Modelling strategies for thin imperfect interfaces and layers

Mathieu Gaborit

THESE DE DOCTORAT DE

LE MANS UNIVERSITE
COMUE UNIVERSITE BRETAGNE LOIRE
KTH ROYAL INSTITUTE OF TECHNOLOGY

ECOLE DOCTORALE N° 602
Sciences pour l'Ingénieur
Spécialité Acoustique

Par

Mathieu GABORIT

Modelling strategies for thin imperfect interfaces and layers

Thèse présentée et soutenue à Stockholm, le 13/12/2019
Unité de recherche : UMR CNRS 6613, Le Mans & MWL, Stockholm
Thèse N° : 2019LEMA1029

Rapporteurs avant soutenance :

Emeline SADOULET Maître de Conférence, FEMTO-ST, Université de Bourgogne Franche-Comté
Elke DECKERS Assistant Professor, KU Leuven

Composition du Jury :

Président : Annie ROSS Professeur, Ecole Polytechnique de Montréal
Examinateurs : Lucie ROULEAU Maître de Conférences, Conservatoire National des Arts et Métiers

Dir. de thèse : Olivier DAZEL Professeur, Le Mans Université
Co-dir. de thèse : Peter GÖRANSSON Professeur, KTH Royal Institute of Technology

Modelling strategies for thin imperfect interfaces and layers

MATHIEU GABORIT

Doctoral Thesis in Engineering Mechanics
KTH Royal Institute of Technology
Stockholm · Sweden

2019LEMA1029
TRITA-SCI-FOU 2019:52
978-91-7873-356-9

KTH School of Engineering Sciences
SE-100 44 Stockholm
Sweden

Akademisk avhandling som med tillstånd av Kungl Tekniska högskolan framlägges till offentlig granskning för avläggande av doktorexamen i teknisk mekanik på fredag 13 december 2019 i rum F3.

Tryck: Universitetsservice US AB

¿′ *Je possède ce miracle de la vitesse et je campe dans le mouvement.*
Je cherche la consistance *qui me prolongera. Je cherche* le lien.

La Horde du Contrevent, Alain Damasio

Contents

Abstract

The global trend towards quieter environments has been one of the key topics of acoustics research for years. The recent tightening of the regulations on noise exposure as well as the many reports on the impact of noise on human health confirm this situation and stress ever more the need for innovative mitigation strategies. Numerous efforts from many teams allowed to refine existing solutions and explore new approaches towards a lower noise level ultimately leading to a number of promising concepts. Central to this field, the use of poroelastic media and the development of realistic meta-materials are paving the way to tackle the problem. In the meantime, a great part of the most widely adopted systems to mitigate noise, such as acoustics panels for instance, resort to thin resistive screens placed on the surface to protect the bulk and control the properties. Despite often being one of the thinnest components of the systems, they have a non-negligible impact on the overall response and are subject to a number of uncertainties.

The approach chosen in this thesis differs from the global trend of designing new solutions and conversely relies on investigating the effect of uncertainties inherent to all these sound proofing systems. More precisely, the work performed focuses on modelling the impact of uncertain interfaces and uncertain parameters in the thin layers used as protective, tuning or aesthetic elements. These acoustic films, and to a certain extent the thin interface zones resulting from the assembly process, are notably challenging to characterise with precision. The main goal of this thesis is then to propose strategies to account for uncertainties on the parameters of the films and interfaces and predict their impact on the overall response of the systems.

Three different scientific contributions are presented in this thesis. Together they discuss modelling aspects related to the films, propose possible simplifications and demonstrate the effect of parameter uncertainties. Finally they introduce numerical strategies to efficiently account for uncertainties in computations within the context of poroelastic and meta-poroelastic media.

Keywords: uncertainties, thin layers, numerical methods, simplified models, poroelastic materials

Sammanfattning

Den globala trenden mot allt tystare miljöer, har i flera år varit i fokus för forskningen inom teknisk akustik. Den senaste tidens skärpning av de reglementen som berör gränser för tillåten ljud- och bullerexponering, tillsammans med studier av bullers påverkan på hälsa, välbefinnande, inlärningsförmåga etc., understryker behovet av nya innovativa strategier. Dessa inbegriper som exempel förfining av redan existerande lösningar, utforskande av nya vägar till effektiva åtgärder för att uppnå en lägre ljudnivå, med flera. Stommen i de flesta åtgärder för att reducera ljudnivåer har sedan mitten av 1900-talet varit olika former av poroelastiska material och under de senaste decennierna även en utveckling av så kallade metamaterial, d.v.s. material vars egenskaper ej går att finna i naturen förekommande form, vilket även bereder väg för att finna nya lösningar på problemet. I dagsläget används, i de mest allmänt använda systemen för att reducera buller, till största delen tunna resistenta skikt som placeras på ytan för att skydda mot mekanisk påverkan och men även för att kunna kontrollera de akustiska egenskaperna. Trots att dessa ytskikt oftast är en av de tunnaste komponenterna i olika system, så är deras påverkan på det totala resultatet avsevärd och kan inte förbises. På grund av deras design, är tillverkningen ofta behäftad med bristande precision och de bidrar därför ofta till att de totala akustiska egenskaperna hos sammansatta system där de ingår, ofta uppvisar en spridning på grund av denna variation.

I denna avhandling behandlas metoder för kunna undersöka effekten av dessa oundvikliga osäkerheter som finns i alla dessa ljudreducerande system. Mer precist, så har arbetet fokuserat på att modellera den påverkan som osäkerheten i gränsytorna och parametrarna i de tunna ytlagren innebär. Bland annat har arbetet varit inriktat på att hantera de utmaningar som ligger i att med precision karaktärisera de akustiska ytskikten och i viss utsträckning de tunna gränsytornas avskärmning som kommer av monteringsprocessen. Avhandlingens mål är att föreslå strategier för att ta i beaktande de osäkerheter hos filmens och gränsytornas parametrar för att förutse deras påverkan på det totala resultatet av systemet.

Tre olika vetenskapliga bidrag presenteras i denna avhandling. Tillsammans behandlar de modelleringsaspekter relaterade till de tunna ytskikten, föreslår möjliga förenklingar och demonstrerar effekterna av osäkerheter i ingående modellparametrar. Slutligen introduceras numeriska strategier för att genom beräkningar, effektivt kunna beakta osäkerheterna gällande poroelastiska och meta-poroelastiska medier.

Keywords: osäkerheter, tunna lager, numeriska metoder, förenklade modeller, poroelastiska medier

Résumé

La tendance globale poussant à développer des environnements plus calmes est, depuis des années, un des aspects clés de la recherche en acoustique. Le récent durcissement des régulations sur l'exposition au bruit ainsi que les nombreux rapports concernant son impact sur la santé humaine rappellent le besoin criant de stratégies innovante pour palier le problème. Le travail de nombreuses équipes a permis d'améliorer les solutions existantes et d'explorer de nouvelles approches, aboutissant à de nouveaux concepts prometteurs. L'utilisation de matériaux poroélastiques et le développement de matériaux méta-poroélastiques réalistes sont un élément central de ces recherches et préfigurent des pistes viables pour résoudre le problème du bruit. En parallèle, une grande partie des systèmes courants pour le traitement des nuisances sonores, comme les panneaux acoustiques, utilisent de fins films résistifs placés en surface pour protéger les matériaux et contrôler le comportement acoustique du système. Malgré que ces films soient souvent les plus petits composants des panneaux, ils ont un impact non-négligeable sur la réponse globale et sont sujet à un certain nombre d'incertitudes.

L'approche choisie dans cette thèse diffère de la tendance globale poussant au développement de nouveaux système. À l'inverse, ce travail s'emploie à modéliser l'impact des incertitudes concernant les films acoustiques et zones d'interface sur le comportement des absorbeurs et traitement acoustiques. Ces films et zones sont notoirement difficiles à caractériser avec précision à cause de leurs propriétés ou de de leur inaccessibilité. Le principal objectif de cette thèse est de proposer des stratégies pour prendre en compte les incertitudes et interfaces afin de prédire leur impact sur la réponse globale.

Trois contributions scientifiques sont présentées. Ensemble, elle discutent différents aspects de modélisation se rapportant aux films et aux absorbeurs, proposent de possibles simplifications et mettent en lumière l'effet des incertitudes. Finalement, ces contributions introduisent des stratégies au niveau du modèle ou du calcul pour prendre en compte les incertitudes dans le contexte des matériaux poroélastiques et méta-poroélastiques.

Keywords : incertitudes, couches fines, méthodes numériques, modèles simplifiés, matériaux poroélastiques

Acknowledgements

This PhD wouldn't have been possible without the financial support of **Le Mans Acoustique** and **KTH**. Similarly, I'm very grateful to the **DENORMS** [a] COST Action 15125 which provided grants for workshops, training schools, conferences and a research visit 2016. A warm thank you to **Jean-Philippe Groby** for the amazing work him and the DENORMS team did over the last years! Many thanks to the patient **admin team** in Le Mans that managed *not* to kill me despite all I did wrong (especially **Iliana**, **Jana** and **Anne-Marie**).

Many thanks go to all the researchers that I closely collaborated with during the PhD, either for papers, lectures or talks: **Logan Schwan** and **Thomas Weisser** for Paper C, **Gwénaël Gabard** for the first contribution of the PhD, the whole team of **Matelys** for the great discussions, data and inputs and especially **Luc Jaouen** for the collaboration over Paper B and at the EAA, the **board of the YAN** for the work we're doing together and, last but not least, **Timo Lähivaara** for the great times and talks in Finland and whenever we cross(ed) paths.

I would like to thank as well **Gunnar Tibert** for accepting to review this thesis and of course the whole committee for spending some of their reading this document and attending the defence in the middle of the Swedish winter. Thanks to **Lucie Rouleau** for accepting to serve as opponent, **Elke Deckers**, **Émeline Sadoulet**, **Patrik Höstmad** and **Camille Perrot** as examiners and of course to **Annie Ross** for presiding the jury.

On a more personal note, thank you **Olivier** and thank you **Peter** for believing in me and in the project, trusting me and managing to cope with my frenchness outbursts and weird ideas since beginning of the master thesis. I learnt a lot by your side, both scientifically and personally and I couldn't have gotten better guides for my first steps in academia. I have to confess one thing though... you were so easy to contact, chat and interact with that I think I mostly failed at seeing you as formal advisers over the last years. To my eyes, you are closer to trusty & very knowledgeable friends than bosses, and I hope to keep the interface between us thin [b] and the collaboration active!

A few last ones, for my dearest friends and my family. *À **mes parents** et **mon frère**, merci une fois de plus pour tout l'amour et le support que vous m'avez témoigné depuis si longtemps, un de mes rares regrets est de ne pas pouvoir plus souvent passer à Saint Gilles.* Thanks to **Samuel**, **Juan**, **Camille**, **Romuald**, **Florent** and particularly **Fred** and **Charlotte** for all the inspiring talks and moments that made me grow by your side. To **My** finally, for her constant support and life together over the last year and hopefully for the years to come, thank you.

To the many unnamed colleagues, friends and strangers with whom I had fun and talks over the last years in Le Mans, Stockholm or anywhere and that had somewhat an impact: thank you, merci, tack så mycket & kiitos!

a. DEsign for NOise Reducing Materials and Structures. https://denorms.eu
b. No. I'm actually not sorry for the pun.

Preface

The work presented in these pages was funded by Le Mans Acoustique (Le Mans, France) and carried out under an international co-tutelle agreement between the KTH Royal Institute of Technology (Stockholm, Sweden) and Le Mans Université (formerly Université du Maine, Le Mans, France). The supervision of the doctoral project is performed by Pr. Olivier Dazel (LAUM, Le Mans Université) and Pr. Peter Göransson (MWL, KTH Royal Institute of Technology).

The present thesis is composed of three parts: an overview of the work performed, a collection of the corresponding scientific publications re-typeset to match the introductory matter and a collection of the published versions of the papers. The different results discussed hereinafter were also presented at conferences, leading to publications in proceedings that are not included in the present document.

Notations and time conventions

Notations differing between the appended papers, it was chosen to keep the mathematical developments in the papers unchanged but to propose a unified version in the introductory section. In all the thesis, papers included, a positive time convention $e^{\mathrm{j}\omega t}$ is adopted with j the complex variable, ω the angular frequency and t the time variable. Matrices and vectors are written in bold face, the former upper case ($\boldsymbol{A}$, $\boldsymbol{B}_{FEM}$, $\boldsymbol{C}^2$) and the latter lower case ($\boldsymbol{n}$, $\boldsymbol{x}_{FEM}$, $\boldsymbol{b}^2$).

List of Acronyms and Abbreviations

FE(M)	Finite-Element (Method)
TMM	Transfer Matrix Method/Model
PDE	Partial Differential Equation
PEM	PoroElastic Material(s)
JCA	Johnson-Champoux-Allard
WRT/w.r.t.	with respect to (in captions or labels)
UEF	University of Eastern Finland (Kuopio, Finland)

Division of work

Paper A & Erratum: A simplified model for thin acoustic screens

Gaborit performed the analysis and implemented the proposed model with inputs from Dazel and Göransson. Gaborit wrote the paper that was later proofread and refined by Dazel and Göransson.

Paper B: Response envelope generation for thin acoustic screens with uncertain parameters

Gaborit derived and tested the model with input from Dazel. Gaborit and Jaouen designed the experiments, the former ran the measurements and both post-processed the characterisation data. Gaborit post-processed the rest of the data and wrote the paper and complimentary dataset (see Ref. [1]) that were reviewed by all authors.

Paper C: Coupling FEM, Bloch Waves and TMM in Meta Poroelastic Laminates

Gaborit performed the analysis and worked on the implementation of the proposed method in a pre-existing code base from Dazel. Gaborit wrote the paper with inputs from all authors and particularly Göransson and Dazel. Groby and Schwan also provided reference results.

List of appended papers

Paper A: A simplified model for thin acoustic screens
M. Gaborit[1,2], O. Dazel[1], P. Göransson[2]
Published as an Express Letter in the Journal of the Acoustical Society of America
Vol. 144 ***(1)*** *(2018), pp. EL76-EL81,* Doi*: 10.1121/1.5047929*

Paper B: Response envelope generation for thin acoustic screens with uncertain parameters
M. Gaborit[1,2], O. Dazel[1], P. Göransson[2], L. Jaouen[3]
Paper submitted to the Journal of the Acoustical Society of America on the 23rd of September 2019.

Paper C: Coupling FEM, Bloch Waves and TMM in Meta Poroelastic Laminates
M. Gaborit[1,2], L. Schwan[1], O. Dazel[1], J.-P. Groby[1], T. Weisser[4], P. Göransson[2]

Published in Acta Acustica United with Acustica
Vol. 104 (2018), pp. 220-227, DOI*: 10.3813/AAA.919163*

Erratum: A simplified model for thin acoustic screens [J. Acoust. Soc. Am. 144 (1), EL76-EL81 (2018)]
M. Gaborit[1,2], O. Dazel[1], P. Göransson[2]
Published in the Journal of the Acoustical Society of America
*Vol. 146 **(2)** (2019), pp. 1382-1383,* DOI*: 10.1121/1.5121612*

Omitted peer-reviewed paper & additional material

Coupling of finite element and plane waves discontinuous Galerkin methods for time-harmonic problems
M. Gaborit[1,2], O. Dazel[1], P. Göransson[2]
Published in the Intl. Journal for Numerical Methods in Engineering
*Vol. 116 **(7)** (2018), pp. 487-503,* DOI*: 10.1002/nme.5933*

Statistical characterisation and responses of acoustics screens and two-layers systems
M. Gaborit[1,2], L. Jaouen[3], O. Dazel[1], P. Göransson[2]
Dataset published on-line via *Zenodo in 2019,* DOI*: 10.5281/zenodo.3358921*

PLANES: Porous LAum NumErical Simulator
O. Dazel[1], M. Gaborit[1,2]
Software package published on Github,
github.com/OlivierDAZEL/PLANES

PyMLS: Python MultiLayer Solver
M. Gaborit[1,2], O. Dazel[1]
Software package published on Github, DOI*:* 10.5281/zenodo.2558137
github.com/cpplanes/pymls

Affiliations:

1. LAUM, UMR CNRS 6613, Université du Maine, Le Mans, France
2. MWL, KTH Royal Institute of Technology, Stockholm, Sweden
3. Matelys Research Lab, Vaulx-en-Velin, France
4. MIPS Laboratory, Université de Haute Alsace, Mulhouse, France

Part I

Work summary

Chapter 1

Introduction

From the cars in the streets to neighbours watching a film, from the loud construction sites to the faint but endless buzz of plugged electric appliances, the modern world is hooded by noise. Each and every aspect of human life in every country is accompanied by sounds of which an important part is unwanted, unstoppable noise. Recent medical and psychological reports suggest that noise exposure have a non-negligible impact on humans[2–4]. Potential effects of over-exposure range from sleep disorders[5,6] and anxiety[7,8] to hypertension or even cardiovascular diseases[9]. Noise is undoubtedly a global issue that has triggered political[10] and regulatory responses[11] along the years. From an acoustics research point of view, different approaches were developed to better understand the effect of noise, reduce emission and prevent propagation. This thesis relates to the last aspect, reflecting on the engineering and conception of acoustic barriers and absorbing systems.

Central to the design of modern sounds absorption devices, porous materials have been extensively studied over the last years. Broad band multi-layered acoustic absorbers have been developed for years, taking advantage of the dissipative properties of foams that arise from the huge contact surface between the interstitial fluid and the elastic skeleton. Aided by the advances in terms of experimental techniques, the characterisation of foams has become more and more accurate[12–18] allowing to determine which layout is the most suitable for a sound package in a given situation. This improved selection of media and assembly follows the current trend in engineering towards lighter, thinner and more concealed acoustic treatments. On the other hand, it has been established that the performance of multi-layered systems at low frequency is directly related to their thickness[19]. Thus, considering the impact of low frequency noise on human health[3–5], it becomes clear that classical absorbers are not always enough to comply with all the requirements.

Different alternatives have gained interest recently, including other classes of sub-wavelength absorbers. One of these approaches combine the properties of periodic diffractors and the broadband absorption of a poroelastic matrix into so-called meta-poroelastic materials to achieve broadband and low-frequency absorption[20–24].

Such systems have been studied in the light of Brillouin and Bloch-Floquet theories, leading to an extensive literature on the subject. Reports in the literature demonstrated as well how optimisation techniques could be leveraged to tailor the properties of these systems at the design stage[25]. These approaches present a number of advantages as they allow to better explore and exploit the design space, unravelling novel possibilities of combining media and inserts. On the other hand, they suffer a number of drawbacks, the most prominent being the computational effort required at each step of the optimisation. In this context, the need for more efficient techniques to evaluate individual responses is undeniable.

Apart from the very core of the absorbing systems such as the ones discussed above, most commercial acoustic panels also involve surface layers, porous screens or films that may have different uses. Initially added to protect the exposed surface from dust, spills and wear, it was shown in the literature that such thin films could be employed to fine-tune the acoustic response of the overall system[26]. Alternatively, they might be used to change the appearance of the panel and serve as a support for paint or other surface treatments. These films are very thin elements, usually less than a millimetre, and the ones used for acoustic applications are highly resistive with an airflow resistivity several orders of magnitude higher than a melamine foam[13]. The most common examples of films are separated in two groups: woven and non-woven. In the first case, a number of threads are weaved into a fabric, in the second case, short fibres are agglutinated to form a stable. Pictures of woven and non-woven film samples appear in Paper B and are reproduced in Figure 1.1, additional examples can be observed in Ref. [13]. Despite being thin and sometimes almost see-through (such as for the woven sample of Paper B), adding a screen on the surface of a system has a remarkable effect as shown in Figure 1.2.

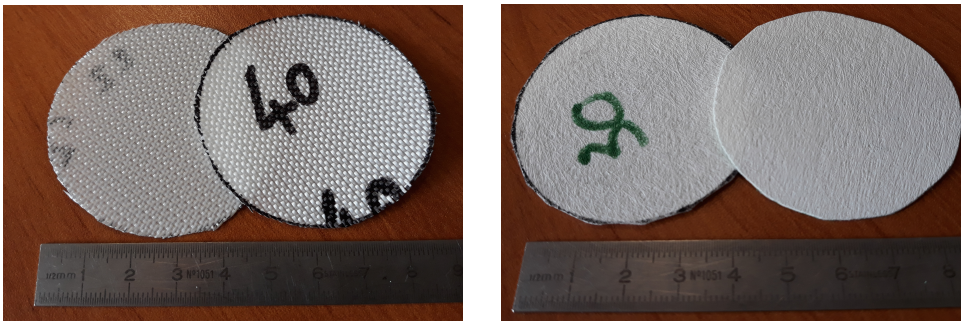

(a) Woven (b) Non-Woven

Figure 1.1 – Samples of acoustic films.

Problematic issues arise when precise values of the parameters are required — to ensure the built panels correspond to the intended design for instance. Indeed, because of their thinness and softness, the physical properties of films are difficult

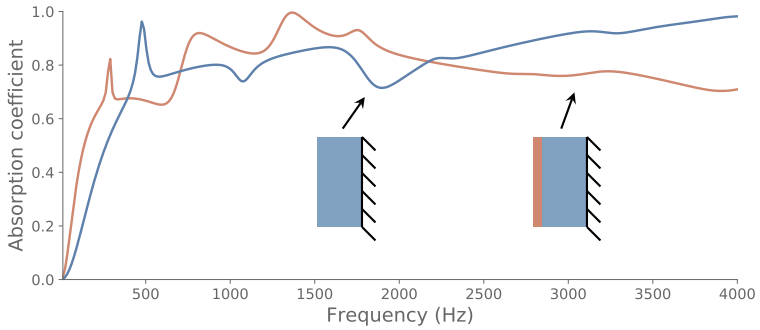

Figure 1.2 – Influence of an acoustic screen added on the surface of an absorber (0.5 mm film on a 5 cm) at 65 deg incidence. The parameters for the two layers are presented in Table 2.1 under the names "Foam" for the backing and "Non-woven" for the screen.

to characterise and some might even change[12,13,19]. For instance, the flow resistivity alone, one of most the important parameters of acoustic screens[26–28], is often associated with a standard deviation of 10 to 20% of the average value[12,13] due to either the measurement process or inherent variability. Accounting for variations in the value of parameters in films and screens, and more generally in all layers, is a key to make the design process more reliable.

Most, if not all, modern sound absorbers involve several materials arranged in various shapes and supposed to hold together to form the complete product. Different techniques might be employed to bond all the components of the panel together into a stable structure and the bonding systematically imply the creation of a small *interface zone* along the frontier. Depending on the bonding strategy, the zone can be one where the materials are compressed thus locally changing the properties, or where a layer of glue has been added, locally creating a stiff layer[19] or even one where a chemical process bonded both solid skeletons, locally changing the porosity and geometry of pores, etc. To a certain extent and provided one can evaluate their properties, interface zone can be represented as thin layers embedded within the global system. Other cases exist but involve specific dynamic effects taking place at the boundary which lie beyond the scope of the thesis.

1.1 Research contributions

In this thesis, some of the challenges exposed in the previous section are addressed. An important part of the work is focused on thin layers and aimed towards the treatment of interface *zones* provided that they can be represented as such. The work includes four scientific contributions, published in international peer-reviewed journals one of which is an erratum. A fifth publication related to the coupling of the Finite-Element Method with a Discontinuous Galerkin approach is omitted here[29] as it is a continuation of a MSc project and is not directly related to interfaces and thin layers.

Amongst the contributions presented here, Papers A and B are specifically targeted towards films. The first of these contributions presents the development of a simplified model for acoustic films and screens, reflecting on the interactions between fields in the medium to propose possible simplifications. This work also presents how such films modify the boundary conditions and stresses the necessity to account for shear effects when modelling these media. The second contribution introduces a strategy to generate response envelopes efficiently and account for the inherent uncertainties in acoustic films. The work is based on a simplification of the propagation model for surface acoustic films on an arbitrary backing. The effect of the screen is isolated and the paper shows how to use these developments to merge precise statistical characterisation of the film properties and a deterministic measurement of the full system response into a meaningful response envelope. Moreover, it is shown that the proposed approach is computationally inexpensive and requires only few operations.

A last contribution, listed as Paper C, discusses a numerical approach to deal with meta-poroelastic systems in the presence of surface layers. By decomposing the fields at the surface of the unit-cell on Bloch modes and using a transfer matrix strategy to propagate loads and unknowns through the layered facings, this work shows that it is possible to include the effect of facings in a Finite Element linear system without meshing them. This technique is validated against a state-of-the-art approach for computation of the responses of meta-poroelastic systems.

1.2 Thesis organisation

This thesis is organised in three parts. The first one is the present introductory matter, which main goal is to introduce the papers, their key results and their conclusions. The second and third parts present the said papers in two different formats. In the former, the content is typeset to resemble the rest of the document in order to ease reading while in the latter, the published versions are reproduced as is. Note that this last section might be missing from the version of this thesis available on-line for copyright reasons.

Part I contains six sections and is organised as follows. After the present introduction, Chapter 2 presents essential background information about poroelastic

models and the Transfer Matrix Method. This chapter is not intended as an exhaustive discussion about any of these topics but instead focuses on introducing the key points on which the rest of the work stands. Then, Chapter 3, 5 and 4 presents each of the appended papers, focusing on the key results and providing, when needed, clarifications on details in the published versions. This part of the thesis is designed for the reader to understand the most important points of each paper, evaluate the quality of the validation and testing process and grasp the underlying goals of the authors. A final chapter concludes, presenting as well thoughts on possible future works.

Chapter 2

Tools: models for poroelastic media and essential aspects of the Transfer Matrix Method

The different parts of this thesis have in common that they all involve porous or poroelastic materials — the latter, abbreviated PEM, implies a deformable skeleton. These media are extensively described in the literature, and a number of models and formulations exist. As an exhaustive review of the pre-existing contributions related to PEM modelling is beyond the scope of this thesis, the next section introduces only key concepts, hypotheses and equations used in the papers.

Similarly, amongst the different computational methods used over the last three years, transfer matrix-based approaches are the most recurring ones. Consequently, the second part of this chapter focuses on key aspects and notations applied in the papers instead of discussing extensively the derivation and implementation of such techniques.

Finally, the two following sections cite relevant items from the literature for the avid reader to get a deeper understanding of the techniques and models involved and apply them anew.

2.1 Selected models for porous and poroelastic media

This thesis deals with porous (or poroelastic) materials and more specifically with open porosity media. Such materials are composed of an all-connected solid skeleton wetted by an all-connected fluid phase. As shown in Figure 2.1 it is seen that for any two points in the fluid (resp. the solid) phase one can always find a path between them that entirely sits in the fluid (resp. solid). In the following and in the papers, the fluid phase is always air although it could be replaced effortlessly by another light fluid. Other works in the literature focus on characterising[17,30] and modelling media filled with a heavy fluid (i.e. water, oil, etc.). There exist a number

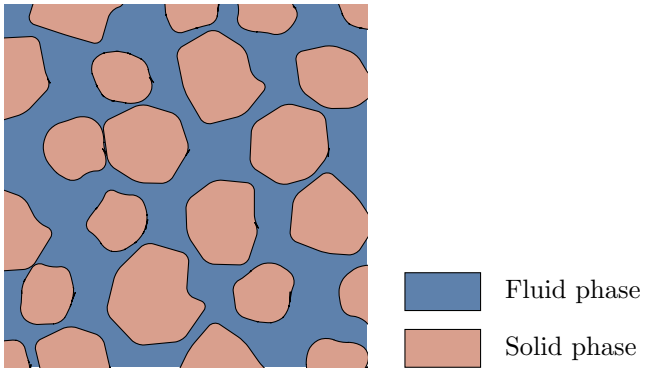

Figure 2.1 – Media studied in this thesis are open-porosity media. Here a slice of medium represent an all-connected fluid phase wetting a solid skeleton connected out of the plane.

of models for such media, either analytical, empirical or semi-phenomenological depending whether or not to account for the skeleton deformation.

Early contributions proposed to consider porous media having a motionless skeleton through the describing of the fluid motion in the pore network. In the light of Kirchoff's theory and provided the pore geometry is simple, one could hypothetically express acoustic indicators based on the topology of the pore networks. This approach gives analytical results[31] but is limited to specific geometries in practice.

On the other hand, some models based on fitting parameters with experiments are widely used in academia and industry[19]. These generally assume that the material under study behaves like a fluid with one or several complex, frequency-dependent parameters to be determined. The equivalent fluid density and compressibility are written as power laws parametrised by coefficients that are determined from the measurements[19,32,33]. Such models lead to a reasonable agreement between predicted and measured responses for some materials and are still widely used, however they do not allow any physical interpretation.

A last class of fluid-based models is of great interest for this thesis. Developed in the second half of the XX$^{\text{th}}$ century, they reflect on the pores topology and the properties of the flow to deduce relations between the equivalent fluid parameters (density and compressibility) and measurable quantities: viscous and thermal characteristic lengths, permeability, tortuosity, etc. Particularly, the model of Johnson *et al.* for the complex density[34] and the one of Champoux and Allard for the compressibility[35] (dynamic bulk modulus) are widely used nowadays to compute the response of media with a motionless skeleton. These models are based on the high or low frequency limits of the parameters and, even though they provide sensible results, are not generally exact. They were later amended to represent more precisely the very low frequency effects, by Pride *et al.*[36] and Lafarge[37] for density

and Lafarge *et al.*[38] for the bulk modulus. Even if they give results agreeing more closely with the measurements, these last two models also require additional parameters (static thermal permeability, static viscous tortuosity and static thermal tortuosity) which limit their adoption. More information on this line of models can be found in the cited works or in the literature[19]. In the following, only the Johnson-Champoux-Allard (JCA) model is considered whenever dealing with media having a motionless skeleton. It is shown when not trivial that the derived expressions can be adapted to othe equivalent models by changing the equivalent density and compressibility. Finally, approaches to model the motion of both the fluid and solid phases exist. The leading strategy in acoustics is then to resort to Biot's theory[39–41]. This model was initially developed for geophysical applications, describing the displacements of the solid skeleton and the interstitial fluid both for isotropic[39,40] or anisotropic[41] cases. It was shown that equivalent fluid models providing expressions for the density and compressibility can be used to represent the fluid phase within Biot's theory[19,42,43]. The case of the Biot's theory used in conjunction with a JCA model is used extensively in the following and referred to as a Biot-JCA model. Note that the Biot's theory was shown to correctly predict the existence of two compressional and a shear waves and that all these were observed experimentally[44–46]. The canonical form of Biot's equations is never used as is in the following and thus is not recalled here. An alternative version,[42] in use everywhere in the thesis is introduced hereinafter while the original one is to be found in the literature.[19,39,41] The canonical form of Biot's wave equations is given in the following for reference but never used as such in the following matter. Instead, an alternative formulation[42] is used in all papers and its formalism is introduced in the following.

2.1.1 Rigid frame: the Johnson-Champoux-Allard model

The Johnson-Champoux-Allard model[34,35] (JCA) is one of the possible models to represent porous materials having a motionless skeleton as an equivalent fluid. This model is based on two main contributions. On one hand, the work of Johnson[34] describes extensively the role of the tortuosity and, through the introduction of the dynamic permeability, can be used to determine an effective mass density for an analogous fluid medium. This work stresses the importance of a parameter to describe the viscous characteristic length denoted Λ which is related to the fluid velocity-weighted ratio between the surface and volume of the pores. On the other hand, a contribution by Champoux and Allard[35] extends the discussion to thermal effects by defining a thermal characteristic length Λ' similar to Λ without the velocity weighting. This second work then allows to define an effective compressibility for the equivalent fluid. The two quantities are complex-valued and frequency dependent, usually represented under their time-harmonic expressions with a dependency on the angular frequency ω.

For the equivalent density, it is:

$$\tilde{\rho}_{eq} = \tilde{\rho}_{eq}(\omega) = \frac{\rho_0 \alpha_\infty}{\phi} \left[1 + \frac{\omega_0}{\mathrm{j}\omega} F(\omega) \right] \tag{2.1}$$

with

$$\omega_0 = \frac{\sigma \phi}{\rho_0 \alpha_\infty}, \quad \omega_\infty = \frac{(\sigma \phi \Lambda)^2}{4 \mu_0 \rho_0 \alpha_\infty^2}, \quad F(\omega) = \sqrt{1 + \frac{\mathrm{j}\omega}{\omega_\infty}}. \tag{2.2}$$

In these equations, ρ_0 and μ_0 are the density and dynamic viscosity of air, ϕ is the porosity, σ is the flow resistivity and α_∞ is the high-frequency limit of the tortuosity.

The equivalent compressibility reads:

$$\tilde{K}_{eq} = \tilde{K}_{eq}(\omega) = \frac{\gamma_0 P_0}{\phi} \left[\gamma_0 - (\gamma_0 - 1) \left(1 + \frac{\omega'_\infty}{2\mathrm{j}\omega} F'(\omega) \right)^{-1} \right]^{-1} \tag{2.3}$$

with

$$F'(\omega) = \sqrt{1 + \frac{\mathrm{j}\omega}{\omega'_\infty}}, \quad \omega'_\infty = \frac{16 \nu'_0}{\Lambda'}$$

in which γ_0, P_0 and ν'_0 are respectively the polytropic coefficient, the static pressure and the viscothermal loss factor of air.

Note that this 5-parameter model uses the high-frequency limits of the different parameters and suffers discrepancies at low frequency. Later works by Pride *et al.*[36] and Lafarge *et al.*[37,38] propose corrections to partly alleviate these issues. Particularly, these corrections allow to account for pore constrictions, introducing a number of additional parameters: static thermal permeability k'_0, static viscous tortuosity α_0 and static thermal tortuosity α'_0. This 8-parameter model is more accurate to represent the low-frequency behaviour but some parameters imply important characterisation challenges which impair its adoption.

Even though never used in the results presented hereafter, this model was sometimes used during the PhD project and is introduced here for reference. The modified versions of the equivalent density and compressibility read:

$$\tilde{\rho}_{eq} = \frac{\rho_0 \alpha_\infty}{\phi} \left[1 + \frac{\omega_0}{\mathrm{j}\omega} F(\omega) \right] \tag{2.4}$$

with

$$F(\omega) = 1 - P + P \sqrt{1 + \frac{\mathrm{j}\omega}{\omega_0} \frac{M}{2P^2}}, \quad M = \frac{8 k_0 \alpha_\infty}{\phi \Lambda^2}, \quad P = \frac{M}{4} \left(\frac{\alpha_0}{\alpha_\infty} - 1 \right)^{-1} \tag{2.5}$$

where ω_0 is the same as for (2.2) and

$$\tilde{K}_{eq} = \frac{\gamma_0 P_0}{\phi}\left[\gamma_0 - (\gamma_0 - 1)\left(1 + \frac{\omega_0'}{\mathrm{j}\omega}F'(\omega)\right)^{-1}\right]^{-1} \tag{2.6}$$

with

$$\omega_0' = \frac{\kappa_0 \phi}{\rho_0 C_p k_0'} \tag{2.7}$$

where κ_0 is the thermal conductivity of air, C_p the specific heat of air at constant pressure and

$$F'(\omega) = 1 - P' + P'\sqrt{1 + \frac{\mathrm{j}\omega}{\omega_0'}\frac{M'}{2P'^2}}, \quad M' = \frac{8k_0'}{\phi\Lambda'^2}, \quad P' = \frac{M'}{4(\alpha_0' - 1)}. \tag{2.8}$$

This refined model is denoted JCAPL (Johnson-Champoux-Allard-Pride-Lafarge)[47].

2.1.2 Elastic frame: the Biot model

Originally created to describe the propagation of waves in geophysical media for oil exploration, Biot's theory was introduced in a set of contributions in the middle of the XX$^{\text{th}}$ century. The theory relies on the modelling of the joint evolution of the fluid and solid phase displacement fields. The approach covers both isotropic[39,40] and anisotropic media[41] in the linear regime although the anisotropic case uses the inter-phase relative displacement instead of the fluid displacement field. The equations are derived by means of an neat Lagrangian formalism which leads to dynamic and constitutive relations. When combining these, one easily obtains two vector wave equations involving a number of coefficients later identified through thought experiments[40] in a similar fashion as in fields theory. The complete derivation of the formalism is to be found in the literature[39–41] and a succinct discussion is available in Ref. [19].

The present thesis does not employ the original formulation of Biot's theory but instead resort to an alternative form[42] that has the advantage of yielding more concise expressions. This alternate form uses the solid displacement $\boldsymbol{u}^s$ and a compound displacement $\boldsymbol{u}^w$ as variables. The latter field writes:

$$\boldsymbol{u}^w = \underbrace{\phi\boldsymbol{u}^f + (1-\phi)\boldsymbol{u}^s}_{\boldsymbol{u}^t} - \frac{K_b}{K_s}\boldsymbol{u}^s \tag{2.9}$$

where K_b is the bulk modulus of the complete foam and K_s the one of the solid material the skeleton is made of. It is straightforward to identify that when the ratio of these moduli is small, i.e. when the foam is soft compared to the material of the skeleton itself, $\boldsymbol{u}^w$ reduces to the so-called total displacement $\boldsymbol{u}^t$. The total displacement is a porosity weighted sum of the displacements in both phases. Using $\boldsymbol{u}^s$ and $\boldsymbol{u}^t$ as variables, one obtains a formulation sometimes referred to as $\{\boldsymbol{u}^s, \boldsymbol{u}^t\}$ based on the following motion equations:

$$\hat{\sigma}_{ij,j} = -\omega^2 \tilde{\rho}_s u_i^s - \omega^2 \tilde{\rho}_{eq} \tilde{\gamma} u_i^t, \qquad -p_{,i} = -\omega^2 \tilde{\rho}_{eq} \tilde{\gamma} u_i^s - \omega^2 \tilde{\rho}_{eq} u_i^t \tag{2.10}$$

using Einstein's convention for summation over repeated indices. The parameters are the interstitial pressure p, the solid-phase density $\tilde{\rho}_s$, the *in vacuo* stress tensor $\hat{\sigma}_{ij}$ and a fluid/solid coupling term $\tilde{\gamma}$. Additionally, the two associated constitutive equations read

$$\hat{\sigma}_{ij} = \hat{A} u_{k,k}^s \delta_{ij} + 2N\varepsilon_{ij}, \qquad p = -\tilde{K}_{eq} u_{k,k}^t \tag{2.11}$$

where δ_{ij} is the Kronecker symbol, $\varepsilon_{ij} = 1/2(u_{i,j}^s + u_{j,i}^s)$ is the *in vacuo* strain tensor and $\hat{A}$ and N are the Lamé coefficients of the solid phase[40,42].

From the motion and constitutive relations, Biot determined that three kinds of waves could propagate in the medium and the same result can be obtained from (2.10) and (2.11). By combining the two sets of equations into a pair of wave equations and considering two scalar potentials, the expressions of the two possible compression waves are obtained. Similarly, the existence of a shear wave is demonstrated by considering a vector potential. This prominent result of Biot's theory was verified experimentally[44–46] providing evidence that the overall approach gives sensible results.

As a final remark, note that the limp model, suitable for very soft foams and used in Paper B, can be derived from (2.10) and (2.11) assuming that the frame stiffness is negligible and using the following effective density that accounts for the inertia of the skeleton:

$$\rho_{limp} = \rho_{eq} \frac{\rho_s - \gamma^2 \rho_{eq}}{\rho_s} \tag{2.12}$$

with ρ_{eq} the equivalent fluid density and ρ_s:

$$\rho_s = \rho_1 + \phi\rho_f \left(\frac{Q}{R}\right)^2 + \phi\rho_f(\alpha_\infty - 1)\left(1 - \frac{Q}{R}\right)^2 \tag{2.13}$$

where ρ_1 is the density of the foam, ρ_f the one of the interstitial fluid, and Q, R are two constitutive coefficients of the poroelastic medium[19,42].

2.2 Computing response of laminates: transfer matrices

Used extensively in the present thesis, Transfer Matrix approaches are a class of efficient methods to compute the acoustic response of layered media. The present section constitutes an introduction to these techniques, focusing on the key points of the approach and the aspects that are the most relevant for understanding the appended papers. A more in-depth presentation can be found in Ref. [19] or Ref. [48] for an alternative approach used in the thesis. The key idea of these approaches is to represent the evolution of the fields in each and every layer by a matrix and finally combine them to represent the whole system.

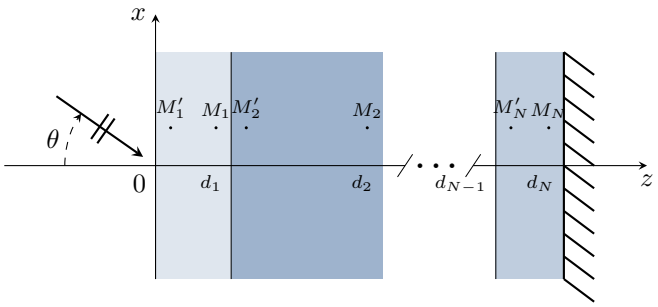

Figure 2.2 – Multiple layers of different media are stacked along the z axis. The objective is to compute the acoustic response of the overall system.

Considering the study model presented in Figure 2.2, one must write, for each layer i, an equation of the form:

$$\boldsymbol{s}_i(M_i') = \boldsymbol{T}_i \boldsymbol{s}_i(M_i) \tag{2.14}$$

where $\boldsymbol{s}_i(M)$ is the so-called state vector containing the values of the fields at a given point M, or quantities that allow to reconstruct them. It is important to understand that for the same media, different sets of quantities might be used, all forming perfectly valid state vectors, the key point being that the enclosed quantities are sufficient to reconstruct the dynamic state within the layer. Some approaches used the amplitudes of waves in the medium,[49] others used the fields in the medium,[19] or a combination of them.[50,51]

2.2.1 Two approaches

To obtain a final expression representing the whole system, a straightforward approach[19,52] is to construct a global matrix associated to a solution vector $\boldsymbol{x}$. This vector contains the fields from the incident and possibly transmitted media and all the different $\boldsymbol{s}_i$. The global matrix is composed of the matrices for each layer as well as of interface operators representing interface conditions. The type of backing or transmission layer finally allows to obtain a square global matrix while the excitation is written in a forcing vector and in the end, the response for all fields is retrieved by inverting the matrix.

Another possible technique[48] is to use a recursive approach that was initially developed to alleviate stability issues[48,53]. The method works in a layer-oriented fashion; starting from the backing, the load is transferred through the layers and interfaces by applying suitable operators. In the end, a matrix representing the whole system and its final load is obtained, linking the excitation to a so-called information vector. After the resolution, the reflection coefficient is directly obtained and a second solution term can be used along with the different matrices to obtain the fields at each layer and the transmission coefficient if applicable.

2.2.2 Deriving transfer matrices

If the interfaces are easily described, the key point of these approaches is to obtain the matrices to propagate through the layers. The literature[19,49–51,54] has examples of how to derive these matrices. For instance, a tedious but common approach using the amplitudes of waves is described in Ref. [19] and more in depths in Refs. [49, 54]. In the scope of this thesis and particularly of Paper A, the so-called Stroh formalism is employed. This approach consists in rewriting the equations governing the propagation through the layer as a first order ordinary differential equation of the state vector $\boldsymbol{s}(z)$ along the depth of the laminate:

$$\frac{\mathrm{d}\boldsymbol{s}(z)}{\mathrm{d}z} = \boldsymbol{\alpha}\boldsymbol{s}(z), \tag{2.15}$$

where $\boldsymbol{\alpha}$ is the co-called state matrix that indicates how the fields interact inside the layer. The complete derivation of this matrix is omitted here as it is out of the scope of this thesis but can be found in the literature[42,51,55]. Note that the present document only uses explicitly the results for isotropic poroelastic media for which the matrix is of size 6×6. The full expression is presented in appendix A.1 of Ref. [48] and reproduced in equation (3.2). Other media have been described in the literature and the reader can refer to the remainder of Ref. [48] for isotropic fluid and solid media or or to Ref. [50] for anisotropic poroelastic materials for instance.

Solving equation (2.15) for a layer of thickness d yields a solution written under the form of a matrix exponential, where $\boldsymbol{T}(d)$ is called the transfer matrix for the said layer:

$$\boldsymbol{s}(0) = \exp(-d\boldsymbol{\alpha})\boldsymbol{s}(d) = \boldsymbol{T}(d)\boldsymbol{s}(d). \tag{2.16}$$

2.2.3 Links with the rest of the thesis

In the present thesis, the ideas of the first approach based on a global system form the strategy of Paper C to account for coatings and facings.

The model presented in Paper A yields a matrix that can be used independently within the scope of both approaches.

All the results presented at "TMM" in the present thesis are generated using the second, recursive, approach[48,53]. More precisely, they are generated using a in house software package written and published[56] as a part of the PhD work. Results from Paper A have also been implemented into the said package by directly inserting the simplified transfer matrix and the appended Erratum was written to acknowledge the detection and correction of an implementation error in the said software.

2.3 Properties of the media used in the examples

The present thesis uses a number of figures presenting acoustic responses of absorbing systems to illustrate parts of the discussion. Figure 1.2 is an example of such graphics. This section gathers the physical parameters of the media used to generate these figures and, when available, indicates the source of the data. Both the films denoted "Woven" and "Non-woven" are originally described in Ref. [13]. The film "Non-woven 2" is taken from Table 11.4 of Ref. [19] and corresponds to a layer of glue. The actual characterised values for this last layer are questionable and thus it is used only in Figure 3.1 to illustrate the difference between models.

Table 2.1 – Parameters of the films and foam used in the examples.[13,19,57] Media specific to a single article are omitted here and directly listed in the said contribution instead.

Parameters (unit)	Foam	Woven	Non-woven	Non-woven 2
Porosity ϕ	0.994	0.72	0.04	0.8
Flow resistivity σ (N·s·m^{-4})	9045	$87{\cdot}10^3$	$775{\cdot}10^3$	$3.2 \cdot 10^6$
HF Limit of tortuosity $\tilde{\alpha}_\infty$	1.02	1.02	1.15	2.56
Thermal CL Λ' (μm)	197	480	230	24
Viscous CL Λ (μm)	103	480	230	6
Foam density ρ_1 (kg·m^{-3})	8.43	171	809	125
Poisson's ratio ν	0.42	0	0.3	0.3
Young's Modulus E (Pa)	$194.9{\cdot}10^3$	$50{\cdot}10^3$	$260{\cdot}10^6$	$2.6 \cdot 10^6$
Loss factor η	0.05	0.5	0.5	0.1

Chapter 3

Towards simpler models for films and interface zones

This section discusses the modelling of thin layers from an acoustic viewpoint. In Paper A a simplified model for acoustic screens is introduced enabling a better understanding of the effects at play within these films. Particularly, some examples related to aspects that could not have been extensively discussed in a letter are provided here. An additional paragraph presents an erratum submitted to amend the figures of the original letter after an implementation mistake was detected.

It has been established that acoustic films and screens tend to be challenging on different levels. Given their specificities in terms of thickness or parameter range, one might wonder which model is the best suited to represent this kind of media. Previous contributions have presented how films are used to control the response of the host system[26] for instance or strategies to represent them by means of rigid frame models[27].

Because it might be challenging or costly to correctly retrieve the elastic properties of films[15,58] and use a Biot-JCA model, equivalent fluid models are often used to obtain an approximate result[19]. This approach has the benefit of giving reasonable results but completely overlooks a number of resonant effects as seen in Figure 3.1 for a two-layer system such as the one in Figure 3.2.b. This is explained by the fact that an equivalent fluid medium model does not only neglect all elastic effects within the layer but also leads to a completely different boundary condition applied on the surrounding layers. Using a complete Biot-JCA model to address these discrepancies is an overly complicated approach in the case of thin screens as the complex interactions between fields do not happen in such thin layers. The approach of Paper A is then to derive a simpler model for the screens able to represent most dynamic effect and conserving accurate interface conditions with the surrounding layers. It is important to understand that the key objective during the development of the proposed approach was to remove as many terms as possible from the matrix while keeping responses close to the reference ones. Many different

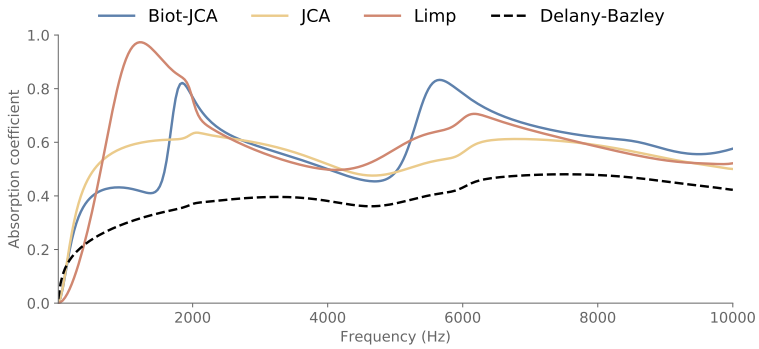

Figure 3.1 – Influence of the choice of model on the resolution of the resonances for a system such as the one in Figure 3.2.b for different models for the film. The foam and films parameters are listed in Table 2.1 under the names “Foam” and ”Non-woven 2”.

types of films were used to assess the effect of neglecting each of the terms. The focus was then to find the best compromise between a simpler model and a sufficient precision.

3.1 Derivation of the simplified model

The derivation relies on an analysis of the transfer matrix and the identification of negligible terms when considering a number of assumptions and observations related to screens. There are different methods to derive transfer matrices to represent poroelastic layers such as acoustic screens[19,48,49] and Paper A employs the so-called Stroh formalism introduced in Section 2.2.2 as it creates a natural basis for simplifications. To represent the film, Paper A resorts to the alternative $\{\boldsymbol{u}^s, \boldsymbol{u}^t\}$ formulation[42] of Biot's equations as presented in section 2.1.2. The equations of this formulation can easily be manipulated to obtain the same form as in (2.15) using the following state vector:

$$\boldsymbol{s}(z) = \left\{\hat{\sigma}_{xz},\ u_z^s,\ u_z^t,\ \hat{\sigma}_{zz},\ p,\ u_x^s\right\}^T \tag{3.1}$$

and the associated state matrix:

$$\boldsymbol{\alpha} = \begin{bmatrix} 0 & 0 & 0 & \mathrm{j}k_x \frac{\hat{A}}{\hat{P}} & \mathrm{j}k_x\tilde{\gamma} & -\frac{\hat{A}^2-\hat{P}^2}{\hat{P}}k_x^2 - \tilde{\rho}\omega^2 \\ 0 & 0 & 0 & \frac{1}{\hat{P}} & 0 & \mathrm{j}k_x\frac{\hat{A}}{\hat{P}} \\ 0 & 0 & 0 & 0 & -\frac{1}{\tilde{K}_{eq}} + \frac{k_x^2}{\tilde{\rho}_{eq}\omega^2} & -\mathrm{j}k_x\tilde{\gamma} \\ \mathrm{j}k_x & -\rho_s\omega^2 & -\tilde{\rho}_{eq}\tilde{\gamma}\omega^2 & 0 & 0 & 0 \\ 0 & \tilde{\rho}_{eq}\tilde{\gamma}\omega^2 & \tilde{\rho}_{eq}\omega^2 & 0 & 0 & 0 \\ \frac{1}{N} & \mathrm{j}k_x & 0 & 0 & 0 & 0 \end{bmatrix}. \quad (3.2)$$

As described alongside equation (2.16), solving Stroh's differential equation leads to a transfer matrix under the form of a matrix exponential. Considering that typical films and screens exhibit a thickness within the millimetre range, one can assume $d \ll 1$ and thus replace the exponential by its Taylor expansion:

$$\boldsymbol{T}(d) = \exp(-d\boldsymbol{\alpha}) \quad \xrightarrow{kd\ll 1} \quad \boldsymbol{T}(d) \approx \boldsymbol{I} - d\boldsymbol{\alpha} \quad (3.3)$$

where $\boldsymbol{I}$ is the identity matrix.

Interestingly enough this reformulation correspond to a form proposed by Pierce[28] who would model blankets through a pressure jump. With the transfer matrix rewritten as a sum, it becomes straightforward to compare the order of magnitude of the terms and identify those that can be neglected. To this end, Paper A introduces a number of considerations that allow sieving the matrix $d\boldsymbol{\alpha}$ and ultimately reduce the number of terms and equations.

One of these simplifications concerns the solid displacement fields. Noting that there always exists a wavenumber k_s greater or equal than all the others ($k_s \geq k_{x,z}$) and substituting this inequality into the constitutive equations for the thin layer ($k_s d \ll 1$) it is shown that

$$\boldsymbol{u}^s(0) \approx \boldsymbol{u}^s(d). \quad (3.4)$$

This result allow to neglect all alteration of the solid displacement and to remove three terms from $\boldsymbol{T}$. From a physical point of view, it is equivalent to saying that the film's skeleton moves as a whole and neither shears nor expands. In order to further simplify the matrix, two other assumptions are used. First, the coupling of the tangential solid and the total normal displacement is neglected and so is the influence of the saturating fluid on the *in vacuo* stresses. These two assumptions are supported by the thickness of the screens which do not allow for the effect of these couplings to build up. Four terms can then be neglected in the matrix, $\boldsymbol{T}_{15}$ and $\boldsymbol{T}_{36}$ for the first statement and $\boldsymbol{T}_{14}$ and $\boldsymbol{T}_{41}$ for the second.

Applying these simplifications yields:

$$\boldsymbol{T}(d) \approx \boldsymbol{I} - d \begin{bmatrix} 0 & 0 & 0 & 0 & 0 & -\frac{\hat{A}^2-\hat{P}^2}{\hat{P}}k_x^2 - \tilde{\rho}\omega^2 \\ 0 & 0 & 0 & 0 & 0 & 0 \\ 0 & 0 & 0 & 0 & -\frac{1}{\tilde{K}_{eq}} + \frac{k_x^2}{\tilde{\rho}_{eq}\omega^2} & 0 \\ 0 & -\rho_s\omega^2 & -\tilde{\rho}_{eq}\tilde{\gamma}\omega^2 & 0 & 0 & 0 \\ 0 & \tilde{\rho}_{eq}\tilde{\gamma}\omega^2 & \tilde{\rho}_{eq}\omega^2 & 0 & 0 & 0 \\ 0 & 0 & 0 & 0 & 0 & 0 \end{bmatrix}. \tag{3.5}$$

In Paper A, a final assumption is proposed regarding the equivalent fluid density $\tilde{\rho}_{eq}$ and compressibility $\tilde{K}_{eq}$. Neglecting the effects of tortuosity ($\alpha_\infty = 1$) the compressibility is rewritten in a form similar to the one for isothermal compression:

$$\tilde{K}_{eq} \approx \frac{P_0}{\phi} \tag{3.6}$$

where P_0 is the atmospheric pressure and ϕ the porosity of the film.

The new expression of the density then corresponds to the one proposed in Ref [28] with a real-valued corrective term for high frequencies:

$$\tilde{\rho}_{eq} \approx \frac{\rho_0}{\phi} + \frac{\sigma}{\mathrm{j}\omega}. \tag{3.7}$$

Altogether, the proposed simplifications lead to a number of consequences regarding the accuracy of the computed responses. First, because of the assumption that the film is thin with respect to the wavelength (i.e. $k_f d \ll 1$), the agreement between the proposed model and a complete Biot-JCA approach is expected to worsen as the frequency increases. As the wavenumber k_f depends on the physical properties of the medium, the frequency range where this model may be used might vary slightly between films. On another level, the validity of the Taylor expansion (3.3) as well as the one of other assumptions might be challenged if the angle of incidence is too close to grazing incidence. Indeed, at these angles, the path travelled by the wave in the medium is long and some of the effects deemed negligible might have enough space to build up. Similar effects can also happen at resonance frequencies where the high amplitudes of some of the fields might trigger coupling effects.

3.2 Validation of the approach

In order to validate the approach, Paper A proposes two tests: first, the method is tested on generating a frequency response for a film or a film on a foam layer on a rigid backing for two different angles. The responses are compared to references with the film modelled using Biot-JCA. A second test asserts the agreement of the model for a wide range of angles and frequencies. In this section, only the second test is reproduced.

Note that an erratum was recently published regarding the figures in the original contribution. In an earlier version, due to a mistake regarding the implementation of the backing condition, the *in vacuo* stresses were considered null and the solid displacement field unknown along the backing. The proposed simplification being completely independent from the backing, the original conclusions still hold and only the figures were corrected in the erratum. The figures hereafter are obviously the new ones.

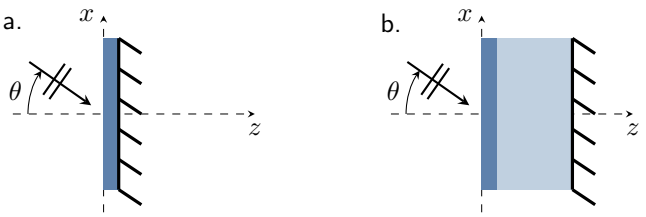

Figure 3.2 – Configurations used for validating the proposed models. **a.** film set on a rigid backing; **b.** film set on a poroelastic layer and a rigid backing

The validation procedure proposed in the paper uses the configurations depicted in Figure 3.2 and consists in varying the angle of incidence between 0 deg and 89 deg (normal to grazing incidence) and the frequency from 0 to 4 kHz. Two absorption coefficients are computed over the (f, θ) plane: α_{biot} using a Biot-JCA model for the film (and the backing PEM if applicable) and α_{screen} using the proposed approach. In order to compare the two, the following metric is used:

$$\epsilon = |\alpha_{\text{biot}} - \alpha_{\text{screen}}|. \tag{3.8}$$

The resulting maps are shown in Figure 3.3 where high values of ϵ correspond to darker shades. Looking at the colour bar of each map, it is very clear that the proposed method gives satisfactory results with respect to the metric. It is interesting to note that the discrepancies discussed at the end of section 3.1 are observed in Figure 3.3 without really challenging the applicability of the model.

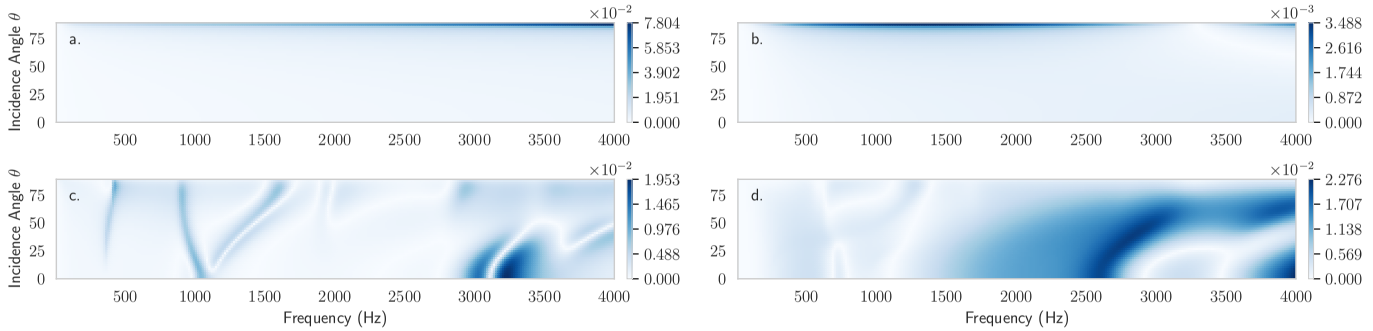

Figure 3.3 – Error distance to the reference solution over the (f, θ) plane. For two types of film (non woven for a. & c. and woven for b. & d.) and two configurations (Figure 3.2.a for a. & b. and Figure 3.2.b. for c. & d.). Parameters for the media are disclosed in Table 2.1 under the names "Foam", "Woven" and "Non-woven".

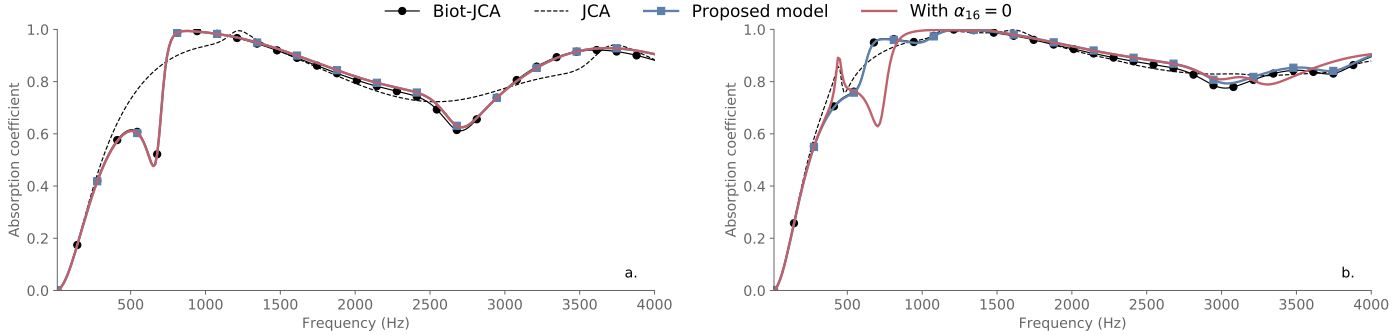

Figure 3.4 – Differences induced by neglecting the shear term in the transfer matrix (3.5), reference curves provided with the film modelled with Biot-JCA or JCA approaches. Responses computed for the system presented in Figure 3.2.b at two different angles of incidence **a.** $\theta = 0\,\text{deg}$ and **b.** $\theta = 45\,\text{deg}$. The physical parameters are the same as for Figure 3.3.

3.3 Closing words and the effect of further simplifications

The method presented in the present section and in Paper A allows to obtain sensible responses for thin screens while using a simpler model than a complete Biot-JCA approach. Particularly, using the proposed approach, two of the six equations describing the link between the two sides are replaced by an identity relation. The simplifications on the equivalent fluid constants and some coupling terms are supported by the special nature of acoustic screens within which some of the effects predicted by Biot's theory do not take place. The proposed approximations leading to considering $\alpha_\infty = 1$ must be treated with care as it was shown that the dynamic tortuosity might have an effect on how the layers couple together[19,27].

To a certain extent, it is interesting to identify the terms remaining in the transfer matrix (3.5) and their effect. Reproducing the matrix of jumps across the layer and the state vector (3.1) one might identify several terms:

$$\boldsymbol{s} = \begin{Bmatrix} \hat{\sigma}_{xz} \\ u_z^s \\ u_z^t \\ \hat{\sigma}_{zz} \\ p \\ u_x^s \end{Bmatrix}, \qquad d \begin{bmatrix} 0 & 0 & 0 & 0 & 0 & -\frac{\hat{A}^2-\hat{P}^2}{\hat{P}}k_x^2 - \tilde{\rho}\omega^2 \\ 0 & 0 & 0 & 0 & 0 & 0 \\ 0 & 0 & 0 & 0 & -\frac{1}{\tilde{K}_{eq}} + \frac{k_x^2}{\tilde{\rho}_{eq}\omega^2} & 0 \\ 0 & -\rho_s\omega^2 & -\tilde{\rho}_{eq}\tilde{\gamma}\omega^2 & 0 & 0 & 0 \\ 0 & \tilde{\rho}_{eq}\tilde{\gamma}\omega^2 & \tilde{\rho}_{eq}\omega^2 & 0 & 0 & 0 \\ 0 & 0 & 0 & 0 & 0 & 0 \end{bmatrix} \tag{3.9}$$

The complex framed in blue is linked to couplings between the compression stresses and normal displacements, related to longitudinal waves in the medium. The one in green is purely linked to shear effects, describing the connection between the tangential displacement in the solid and the modification of shear stresses. This term is particularly important to correctly describe how the screen modifies the condition at the surface of the backing. In order to illustrate this last point, Figure 3.4 compares the responses computed with the proposed model and when neglecting the shear coupling term. It then becomes clear that shear stresses play a prominent role in determining the overall response and cannot be neglected. Though, it is interesting to note that the approach described here does not allow for shear to compression conversion within the film as all the relevant terms (in orange) are null in the matrix.

Chapter 4

Response envelopes and the effect of film uncertainties

Films and coatings used in acoustic panels are challenging in different ways and particularly in terms of characterisation. Their small thickness and the range of values their mechanical and acoustical properties might take tend to render characterisation difficult and even push some of the procedures to their limits. Methods do exist to determine the value of the different properties through acoustic measurements[13,59] and start to be included in the newest versions of international standards, see Ref.[12] for flow resistivity for instance. Despite these efforts towards a better determination of the production values of acoustic screens properties, these quantities tend to be altered during panel assembly or even manipulation. Indeed, the films are often the most exposed layers in the panels which implies a certain wear over time and ends up deviating the properties away from their nominal values.

As discussed in the introduction, acoustic films are mostly used for their resistive behaviour and have a strong influence on the response of the whole panel. Two parameters are particularly important in this context: the flow resistivity σ and the thickness d[19,26,28]. Just as any others, these parameters are subject to uncertainties linked either to the characterisation process or to variations inherent to the medium and its handling.

Paper B proposes a simple way to compute response envelopes that better represent the effect of parameters uncertainty. Apart from the usual theory and validation sections, the paper also comprises an experimental part which required characterising a large number of film samples and measuring their response when associated to a poroelastic backing layer. The target of this set of measurement was to obtain reliable statistical data on the screens both to apply the proposed method and assess the validity of the assumptions. A result from these characterisation is presented in Figure 4.1 (and in Figure 11 in the paper) showing the range of variation of the different JCA parameters for two different films: woven and non-woven (refer to Section 2.1.1). Pictures of both films are shown in Figure 4.2.

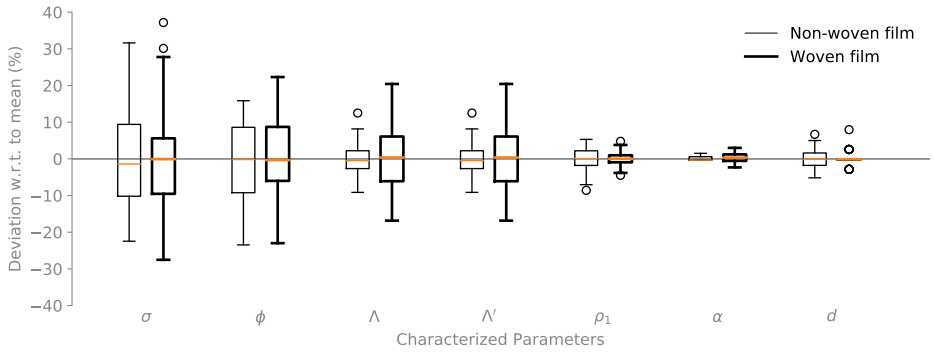

Figure 4.1 – Spread of the JCA parameters and thickness for both facings. The orange line marks the median, outliers are represented with circles and the box spans between the first and third quartiles. Thin lines correspond to the non-woven facing, thick ones to the woven film.

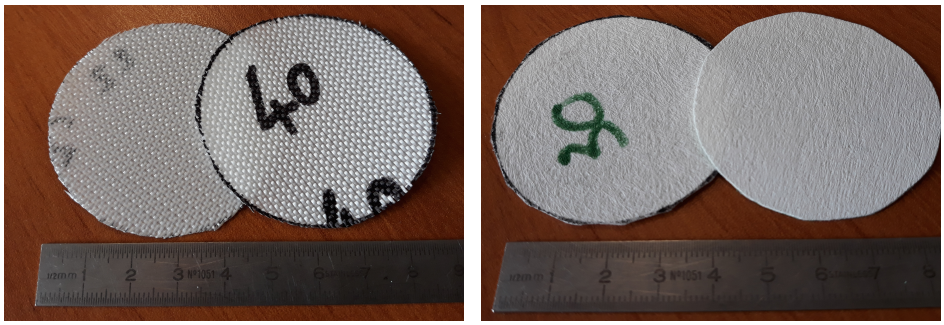

(a) Woven facing (b) Non-woven facing

Figure 4.2 – Pictures of screen samples.

The characterisation of the two media was performed following standards and techniques from the literature[12,13,16]. It is very clear in Figure 4.1 that the flow resistivity is the most varying parameter with about 11% of deviation with respect to the average value, closely followed by the porosity with 9%. Of course, the precise values directly depends on the film involved.

4.1 Theoretical background

In order to derive an expression for the response where the effect of the uncertainties can be isolated, Paper B proposes a strategy based on a very simple system shown in Figure 4.3.

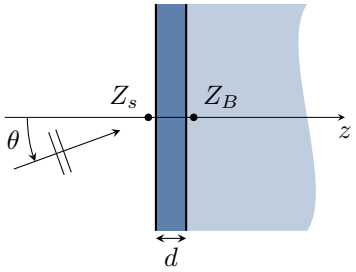

Figure 4.3 – System schematic

The contribution relies on two main assumptions: first that the effect of the film can be coarsely approximated by an equivalent fluid model and second that the film is thin compared to the wavelength i.e. $k_f d \ll 1$ where k_f is the wavenumber of the equivalent fluid model. The first of these assumptions is generally verified as the global trend is usually correctly approximated, even though the resonances are not quite recovered with an equivalent fluid model. The second assumption holds up to a few kilohertz as most films have a thickness of under a millimetre[13,19,27].

Taking advantage of the equivalent fluid model, a first step towards isolating the influence of uncertainties is then to use the impedance translation formula[19] to represent the film and determine Z_s knowing Z_B. This formula involves $\tan(k_f d)$ terms which can be approximated by their first order Taylor expansion based on the second assumption:

$$Z_s = \frac{Z_B + \mathrm{j} Z_f k_f d}{1 + \mathrm{j} Z_B Z_f^{-1} k_f d} \tag{4.1}$$

where Z_f is the characteristic impedance of the equivalent fluid model. Note that the usual relations for fluids hold:

$$Z_f = \sqrt{\rho_f K_f}, \qquad k_f = \omega \cos\theta \sqrt{\rho_f / K_f} \tag{4.2}$$

where ρ_f and K_f are the equivalent fluid density and compressibility.

Considering that the term in the denominator of (4.1) is often small due to the thickness and the low impedance contrast between the film and the backing system a second Taylor expansion is employed. This simplification allows to turn the ratio into a sum and to after substitution of the expression for k_f and ρ_f and simplification, it yields:

$$Z_s = Z_B + \underbrace{\mathrm{j}\omega \cos\theta d \left(\rho_f - Z_b^2 K_f^{-1}\right)}_{Z_F} \tag{4.3}$$

In this equation, the influence of the film is clearly contained in the last term, incidentally called Z_F. To determine how the uncertainties on the parameters of the film influence the overall response then means understanding what contributes to the deviation of Z_F. In Paper B, four different cases are considered depending on which variable is uncertain: either ρ_f or K_f alone, both at once or the thickness d. These cases correspond to the different possibilities when the film is represented with a JCA model, see Section 2.1 for more details. Indeed in this case model a deviation of ρ_f could correspond for instance to an uncertainty on the flow resistivity σ, whereas if ϕ is uncertain it will impact both ρ_f and K_f. For each quantity ξ one can consider that it can be separated into an average component $\bar{\xi}$ and a deviation $\Delta\xi$. Paper B presents the different expressions of ΔZ_F for the different cases and these are recalled in Table 4.1.

Table 4.1 – Different expressions for Z_F, corresponding to equations (7) to (10) in Paper B

Varying parameter(s)	**Expression for $\boldsymbol{\Delta Z_F}$**
ρ_f	$\mathrm{j}\omega \cos\theta d \Delta\rho_f$
K_f	$\mathrm{j}\omega \cos\theta d Z_b^2 \frac{\Delta K_f}{\bar{K}_f^2}$
ρ_f and K_f	$\mathrm{j}\omega \cos\theta d \left(\Delta\rho_f - Z_B^2 \frac{\Delta K_f}{\bar{K}_f^2}\right)$
d	$\mathrm{j}\omega \cos\theta \left(\rho_f - Z_b^2 K_f^{-1}\right) \Delta d$

Once the deviation ΔZ_F is known it is straightforward to determine Z_s and the reflection and absorption coefficients:

$$R = \underbrace{\frac{\bar{Z}_s - Z_0}{\bar{Z}_s + Z_0}}_{\bar{R}} \left(1 + \underbrace{\frac{2Z_0 \Delta Z_s}{\bar{Z}_s^2 - Z_0^2}}_{\eta}\right), \qquad \alpha = 1 - |\bar{R}|^2 |1 + \eta|^2 \tag{4.4}$$

4.2 Validation and applications

Paper B discusses a number of cases to demonstrate the possibilities of the approach using either numerical Monte Carlo results or experimental data as reference. In this section, only two of the examples are presented. A first numerical application uses the current approach to generate a response envelope that is compared to Monte Carlo results. A second example based on experimental data[1] is then introduced to demonstrate the potential of the method to generate an envelope based on a pre-existing response. These two cases are completed with additional applications in Paper B.

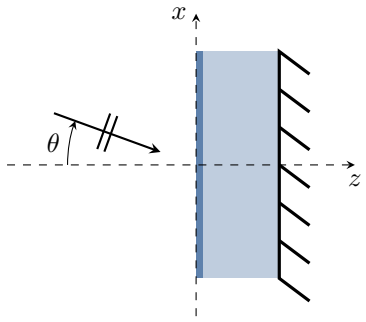

Figure 4.4 – One of the systems used for numerical validation. A film (dark shade) is placed on a layer of PEM (light shade) bonded onto a rigid backing.

In the first case, a film is placed over a poroelastic layer and a rigid backing such as in Figure 4.4. The physical parameters for the media are gathered in the Table 1 of Paper B (see p.82). For two different films and angles, absorption coefficient envelopes are computed with the proposed approach for different deviations of the flow resistivity:

$$\sigma = \bar{\sigma} + n\mathrm{std}(\sigma), \qquad n = 1, 2, 3 \tag{4.5}$$

The results are compared to Monte Carlo simulations for which all samples are drawn from a normal distribution $\mathcal{N}(\bar{\sigma}, \mathrm{std}(\sigma))$. For both bases, the standard deviation $\mathrm{std}(\sigma)$ is set to 10% of the average value $\bar{\sigma}$. The different possible values of the multiplier n allow to reach different confidence intervals. The results are shown in Figure 4.5.

In the paper and by extension in the present section, the results are either presented as an absorption coefficient or as a so-called centred envelope. In the latter case, the mean value of the quantity to represent is subtracted to the data, leading to a zero-centred representation indicating the spread of the envelope with respect to frequency.

In this figure, both the absorption coefficient and the centred envelopes are plotted, the latter allowing to check the amplitude of the envelope. An interesting aspect is that the $n = 1$ curve follow closely the Monte Carlo standard deviation envelope. Similarly the $n = 3$ envelope corresponding to the 99.7% confidence interval stays close to the extremal response envelopes and no complete outlier

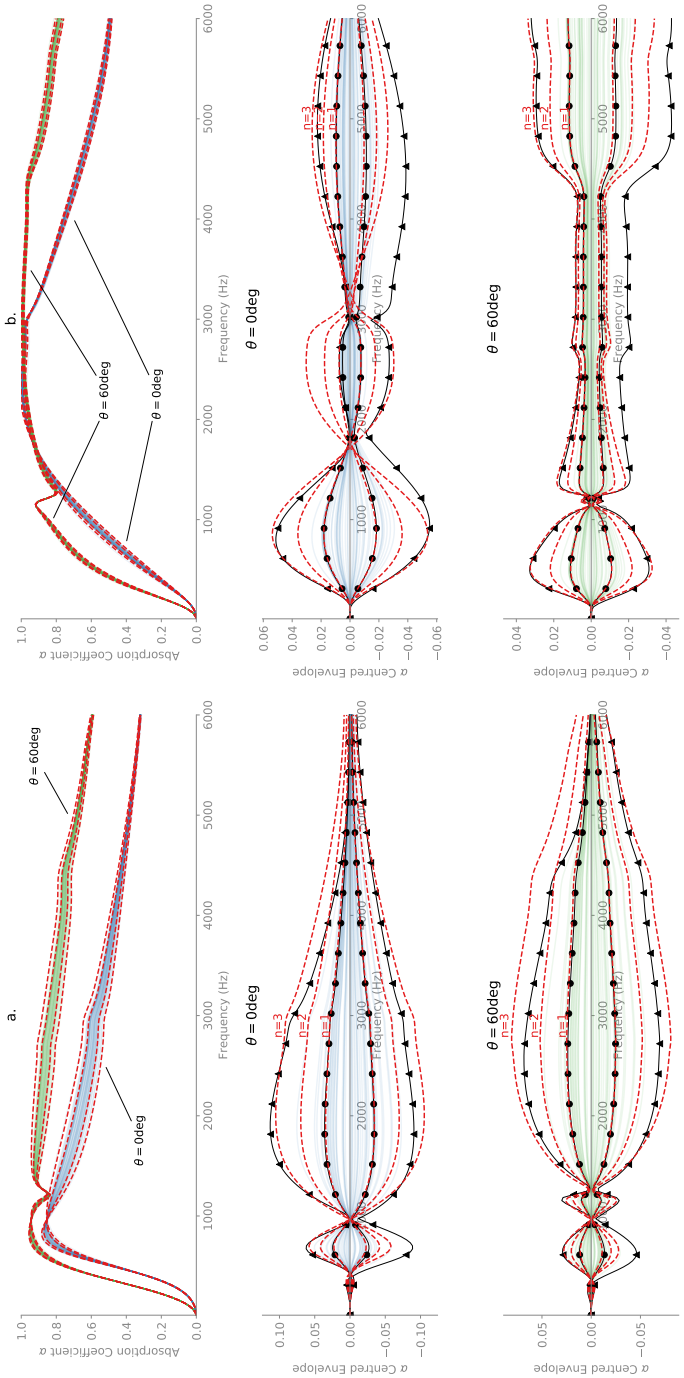

Figure 4.5 – Comparison between Monte Carlo envelopes (realisations in blue/green, realisation-wise standard deviation envelope with bullets • and extremal envelopes with triangles ▲) and envelopes from the proposed method (dashed red, n being the multiplier to the standard deviation of the varying parameter). Absorption coefficient (two top most axes) and centred envelopes (four lower axes) for two films (**a.** non-woven, **b.** woven) and two angles of incidence (0 in blue and 60 deg in green).

is observed. Despite the rather aggressive approximation strategy, the envelopes provided by the presented techniques are plausible for the different angles and over the whole frequency band.

A second test based on experimental measurements of the response of a screen and melamine system with a rigid backing in an impedance tube. The responses for twenty samples of film on the same PEM are measured. In order to use the proposed technique and generate the envelope. One might need to access Z_B which, in this case, is not directly measured. A possible approach is then to use the impedance translation formula backwards and obtain a value from Z_B from a measurement of Z_s. The parameters of the film used for the impedance translation are the average characterised values. The results for two different screens (woven and non-woven) are presented in Figure 4.6 and the physical properties of the media can be found in Table 2 from the paper (p. 87). This time, the results from the proposed approach are compared to naive solutions consisting in generating one maximal (resp. minimal) response using the maximum (resp. minimum) value of the varying parameter.

In Figure 4.6, it is seen that the envelopes generated by the proposed approach for $n = 1$ follows closely the empirical results and particularly the standard deviation envelope.

4.3 Concluding remarks

Despite its simplicity, the proposed model allows to efficiently merge statistical characterisation data for films and deterministic responses from systems into sensible response envelopes. It should be noted that the resulting envelopes come at the price of some simplifications and assumptions and might not be suitable for an in-depth analysis of uncertainties. Other techniques such as polynomial chaos approaches might be used to better quantify the effect of the uncertainties.

Another interesting point of the presented contribution is that it allowed to generate an extensive dataset of impedance tube traces and associated characterisations for a rather large number of samples of two different acoustic films. This dataset has been made available to the community as an independent, citable entry and can be reused for further investigation[1].

A last aspect is worth noting. Observing all the envelope curves, both experimental and simulated, one easily spots a set of constrictions of the envelopes i.e. points where the uncertainties have no influence. The authors have contemplated the idea of investigating what could cause such an effect and what determines the frequency of the constrictions.

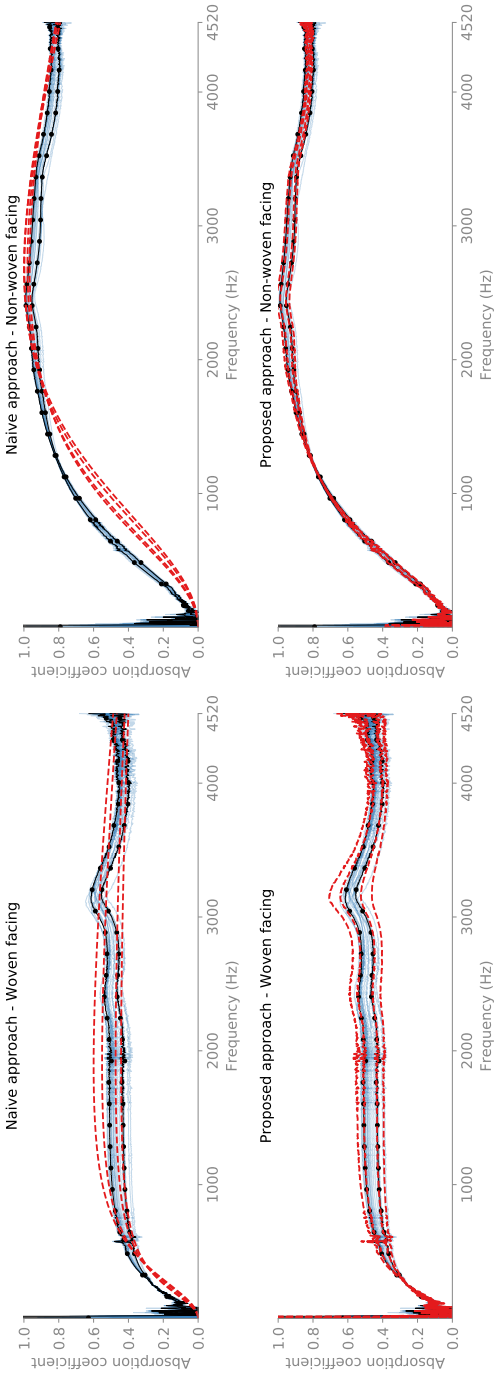

Figure 4.6 – Case of a melamine backing. Comparison of envelopes (in dashed red) generated from the system trace and proposed approach (bottom) and envelopes generated using the JCA characterisation of the backing and the film (top). For a woven film (left) and a non-woven (right). The blue light traces are sample responses and the black curve with bullets • is the standard deviation envelope.

Chapter 5

Coupling TMM and FEM for meta-poroelastic systems

As said in the introduction, poroelastic media have the ability to absorb over a large band but their effectiveness at low frequencies is limited by the total thickness. In an attempt to overcome this limitation, different solutions have been proposed such as double-porosity[60,61] or meta-poroelastic media[62]. This last option consist in embedding arrays of diffractors or resonators inside a poroelastic matrix. The usual way to analyse such media is to consider one of the repeated sections, thus defining a so-called unit cell[62]. Examples of unit cells from the literature[20,21,23,24,63] are shown in Figure 5.1. Additionally, attempts to use optimisation techniques to come up with promising architectures have also been investigated[25].

To control the response even further or anticipate real-life cases, facings might then be added to the meta-poroelastic panels. This is used to trigger a different kind of coupling between the surrounding air and the matrix (for example with an elastic layer) or simply to alter and tune the response[26].

When it comes to numerical evaluation, different methods have been used. Among others, one can cite the homogenisation approach[20] that allows to derive the properties of an equivalent medium from the topology of the unit cell, or the Multiple Scattering Theory[22,64] that accounts for the diffraction due to each element of the array. Both of these methods have been extensively used and give either analytical or semi-analytical results. Even though such methods could potentially be used to evaluate the response of any system, it might be particularly difficult to actually write the relevant relations and solve the problem. On the other hand, the versatility of FEM allows to cope with arbitrarily intricate core and inclusion designs. The key issue of the approach being to accurately account for thin coating layers that might force the mesh refinement up. Indeed, these tend to require several elements through the thickness and to avoid distortion of the mesh, it tends to impact the size of the elements surrounding the thin part as well. An example of such an effect is shown in Figure 5.2 where the elements besides the inserted thin

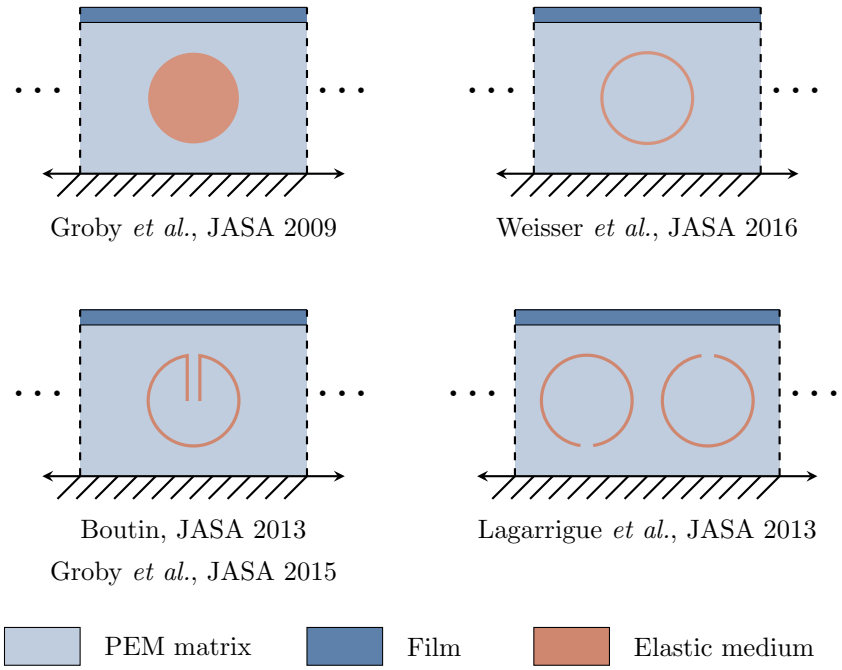

Figure 5.1 – Examples of unit cell from meta-poroelastic systems.

layer gradually get bigger as the distance to the film surface increases.

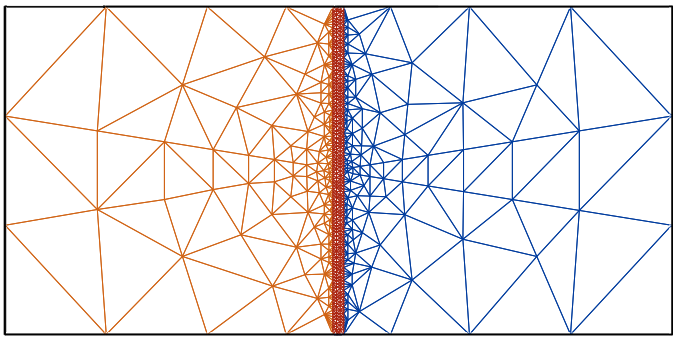

Figure 5.2 – A thin layer meshed in red with 3 elements in the thickness is inserted between two large domains. The mesh refinement in the surrounding domains is driven up to cope with the element size in the thin layer.

To overcome the mesh refinement issues, Paper C proposes a hybrid strategy to embed a mesh-less representation of the fields into a FEM linear system describing

an arbitrarily complex core.

5.1 Coupling strategy

The contribution is based on the idea of rewriting the boundary operator from the Finite Element model of the core in order to correctly account for the load applied through the coating layers. The chosen system is shown in Figure 5.3 where these two areas, poroelastic core and coatings, can be identified. In the case studied in Paper C, the coating is composed of only one layer of elastic medium and the part of the core in contact with the said coating is made of poroelastic medium. This setting allows to present the most important points of the derivation in Paper C while keeping reasonably concise expressions. The method can be easily extended to other types of core and coatings, even though it might require a few adjustments[65]. The system represented in Figure 5.3 is a single unit cell of width D that is repeated to form the whole medium. In the case of Paper C, the repetition is done through the use of periodic boundary conditions on the FEM domain.

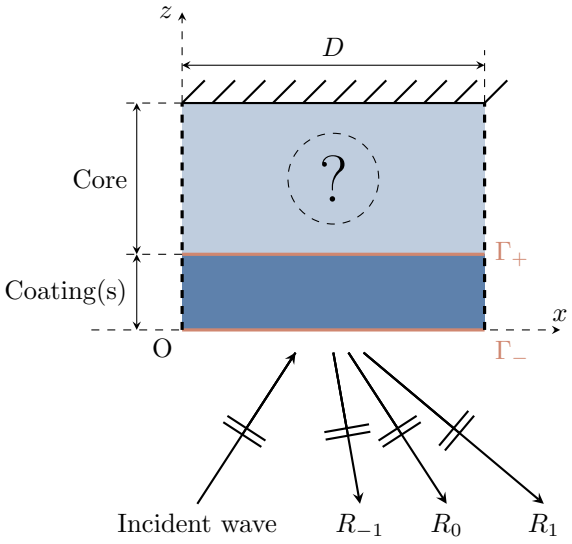

Figure 5.3 – System under study, a possibly complex core is lined with a flat coating on its free surface. The system is of size D and periodic along the x-axis. The two interfaces Γ_- and Γ_+ are central to the proposed approach as they separate key domains of the problem.

In the light of these elements, the proposed procedure goes as follow. First, taking advantage of the periodicity of the system, the fields in the incident medium and coating are rewritten as a sum of Bloch waves. The matching conditions

between the fields in air and in the coating is made in a Bloch mode-oriented approach and each of these components is propagated through the coating using a separate transfer matrix. The different Bloch components of the fields in the layer are included in the FEM domain using the boundary conditions and replacing the expression in the relevant boundary operator. Finally, to balance the system, the fields are projected on the different Bloch components. A complete exposition of these various steps follows.

As said, the periodicity allows to write the fields in the incident medium as a sum of Bloch waves. For the pressure field, one obtains:

$$p^a(\boldsymbol{r}) = \sum_{l\in\mathbb{Z}} \left[\delta_{0l} e^{-\mathrm{j}k_z^l z} + R_l e^{+\mathrm{j}k_z^l z}\right] e^{-\mathrm{j}k_x^l x} \tag{5.1}$$

where δ_{0l} is the Kronecker symbol, R_l are the complex-valued reflection coefficients for each wave l and k_x^i, k_x^l and k_z^l are respectively the incident and Bloch reflected wavenumbers along x and z axis depending on the index. While k_x^i is imposed by the excitation, k_x^l and k_z^l on the other hand are defined by the Bloch theorem such that

$$k_x^l = k_x^i + \frac{2\pi l}{D}, \qquad k_z^l = \sqrt{\left(\frac{\omega}{c}\right)^2 - \left(k_x^l\right)^2} \tag{5.2}$$

where c is the speed of sound in the incident medium.

As Paper C uses the example of an elastic coating, the first interface relations link air from the incident medium to the fields in the coating. Mathematically, this translates into the continuity of normal displacements (u^a for the incident medium, u_z^e for the elastic coating) and compression stresses (p^a and σ_{zz}^e). It also requires enforcing null shear stresses along the surface of the coating σ_{zx}^e. Formally, this reads:

$$\sigma_{zx}^e = 0, \qquad \sigma_{zz} = -p^a, \qquad u_z^e = u_z^a, \qquad u_x^e \text{ unknown} \qquad \text{along } \Gamma_-. \tag{5.3}$$

Note that in the present case, the tangential component of the displacement field u_x^e remains unconstrained by the interface relations and thus must be considered an additional unknown of the final system.

In order to cross the first interface Γ_-, it is proposed in Paper C to take advantage of the completeness of the basis of Bloch waves and to decompose all the fields in the coating. Each field ξ (including u_x^e) is then replaced by the following expression along Γ_- and Γ_+:

$$\xi(x, z_\pm) = \sum_{l\in\mathbb{Z}} \xi^l(z_\pm) e^{\mathrm{j}k_x^l x}. \tag{5.4}$$

To rewrite the interface relations (5.3) in terms of Bloch waves one must also determine the expansion of the incident displacement field using the momentum

conservation equation, see equations (4) and (5) in Paper C. To use a transfer matrix approach to transfer each of the fields from Γ_- to Γ_+ within the coating, they are gathered in a vector which for an elastic coating reads:

$$\boldsymbol{s}_l^{\pm} = \{u_x^{e,l}(z_\pm),\ u_z^{e,l}(z_\pm),\ \sigma_{zx}^{e,l}(z_\pm),\ \sigma_{zz}^{e,l}(z_\pm)\}^T \tag{5.5}$$

and using the expansions for the different fields and the interface relations (5.3), it comes:

$$\boldsymbol{s}_l^- = \boldsymbol{e}^- \delta_{0l} + \boldsymbol{I}_l^- \boldsymbol{q}_l, \quad \forall l \in \mathbb{Z} \tag{5.6}$$

where the expressions of the quantities $\boldsymbol{e}^-$ and $\boldsymbol{I}_l^-$ are detailed in equation (12) from the original paper. In this expression, $\boldsymbol{e}^-$ describes the contribution of the incident wave and specular reflection ($l = 0$) on the fields in the coating and $\boldsymbol{I}^-$ is the actual interface matrix that indicates the coupling between the coating and the other reflected Bloch modes. Finally, $\boldsymbol{q}_l$ is the vector of unknown coefficients for each Bloch wave i.e. the reflection coefficient and any field left unknown within the coating. Note that for some cases, such as a fluid or and equivalent fluid[19] coating, $\boldsymbol{q}_l$ is not a vector but simply a scalar whereas for others facings, such as poroelastic media, $\boldsymbol{q}_l$ will involve several fields[65].

Having successfully transferred the incident fields to the coating, one then uses a transfer matrix approach to obtain the expression of the expanded fields on the other side of the coatings, along Γ_+. It is of prime importance to understand that the transfer matrices cannot propagate all modes at once. A different matrix $\boldsymbol{T}_l$ has to be used for each Bloch wavenumber k_x^l. Each of the components $\boldsymbol{s}_l^-$ of the overall vector has to be transferred using the corresponding matrix in order to determine the corresponding $\boldsymbol{s}_l^+$:

$$\boldsymbol{s}_l^+ = \boldsymbol{T}_l \boldsymbol{S}_l^- . \tag{5.7}$$

The expressions of these matrices for different coatings and how to construct in the case of multilayer facings are to be found in Section 2.2 or in the literature[19,48].

The vector $\boldsymbol{s}_l^+$ can be formally written as $\boldsymbol{s}^l$ in (5.6) using the transfer matrices such that:

$$\boldsymbol{s}_l^+ = \boldsymbol{e}^+ \delta_{0l} + \boldsymbol{I}_l^+ \boldsymbol{q}_l, \quad \text{with } \boldsymbol{e}^+ = \boldsymbol{T}_0 \boldsymbol{e}^- \quad \text{and} \quad \boldsymbol{I}_l^+ = \boldsymbol{T}_l \boldsymbol{I}_l^- . \tag{5.8}$$

Once this vector is determined, the fields must be injected into the FEM formulation for the core.

As said in the introduction, one of the assumption is that the part of the core in contact with the coating is only PEM. From a FEM viewpoint, different strategies exists to represent PEM[66–68]. In Paper C, a mixed pressure-displacement formulation that naturally couples with elastic media[67] is selected, mostly to keep the

mathematical expressions concise. It can be shown without difficulties that the approach is valid for other formulations[65]. The weak form of this formulation[67] uses the interstitial pressure p and the solid displacement $\boldsymbol{u}^s$ as primary variables, i.e. fields to be solved for. The corresponding secondary variables, used in the boundary operator, are the total stress tensor $\underline{\underline{\sigma}}^t$ and the relative fluid/solid displacement $\boldsymbol{w}$. While the complete expression of the weak form is beyond the scope of the present work and can be found in the literature[67], the expression of the boundary operator $\mathcal{I}$ is of importance:

$$\mathcal{I} = \int_{\Gamma_+} \delta\boldsymbol{u}^s \cdot [\underline{\underline{\sigma}}^t \cdot \boldsymbol{n}] \, \mathrm{d}\Gamma + \int_{\Gamma_+} \delta p [\boldsymbol{w} \cdot \boldsymbol{n}] \, \mathrm{d}\Gamma \tag{5.9}$$

where $\delta\boldsymbol{u}^s$ and δp are the solid displacement and pressure test fields and $\boldsymbol{n}$ is the normal to the interface.

It is trivial to identify that applying an impervious elastic layer on the surface, such as along Γ_+, will force the relative inter-phase displacement to be null and that both the stresses and solid displacement will be continuous. Paying attention to the orientation of the boundary, the following relations hold:

$$\boldsymbol{w} \cdot \boldsymbol{n} = 0, \qquad \underline{\underline{\sigma}}^t \cdot \boldsymbol{n} = -\boldsymbol{\sigma}^e, \qquad \boldsymbol{u}^s = \boldsymbol{u}^e \qquad \text{along } \Gamma_+. \tag{5.10}$$

Using the definition of $\boldsymbol{s}_+$ from equation (5.8) and substituting the corresponding interface conditions into the boundary operator yields

$$\mathcal{I} = -\int_{\Gamma^+} \left(\boldsymbol{e}^+ \Big|_{3,4} e^{-\mathrm{j}k_x^0 x} \right) \cdot \delta\boldsymbol{u}^s \, \mathrm{d}\Gamma - \sum_{l\in\mathbb{Z}} \int_{\Gamma_+} \left(\boldsymbol{I}_l^+ \Big|_{3,4} \boldsymbol{q}_l e^{-\mathrm{j}k_x^l x} \right) \cdot \delta\boldsymbol{u}^s \, \mathrm{d}\Gamma \tag{5.11}$$

where a vertical bar followed by indices (here $3,4$) indicates that only the corresponding lines of the subscripted matrix or vector are considered.

This expression of the FEM boundary operator implies once again that additional unknowns must be considered which in this context are the ones of the $\boldsymbol{q}_l$ vectors. For the problem to be well posed, additional equations should be added to balance these new variables. To this end, Paper C proposes to use the interface conditions related to the primary fields of the FEM system and project them on the Bloch waves. Taking advantage of the orthogonality of the basis of Bloch wave, one might project the continuity equation for primary field on each mode and generate additional equations to balance each of the added unknowns. In the case of Paper C:

$$\int_0^D \boldsymbol{u}^s(x, z_+) e^{jk_x^l x} \, \mathrm{d}x = D\boldsymbol{e}^+ \Big|_{1,2} \delta_{0l} + D\boldsymbol{I}_l^+ \Big|_{1,2} \boldsymbol{q}_l. \tag{5.12}$$

The last important aspect of the theoretical development of the paper is then to include equations (5.11) and (5.12) into the FEM linear system. The said system formally reads $\boldsymbol{A}\boldsymbol{x} = \boldsymbol{f}_0$, with $\boldsymbol{A}$ the global matrix, $\boldsymbol{x}$ the solution vector and $\boldsymbol{f}_0$ the

forcing vector which encompasses all forcing terms applied on the domain that cannot be represented as plane waves. Even though the whole discussion until now has been dealing with infinite series of Bloch waves they must be truncated in practice. A rule of thumb, involving the frequency, the size of the cell and the incident tangential wavenumber, was devised based on previous numerical experiments.[22,69,70] It is provided in equation (24) of Paper C and indicates a number N of positive/negative modes to keep. The truncated series then span over $2N+1$ possible values of l and it is possible to include it in the FEM domain through equations (5.11) and (5.12).

The final linear system writes:

$$\begin{bmatrix} \boldsymbol{A} & \boldsymbol{C} \\ \boldsymbol{C}' & \boldsymbol{A}' \end{bmatrix} \begin{Bmatrix} \boldsymbol{x} \\ \boldsymbol{q} \end{Bmatrix} = \begin{Bmatrix} \boldsymbol{f} \\ \boldsymbol{f}' \end{Bmatrix} + \begin{Bmatrix} \boldsymbol{f_0} \\ \boldsymbol{0} \end{Bmatrix} \tag{5.13}$$

where $\boldsymbol{f}$ and $\boldsymbol{C}$ come from discretising the first and second terms of (5.11) and $\boldsymbol{C}'$, $\boldsymbol{f}'$ and $\boldsymbol{A}'$ come from (5.12) (left hand side for the first one and right hand side for the others). Note that $\boldsymbol{q}$ is a vector gathering all the $\boldsymbol{q}_l$, thus containing all the added unknowns.

This final system can then be solved so as to retrieve the FEM solution vector as well as the reflections coefficients R_l for each wave and all the unconstrained fields.

It must be stressed that even though the technique is presented for a coating composed of a single elastic layer and on a reflection problem, it can be extended to more general cases. The first kind of extension would be to consider a transmission problem. From a FEM point of view, it simply changes the boundary operator along another boundary and the same approach can be used to couple with the TMM and the surrounding medium. From a Transfer Matrix point of view, the same Bloch expansion can be written and a very similar development will follow without the excitation term. Obviously, new variables will have to be added to the solution vector and the associated matrices to the global operator.

Another possible extension consists in dealing with more complicated coatings, possibly involving multiple layers. Once again, adapting the method is rather straightforward as the propagation through the coating is accounted for through the $\boldsymbol{T}_l$ matrices only. An important note though is that other fields might potentially be unknown at some of the interfaces such as the tangential displacement in this case which implies adding them to the corresponding $\boldsymbol{q}_l$.

5.2 Validation and results

In order to validate the approach and demonstrate its potential Paper C includes a number of experiments. The validation process involves three different reference methods: TMM for a sanity check on a case with no inclusion, Multiple Scattering Theory for examples of periodic media, and FEM for more complex cases. All these examples are presented in section 3 of the original paper.

In the present section, only two examples are discussed: an illustration of the advantages of the method compared to a pure FEM approach and a comparison with a state-of-the-art method used in the meta-materials community.

The first of the examples compares the proposed approach to a pure FEM solution on a simple three-layers system. The model is presented in Figure 5.4.a.

The test is performed as follows: a FEM solution is set-up and prepared so as to be fully converged at 1000 Hz with both coatings and the core meshed. Without changing the number of the elements in the core, both coatings are removed from the FEM domain and instead represented with the proposed method. The two solutions as well as a TMM reference are computed from 10 Hz to 5 kHz and are plotted in Figure 5.5.

This figure illustrates one of the advantages of the proposed approach. The reason why the precision drops for the FEM solution is that as the frequency increases, the wavelength reaches the same order of magnitude as the thickness of the film. At this point, the FEM mesh is not refined enough to deal with the phenomena taking place in the coatings. On the other hand, the proposed approach is not impaired by such effects as the coatings are represented with the same precision as for the pure TMM reference.

Another example compares the results of the hybrid method and results from the Multiple Scattering theory. This technique is a semi-analytical approach, possibly leading to an excellent precision. In this example, two different systems are considered, both featuring an inclusion, presented in Figure 5.4.b and Figure 5.4.c.

The results are shown in Figure 5.6. It appears clearly on the figure that both methods give very similar results. The proposed approach has the advantage over existing techniques that it benefits from the versatility of FEM without the need for an over-refined mesh to cope with the thin facings.

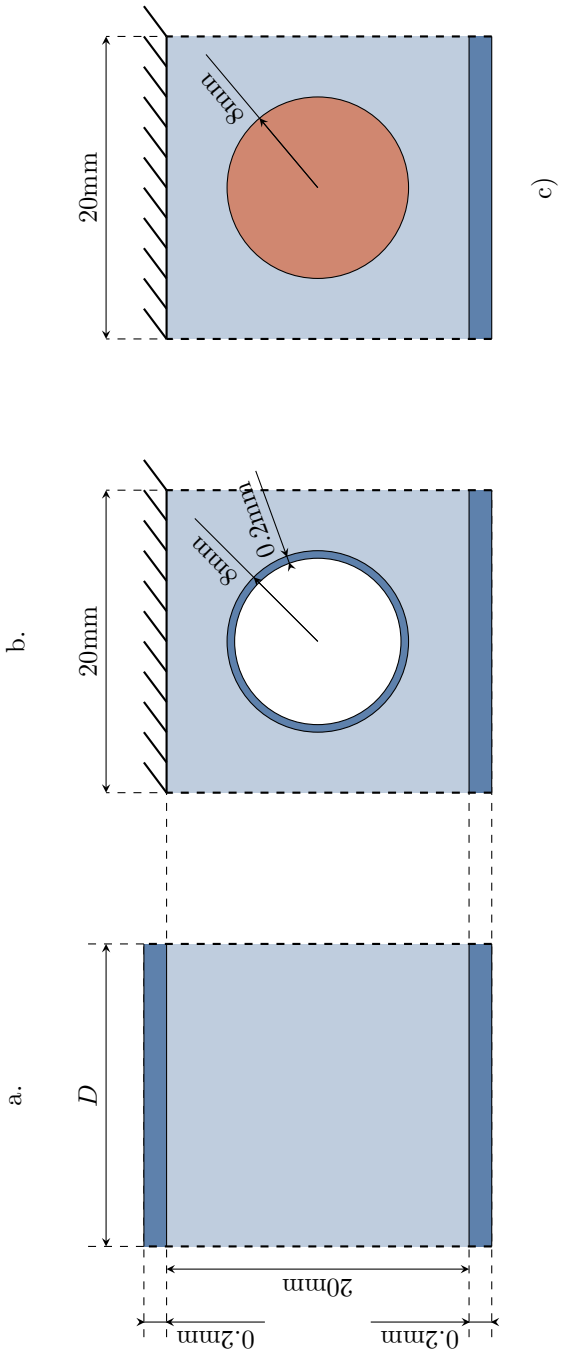

Figure 5.4 – Different configurations used in the applications, coatings are always rubber. **a.** poroelastic core and transmission setting; **b.** with an air-filled rubber shell inclusion; **c.** with a poroelastic inclusion

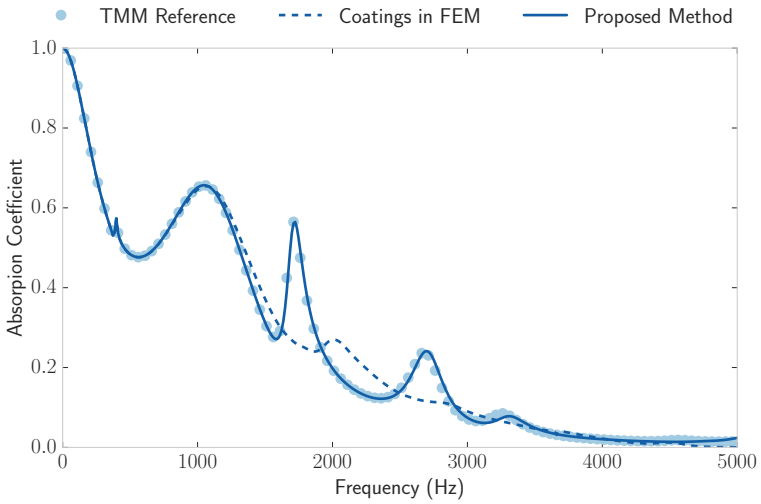

Figure 5.5 – Comparison of the absorption coefficient computed using TMM (circle markers), the proposed method (solid line) or including the coatings in a Finite Element model (dashed line). The number of elements in the core is the same for the two last methods, chosen such as one of them cat least complies with the reference.

5.3 Perspectives

The approach presented in this contribution is promising in a number of ways. First, by separating the facings from the core and resorting to a mesh-less approach for representing the surface layers, the method has a much lower computational overload than pure FEM.

Second, the technique can easily be adapted to account for a FEM domain up- and downstream of the (multi-)layered zone. This change brings the proposed approach closer to other techniques for coupling FEM domains in the literature[71], the method presented here having the advantage that it does not require conformal meshes on both sides of the modelled layer.

Finally, note that the coupling between the core-related FEM linear system and the added unknowns and equations is rather weak. Without reassembling the FEM system, it is then possible to change the surface layers at a reduced cost. This paves the way to explore the effects of statistical variability of the surface layers or even to quickly test different facings over the same core and guide design decisions.

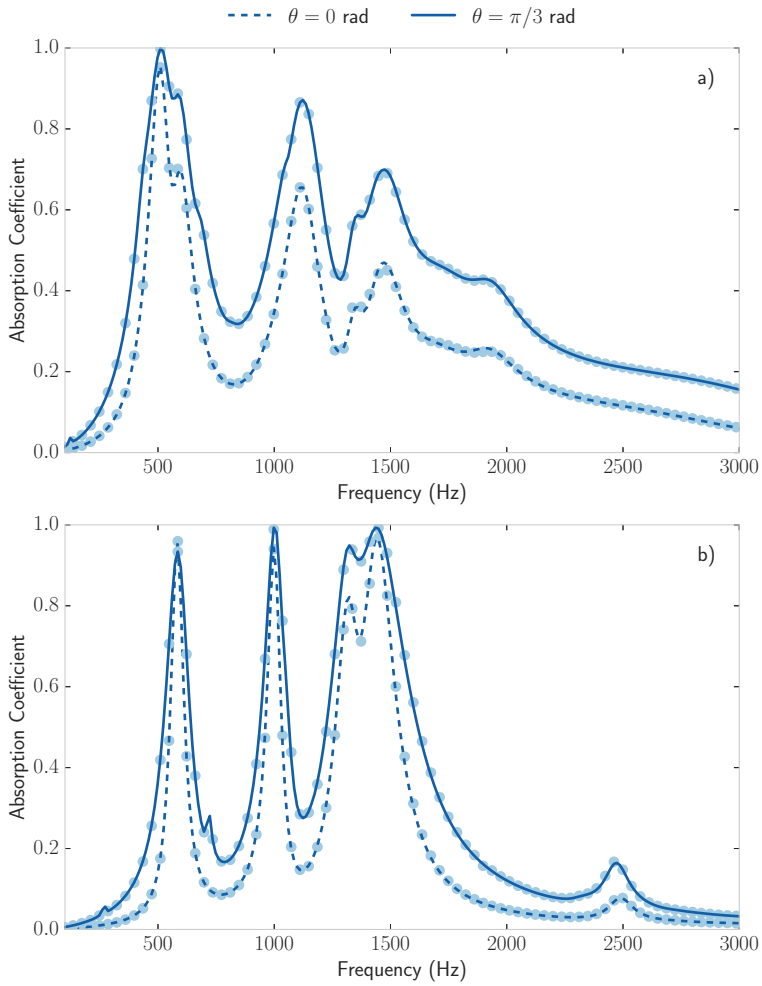

Figure 5.6 – Absorption coefficient for two meta porous panels bonded on a rigid backing with a) an air-filled rubber shell or b) a poroelastic circular inclusion. The panels are coated with rubber and excited by a plane wave for two different incidence angles $\theta = 0\,\text{rad}$ (dashed) and $\theta = \pi/3\,\text{rad}$ (solid). Results from the Multiple Scattering Theory are used as reference and shown with circle markers.

Chapter 6

Conclusion

In the present summary, three works and a correction were presented, discussing different aspects of the modelling of acoustic screens, films and interfaces. Over the course of the PhD project, the focus has always been to devise efficient approaches to account for films, interfaces and their associated uncertainties both from a numerical and physical viewpoint.

6.1 Key aspects

Paper A presents a simplified model for screens, stressing that some of the interactions predicted by Biot's theory do not play a role in these media. The associated investigation shows, on the other hand, that preserving shear effects is crucial to correctly account for the load applied by the film on the backing system.

Paper B introduces a strategy to obtain response envelopes with a minimal effort from the statistical characterisation of the parameters and a deterministic system response. With this simplifying approach to express the effect of the film on the response and then by separating the contribution of the uncertainties from the average value, this contribution offers a cost-efficient solution to generate response envelopes. From an engineering point of view it also presents a number of advantages, particularly as it decouples the determination of the spread of the films parameters from the generation of the actual envelope.

Paper C finally renders computing the response of meta-poroelastic systems more efficient by extracting the components that could drive the mesh refinement up. This approach can be combined with different techniques to evaluate the effect of film uncertainties on the overall response without having to re-assemble the whole FEM system. Even though it was not explicitly exploited here, this option is a straightforward extension of the published work. In addition to the paper itself, a talk at the French-Chinese Acoustics Congress presented an adaptation of the formulation for various media, including the screen model from paper A.

One might note that this thesis gathers contributions centred on the techniques, providing validation cases but no lengthy application sections. During the PhD project, it was decided to explore different approaches and methods, knowing that some of these would not be ready for publication before the end. Therefore, the work was focused on releasing usable techniques related to different aspects of the modelling and computation fast so they can be used and improved by more teams over time. Other projects and ideas than the ones presented in this document were also investigated and are yet to be developed.

Keeping in mind that research should be reproducible, all software components, scripts and utilities used in the papers are freely available on-line or on demand. Particularly, the two main software packages, PLANES[72] and PyMLS,[56] can be downloaded on Github [a] under licenses that allow re-utilisation, modification and even redistribution.

6.2 Outlooks

A number of aspects related to films, screens and interfaces are left to explore.

Amongst other things, the precise description of interface zones appears an important milestone for future absorbers. A better understanding of their properties and how to tune them would make it possible to use these inevitable by-products of the assembly process as actual component of future absorbers. Indeed, in some cases, such as a very stiff but non-continuous layer of glue, the interface might trigger specific dynamic phenomena[19,73], possibly random, both in terms of parameters and of spatial localisation. In order to further the description of interface zones, it is necessary to gather more information and data and, in turns, this imply developing suitable *in-situ* measurement and characterisation techniques.

The concept of interface extends far beyond a physical element present between two given domains and encompasses as well the local change of boundary condition along the frontier between different media. Particularly, its has been established that the type of bonding between poroelastic media had a lot of influence on the response[19]. Depending on the bonding strategy, the whole surface of the interface is not necessarily governed by the same continuity conditions (due to debonding for instance) and the description and modelling of such cases is still undone.

Films and interfaces have been shown to be subject to uncertainties linked both to the production or creation process and to imprecisions in the characterisation. Even though techniques exist to quantify the effect of uncertainties, the complexity of poroelastic models and the number of components used in modern absorbers makes them challenging to use. While first thoughts are presented in the thesis or were introduced in conferences[74], an effort to develop uncertainty quantification approaches tailored to poroelastic and meta-poroelastic media is in order. To a certain extent, canonical techniques from the uncertainty quantification framework such as polynomial chaos[75,76] or Karhunen-Loève[77] expansions might be used but

a. github.com/OlivierDAZEL/PLANES and github.com/cpplanes/pymls

the intricate mathematical models at play with poroelastic media poses a formidable challenge.

Bibliography

[1] M. Gaborit et al. Statistical Characterisation and Responses of Acoustics Screens and Two-Layers Systems. 2, 2019. DOI: 10.5281/zenodo.3358921.

[2] C. Eriksson et al. Environmental Noise and Health: Current Knowledge and Research Needs. 6553. Stockholm: Swedish Environmental Protection Agency, 2013.

[3] G. Bluhm, E. Nordling, and N. Berglind. Road Traffic Noise and Annoyance–an Increasing Environmental Health Problem. *Noise & Health*, 6 (**24**), 2004, pp. 43–49. pmid: 15703140.

[4] D. J. M. Houthuijs et al. Health Implication of Road, Railway and Aircraft Noise in the European Union: Provisional Results Based on the 2nd Round of Noise Mapping. RIVM Report 2014-0130. The Netherlands: National Institute for Public Health and the Envrionment, 2014.

[5] K. Hume, M. Brink, and M. Basner. Effects of Environmental Noise on Sleep. *Noise and Health*, 14 (**61**), 2012, pp. 297–302. DOI: 10.4103/1463-1741.104897.

[6] World Health Organization. Night Noise Guidelines for Europe. Ed. by C. Hurtley. Copenhagen, Denmark: World Health Organization Europe, 2009. 162 pp.

[7] W. Babisch. The Noise/Stress Concept, Risk Assessment and Research Needs. *Noise & Health*, 4 (**16**), 2002, pp. 1–11. pmid: 12537836.

[8] M. E. Beutel et al. Noise Annoyance Is Associated with Depression and Anxiety in the General Population- The Contribution of Aircraft Noise. *PLOS ONE*, 11 (**5**), 19, 2016. Ed. by M. A. Andrade-Navarro, e0155357. DOI: 10.1371/journal.pone.0155357.

[9] World Health Organisation. Burden of Disease from Environmental Noise: Quantification of Healthy Life Years Lost in Europe. Ed. by F. Theakston. Copenhagen, Denmark: World Health Organization Europe, 2011. 106 pp.

[10] The European Parliament. Directive 2002/49/EC of the European Parliament and of the Council of 25 June 2002 Relating to the Assessment and Management of Environmental Noise. *Official Journal of the European Communities*, L189, 25, 2002, pp. 12–25.

[11] The European Parliament. Regulation (EU) No 540/2014 of the European Parliament and of the Council of 16 April 2014 on the Sound Level of Motor Vehicles and of Replacement Silencing Systems, and Amending Directive 2007/46/EC and Repealing Directive 70/157/EEC. *Official Journal of the European Communities*, L158, 16, 2014, pp. 131–195.

[12] ISO. ISO 9053-1 - Acoustics - Determination of Airflow Resistance - Static Airflow Method. 2018.

[13] L. Jaouen and F.-X. Bécot. Acoustical Characterization of Perforated Facings. *The Journal of the Acoustical Society of America*, 129 (**3**), 2011, pp. 1400–1406. DOI: 10.1121/1.3552887.

[14] J.-D. Chazot, E. Zhang, and J. Antoni. Acoustical and Mechanical Characterization of Poroelastic Materials Using a Bayesian Approach. *The Journal of the Acoustical Society of America*, 131 (**6**), 2012, pp. 4584–4595.

[15] O. Doutres et al. Evaluation of the Acoustic and Non-Acoustic Properties of Sound Absorbing Materials Using a Three-Microphone Impedance Tube. *Applied Acoustics*, 71 (**6**), 2010, pp. 506–509. DOI: 10.1016/j.apacoust.2010.01.007.

[16] T. Iwase, Y. Izumi, and R. Kawabata. A New Measuring Method for Sound Propagation Constant by Using Sound Tube without Any Air Spaces Back of a Test Material. *INTER-NOISE and NOISE-CON Congress and Conference Proceedings*. Vol. 1998. 1998, pp. 1265–1268.

[17] M. Niskanen et al. Deterministic and Statistical Characterization of Rigid Frame Porous Materials from Impedance Tube Measurements. *The Journal of the Acoustical Society of America*, 142 (**4**), 2017, pp. 2407–2418. DOI: 10.1121/1.5008742.

[18] F. Pompoli et al. How Reproducible Is the Acoustical Characterization of Porous Media? *The Journal of the Acoustical Society of America*, 141 (**2**), 2017, pp. 945–955.

[19] J.-F. Allard and N. Atalla. Propagation of Sound in Porous Media: Modelling Sound Absorbing Materials. 2nd. Hoboken, N.J: Wiley, 2009. 358 pp.

[20] C. Boutin. Acoustics of Porous Media with Inner Resonators. *The Journal of the Acoustical Society of America*, 134 (**6**), 2013, pp. 4717–4729. DOI: 10.1121/1.4824965.

[21] J.-P. Groby et al. Acoustic Response of a Rigid-Frame Porous Medium Plate with a Periodic Set of Inclusions. *The Journal of the Acoustical Society of America*, 126 (**2**), 2009, pp. 685–693. DOI: 10.1121/1.3158936.

[22] J.-P. Groby, A. Wirgin, and E. Ogam. Acoustic Response of a Periodic Distribution of Macroscopic Inclusions within a Rigid Frame Porous Plate. *Waves in Random and Complex Media*, 18 (**3**), 2008, pp. 409–433. DOI: 10.1080/17455030802061300.

[23] C. Lagarrigue et al. Absorption of Sound by Porous Layers with Embedded Periodic Arrays of Resonant Inclusions. *The Journal of the Acoustical Society of America*, 134 (**6**), 2013, pp. 4670–4680. DOI: 10.1121/1.4824843.

[24] T. Weisser et al. Acoustic Behavior of a Rigidly Backed Poroelastic Layer with Periodic Resonant Inclusions by a Multiple Scattering Approach. *The Journal of the Acoustical Society of America*, 139 (**2**), 2016, pp. 617–629. DOI: 10.1121/1.4940669.

[25] C. Lagarrigue et al. Design of Metaporous Supercells by Genetic Algorithm for Absorption Optimization on a Wide Frequency Band. *Applied Acoustics*, 102, 2016, pp. 49–54. DOI: 10.1016/j.apacoust.2015.09.011.

[26] F. Chevillotte. Controlling Sound Absorption by an Upstream Resistive Layer. *Applied Acoustics*, 73 (**1**), 2012, pp. 56–60. DOI: 10.1016/j.apacoust.2011.07.005.

[27] N. Atalla and F. Sgard. Modeling of Perforated Plates and Screens Using Rigid Frame Porous Models. *Journal of Sound and Vibration*, 303 (**1-2**), 2007, pp. 195–208. DOI: 10.1016/j.jsv.2007.01.012.

[28] A. D. Pierce. Acoustics: An Introduction to Its Physical Principles and Applications. 1989th ed. Woodbury, N.Y: Acoustical Society of America, 1989. 678 pp.

[29] M. Gaborit et al. Coupling of Finite Element and Plane Waves Discontinuous Galerkin Methods for Time-Harmonic Problems. *International Journal for Numerical Methods in Engineering*, 116 (**7**), 16, 2018, pp. 487–503. DOI: 10.1002/nme.5933.

[30] M. Niskanen et al. Estimating the Material Parameters of an Inhomogeneous Poroelastic Plate from Ultrasonic Measurements in Water. *The Journal of the Acoustical Society of America*, 146 (**4**), 2019, pp. 2596–2607. DOI: 10.1121/1.5129369.

[31] C. Zwikker and C. Kosten. Sound Absorbing Materials. Elsevier Publishing Company, 1949.

[32] M. E. Delany and E. N. Bazley. Acoustical Properties of Fibrous Absorbent Materials. *Applied acoustics*, 3 (**2**), 1970, pp. 105–116.

[33] Y. Miki. Acoustical Properties of Porous Materials-Modifications of Delany-Bazley Models. *Journal of the Acoustical Society of Japan (E)*, 11 (**1**), 1990, pp. 19–24.

[34] D. L. Johnson, J. Koplik, and R. Dashen. Theory of Dynamic Permeability and Tortuosity in Fluid-Saturated Porous Media. *Journal of fluid mechanics*, 176 (**1**), 1987, pp. 379–402.

[35] Y. Champoux and J.-F. Allard. Dynamic Tortuosity and Bulk Modulus in Air-Saturated Porous Media. *Journal of Applied Physics*, 70 (**4**), 1991, p. 1975. DOI: 10.1063/1.349482.

[36] S. R. Pride, F. D. Morgan, and A. F. Gangi. Drag Forces of Porous-Medium Acoustics. *Physical Review B*, 47 (**9**), 1, 1993, pp. 4964–4978. DOI: 10.1103/PhysRevB.47.4964.

[37] D. Lafarge et al. Dynamic Compressibility of Air in Porous Structures at Audible Frequencies. *The Journal of the Acoustical Society of America*, 102 (**4**), 1997, pp. 1995–2006. DOI: S0001-4966~97!00310-X.

[38] D. Lafarge. Propagation du son dans les materiaux poreux à structure rigide satures par un fluide viscothermique. PhD. Le Mans: Université du Maine, 1993.

[39] M. A. Biot. Theory of Propagation of Elastic Waves in a Fluid-Saturated Porous Solid. *The Journal of the Acoustical Society of America*, 28 (**2**), 1956, p. 168. DOI: 10.1121/1.1908239.

[40] M. A. Biot and D. Willis. The Elastic Coefficients of the Theory of Consolidation. *Journal of Applied Mechanics*, 1957.

[41] M. A. Biot. Mechanics of Deformation and Acoustic Propagation in Porous Media. *Journal of Applied Physics*, 33 (**4**), 1962, p. 1482. DOI: 10.1063/1.1728759.

[42] O. Dazel et al. An Alternative Biot's Displacement Formulation for Porous Materials. *The Journal of the Acoustical Society of America*, 121 (**6**), 2007, p. 3509. DOI: 10.1121/1.2734482.

[43] F.-X. Bécot and L. Jaouen. An Alternative Biot's Formulation for Dissipative Porous Media with Skeleton Deformation. *The Journal of the Acoustical Society of America*, 134 (**6**), 2013, pp. 4801–4807. DOI: 10.1121/1.4826175.

[44] T. J. Plona. Observation of a Second Bulk Compressional Wave in a Porous Medium at Ultrasonic Frequencies. *Applied Physics Letters*, 36 (**4**), 15, 1980, pp. 259–261. DOI: 10.1063/1.91445.

[45] J. M. Hovem. Transmission of Sound through a Porous Disk. *Applied Physics Letters*, 39 (**8**), 15, 1981, pp. 590–591. DOI: 10.1063/1.92834.

[46] J. G. Berryman. Confirmation of Biot's Theory. *Applied Physics Letters*, 37 (**4**), 15, 1980, pp. 382–384. DOI: 10.1063/1.91951.

[47] L. Jaouen and F. Chevillotte. APMR. 2019. URL: apmr.matelys.com.

[48] O. Dazel et al. A Stable Method to Model the Acoustic Response of Multilayered Structures. *Journal of Applied Physics*, 113 (**8**), 2013, p. 083506. DOI: 10.1063/1.4790629.

[49] J. F. Allard et al. Inhomogeneous Biot Waves in Layered Media. *Journal of Applied Physics*, 66 (**6**), 1989, p. 2278. DOI: 10.1063/1.344284.

[50] J. P. Parra Martinez et al. Acoustic Analysis of Anisotropic Poroelastic Multilayered Systems. *Journal of Applied Physics*, 119 (**8**), 28, 2016, p. 084907. DOI: 10.1063/1.4942443.

[51] J. P. Parra Martinez et al. Derivation of the State Matrix for Dynamic Analysis of Linear Homogeneous Media. *The Journal of the Acoustical Society of America*, 140 (**2**), 2016, EL218–EL220. DOI: 10.1121/1.4960624.

[52] L. M. Brekhovskikh. Waves in Layered Media. Burlington: Elsevier Science, 1960.

[53] H.-Y. D. Yang. A Spectral Recursive Transformation Method for Electromagnetic Waves in Generalized Anisotropic Layered Media. *IEEE Transactions on Antennas and Propagation*, 45 (**3**), 1997, pp. 520–526.

[54] B. Brouard. Validation Par Holographie Acoustique de Nouveaux Modèles Pour La Propagation Des Ondes Dans Les Matériaux Poreux Stratifiés. 1994.

[55] Q. Serra, M. N. Ichchou, and J.-F. Deü. On the Use of Transfer Approaches to Predict the Vibroacoustic Response of Poroelastic Media. *Journal of Computational Acoustics*, 24 (**02**), 2016. DOI: 10.1142/S0218396X15500204.

[56] M. Gaborit and O. Dazel. Pymls: Multilayer Solver in Python for Acoustic Problems, 2019. DOI: 10.5281/zenodo.2558137.

[57] M. Gaborit, O. Dazel, and P. Göransson. A Simplified Model for Thin Acoustic Screens. *The Journal of the Acoustical Society of America*, 144 (**1**), 2018, EL76–EL81. DOI: 10.1121/1.5047929.

[58] L. Jaouen, A. Renault, and M. Deverge. Elastic and Damping Characterizations of Acoustical Porous Materials: Available Experimental Methods and Applications to a Melamine Foam. *Applied Acoustics*, 69 (**12**), 2008, pp. 1129–1140. DOI: 10.1016/j.apacoust.2007.11.008.

[59] L. Jaouen, E. Gourdon, and M. Edwards. 6-Parameter Acoustical Characterization of Porous Media Using a Classical Impedance Tube. 2018.

[60] F. Sgard et al. On the Use of Perforations to Improve the Sound Absorption of Porous Materials. *Applied Acoustics*, 66 (**6**), 2005, pp. 625–651. DOI: 10.1016/j.apacoust.2004.09.008.

[61] N. Atalla et al. Acoustic Absorption of Macro-Perforated Porous Materials. *Journal of Sound and Vibration*, 243 (**4**), 2001, pp. 659–678. DOI: 10.1006/jsvi.2000.3435.

[62] V. Romero-García and A. Hladky-Hennion, eds. Fundamentals and Applications of Acoustic Metamaterials: From Seismic to Radio Frequency. 1st ed. Wiley, 15, 2019. DOI: 10.1002/9781119649182.

[63] J.-P. Groby et al. Enhancing the Absorption Properties of Acoustic Porous Plates by Periodically Embedding Helmholtz Resonators. *The Journal of the Acoustical Society of America*, 137 (**1**), 2015, pp. 273–280. DOI: 10.1121/1.4904534.

[64] V. Twersky. Multiple Scattering of Radiation by an Arbitrary Configuration of Parallel Cylinders. *The Journal of the Acoustical Society of America*, 24 (**1**), 1952, pp. 42–46. DOI: 10.1121/1.1906845.

[65] M. Gaborit et al. Extending the Coupling of FEM, TMM and Bloch Waves to Poroelastic Layers and Films. 2nd Franco-Chinese Acoustic Conference. Le Mans, France, 30, 2018.

[66] N. Atalla, R. Panneton, and P. Debergue. A Mixed Displacement-Pressure Formulation for Poroelastic Materials. *The Journal of the Acoustical Society of America*, 104 (**3**), 1998, p. 1444. DOI: 10.1121/1.424355.

[67] N. Atalla, M. A. Hamdi, and R. Panneton. Enhanced Weak Integral Formulation for the Mixed (u,p) Poroelastic Equations. *The Journal of the Acoustical Society of America*, 109 (**6**), 2001, p. 3065. DOI: 10.1121/1.1365423.

[68] P. Göransson. A 3-D, Symmetric, Finite Element Formulation of the Biot Equations with Application to Acoustic Wave Propagation through an Elastic Porous Medium. *International Journal for Numerical Methods in Engineering*, 41 (**1**), 1998, pp. 167–192. DOI: 10.1002/(SICI)1097-0207(19980115)41:1<167::AID-NME285>3.0.CO;2-T.

[69] T. Weisser et al. High Broadband Absorption of Acoustic Waves by Elastic-Framed Metaporous Layer. *Advanced Electromagnetic Materials in Microwaves and Optics (METAMATERIALS), 2016 10th International Congress On*. IEEE, 2016, pp. 322–324.

[70] J.-P. Groby, W. Lauriks, and T. E. Vigran. Total Absorption Peak by Use of a Rigid Frame Porous Layer Backed by a Rigid Multi-Irregularities Grating. *The Journal of the Acoustical Society of America*, 127 (**5**), 2010, pp. 2865–2874. DOI: 10.1121/1.3337235.

[71] D. Blon. 2016LEMA1034 Influence des jonctions sur le comportement vibro-acoustique d'assemblages de structures bois pour le bâtiment. PhD. Le Mans, France: Université du Maine, 2016.

[72] O. Dazel and M. Gaborit. PLANES: Porous LAUM Numerical Simulator. Software Package. LAUM UMR CNRS 6613, 2018.

[73] C. Potel et al. Shear Horizontal Acoustic Waves Propagating along Two Isotropic Solid Plates Bonded with a Non-Dissipative Adhesive Layer: Effects of the Rough Interfaces. *Journal of Applied Physics*, 118 (**22**), 14, 2015, p. 224904. DOI: 10.1063/1.4937150.

[74] M. Gaborit et al. Génération rapide de courbes enveloppes pour les matériaux poro-élastiques. Congrès Français d'Acoustique. Le Havre, France, 2018.

[75] N. Wiener. The Homogeneous Chaos. *American Journal of Mathematics*, 60 (**4**), 1938, p. 897. DOI: 10.2307/2371268. JSTOR: 2371268?origin=crossref.

[76] D. Xiu. Numerical Methods for Stochastic Computations: A Spectral Method Approach. Princeton, N.J: Princeton University Press, 2010. 125 pp.

[77] A. Alexanderian. A Brief Note on the Karhunen-Loève Expansion. North Carolina State University, 2015.

Part II

Appended Papers

Paper A

A simplified model for thin acoustic screens

M. Gaborit[1,2,@], O. Dazel[1], P. Göransson[2]

Published as an Express Letter in the Journal of the Acoustical Society of America
Vol. 144 **(1)** (2018), pp. EL76-EL81, DOI: 10.1121/1.5047929

1. LAUM, UMR CNRS 6613, Université du Maine, Le Mans, France
2. MWL, KTH Royal Institute of Technology, Stockholm, Sweden
@ Corresponding author

Abstract

A generalization of the commonly used pressure jump modelling of thin porous layers, is proposed. The starting point is a transfer matrix model of the layer derived using matrix exponentials. First order expansions of the propagating terms lead to a linear approximation of the associated phenomena and the resulting matrix is further simplified based on physical assumptions. As a consequence the equivalent fluid parameters used in the model may be reduced to simpler expressions and the transfer matrix rendered sparser. The proposed model is validated for different backing conditions, from normal to grazing incidence and for a wide range of thin films. In the paper the physical hypotheses are discussed, together with the origin of the fields jumps.

Thin porous layers, sometimes referred to as screens, films, veils, *etc.*, are commonly applied as protection, both for aesthetic reasons as well as for prevention of wear and tear. Properly designed they may also contribute to the performance of sound packages in various applications. For example, when used in combination with e.g. metamaterials[1–3] or stacked layers of poroelastic materials (foam, fibre panels, ...)[4,5], their properties can be tailored to optimise the overall system performance, at low weight and without increasing the overall thickness of the installation. They may also be used to improve the absorption at low frequencies and despite their small thickness, usually ranging from 0.1 to 1 mm, these coatings commonly have a noticeable impact and cannot be ignored when simulating the behaviour of the absorbers[6,7].

The present work focuses on the numerical modelling of thin permeable films applied as coatings on multilayer poroelastic panels. Depending on which effects need to be accounted for in the simulations, different approaches may be adopted. A minimal one would be the pressure jump model proposed by Pierce[8] or a slightly more refined rigid-frame model[7]. This would however lead to a rather crude prediction of the response, missing system but would also have the advantage of requiring only a few parameters to be characterised in order to simulate the acoustic behaviour. A more accurate approach, particularly for woven screens could be based on models for perforated panels accounting for the *vena contracta* effect and changes of dynamic tortuosity[5]. Finally, an even more accurate description would consider bi-phase models such as Biot's with the refinements proposed by Johnson, Champoux and Allard (JCA) for viscous dissipative effects[9–11] or one of the rewritten sets of equations for poroelastic materials[12,13]. Note that in Ref. [13] a flexible poroelastic model is presented that may be adapted to any existing equivalent fluid model for the dynamic density and compressibility $\tilde{\rho}_{eq}$ and $\tilde{K}_{eq}$, hence allowing for changes in the dissipation model. Even if the thickness is rather small compared to the dimension of the homogenisation volume, the Biot theory has been successfully applied to model screens[7,14].

The present work aims at proposing a simplified model for acoustic screens accounting for the resonant effects while reducing the number of physical parameters needed in the modelling. It is intended as an alternative to the more elaborate modelling approaches used in current Transfer Matrix models. The principles used

to derive a transfer matrix for a poroelastic layer (section 1) are first presented, followed by an introduction of a number of simplifications in section 2. In these, the propagative terms are linearised and a dimensional analysis is applied to neglect the terms of least importance. The approach is validated using numerical simulations where the results using the proposed model are compared to those obtained from a full Biot-JCA simulation, for several films (section 3). An extensive testing of the proposed model was performed however most of these tests are omitted from the paper for conciseness and only two representative films are presented in the results of section 3: one woven and one non-woven. Note that throughout this paper, a positive time convention ($e^{\mathrm{j}\omega t}$) is used.

1 Transfer matrix as an exponential

To describe the acoustic propagation in a poroelastic layer, a Biot model[9,15] is used but without taking into account membrane effects that could be significant in films under tension. In the present case, the model uses the two motion equations corresponding to the strain-decoupled formulation[12]:

$$\hat{\sigma}_{ij,j} = -\omega^2 \tilde{\rho}_s u_i^s - \omega^2 \tilde{\rho}_{eq} \tilde{\gamma} u_i^t, \qquad -p_{,i} = -\omega^2 \tilde{\rho}_{eq} \tilde{\gamma} u_i^s - \omega^2 \tilde{\rho}_{eq} u_i^t, \tag{1}$$

and the associated two constitutive laws:

$$\hat{\sigma}_{ij} = \hat{A} u_{i,i}^s \delta_{ij} + 2N\varepsilon_{ij}, \qquad p = -\tilde{K}_{eq} u_{i,i}^t, \tag{2}$$

where $\boldsymbol{u^s}$ and $\boldsymbol{u^t}$ are respectively the homogenised solid and total displacements, p the interstitial pressure, $\hat{\sigma}$ and ε the in-vacuo stress and strain tensors and δ_{ij} is the Kronecker symbol. The other symbols are physical parameters of the medium that represent densities ($\tilde{\rho}_{eq,s}$), compressibility ($\tilde{K}_{eq}$), Lamé coefficients ($\hat{A}$ and N) and solid/fluid coupling ($\tilde{\gamma}$).

The model is developed assuming a layer of infinite extent in the (x, y) plane and of thickness d excited by a plane wave travelling towards the positive values along the z axis. All the fields have the same dependence $e^{-jk_x x}$ and the wave vector, due to the assumed isotropy, is oriented such that $k_y = 0$. The strategy to derive the transfer matrix is then based on the so-called Stroh formalism[4,16,17]. This approach leads to a set of first order differential equations in the state vector $\boldsymbol{s}(z)$:

$$\frac{\partial \boldsymbol{s}(z)}{\partial z} = \boldsymbol{\alpha} \boldsymbol{s}(z), \qquad \text{with } \boldsymbol{s}(z) = \left\{ \hat{\sigma}_{xz}(z),\ u_z^s(z),\ u_z^t(z),\ \hat{\sigma}_{zz}(z),\ p(z),\ u_x^s(z) \right\}^T. \tag{3}$$

Note that the physical fields absent from the state vector (such as u_x^t and $\hat{\sigma}_{xx}$) can be deduced from linear combinations of the ones present.

As the medium is homogeneous, solving (3) for a layer of thickness d leads to the expression of the transfer matrix $\boldsymbol{T}(d)$ for the state vector $\boldsymbol{s}$ written as a matrix exponential:

$$\boldsymbol{s}(0) = \boldsymbol{T}(d)\boldsymbol{s}(d), \quad \boldsymbol{T}(d) = \exp\left(-d\boldsymbol{\alpha}\right). \tag{4}$$

The derivation of the state matrix $\boldsymbol{\alpha}$ is central to the present work. However, it has been addressed multiple times in the literature (see Ref. [16] for this specific case or Refs. [17, 18] for a more general discussion) and thus will be omitted for conciseness. The matrix used in the present work is identical to the one proposed in the appendix A.1 of Ref. [16] (with $\hat{P} = \hat{A} + 2N$):

$$\boldsymbol{\alpha} = \begin{bmatrix} 0 & 0 & 0 & \mathrm{j}k_x\frac{\hat{A}}{\hat{P}} & \mathrm{j}k_x\tilde{\gamma} & -\frac{\hat{A}^2-\hat{P}^2}{\hat{P}}k_x^2 - \tilde{\rho}\omega^2 \\ 0 & 0 & 0 & \frac{1}{\hat{P}} & 0 & \mathrm{j}k_x\frac{\hat{A}}{\hat{P}} \\ 0 & 0 & 0 & 0 & -\frac{1}{\tilde{K}_{eq}} + \frac{k_x^2}{\tilde{\rho}_{eq}\omega^2} & -\mathrm{j}k_x\tilde{\gamma} \\ \mathrm{j}k_x & -\tilde{\rho}_s\omega^2 & -\tilde{\rho}_{eq}\tilde{\gamma}\omega^2 & 0 & 0 & 0 \\ 0 & \tilde{\rho}_{eq}\tilde{\gamma}\omega^2 & \tilde{\rho}_{eq}\omega^2 & 0 & 0 & 0 \\ \frac{1}{N} & \mathrm{j}k_x & 0 & 0 & 0 & 0 \end{bmatrix}. \tag{5}$$

2 Simplification of the transfer matrix

The key idea of this paper is to use some hypotheses based on the characteristic properties of acoustic screens, which may be used to simplify the transfer matrix $\boldsymbol{T}(d)$ and to reduce the number of required parameters. The most important assumption is that the average thickness of these coatings is rather small, especially compared to the wavelengths of the waves in the media ($kd \ll 1$, with k the wavenumber in air or in the poroelastic layer). This hypothesis allows for an approximation of the matrix exponential of Eq. (4) in terms of its first order Taylor expansion:

$$\boldsymbol{T}(d) \approx \mathbf{I} - d\boldsymbol{\alpha} + \mathcal{O}(d^2) \tag{6}$$

with $\mathbf{I}$ the identity matrix. This approximation replaces the terms representing the transfer of the corresponding fields through the film, with jumps in the values of the field amplitude values between both faces of the layer. Indeed, Eq. (6) suggests that all the fields are transferred and altered by a combination of the other fields described by the state matrix $\boldsymbol{\alpha}$ and proportional to the thickness d.

The next step is to identify the most important contributions in $\boldsymbol{\alpha}$ and neglect all others. For this purpose, the second proposed approximation is introduced. Let k_s be the largest wavenumber in the layer (i.e. $k_s \geq k_{x,z}$, noting that k_s often corresponds to the solid-borne compressional wave) and using the constitutive equations (2), it is easily shown that:

$$|\hat{\sigma}_{zz}| \leqslant k_s\left(\hat{P}u_z^s + \hat{A}u_x^s\right), \qquad |\hat{\sigma}_{xz}| \leqslant 2Nk_s\left(u_x^s + u_z^s\right) \tag{7}$$

From the second and last rows of the transfer matrix (solid displacements), we get

$$u_z^s(0) = u_z^s(d) + \frac{d}{\hat{P}}\hat{\sigma}_{zz}(d) + \mathrm{j}k_x d\frac{\hat{A}}{\hat{P}}u_x^s(d), \qquad u_x^s(0) = u_x^s(d) + \frac{d}{N}\hat{\sigma}_{xz}(d) + \mathrm{j}k_x d u_z^s(d). \tag{8}$$

which can be combined with the two inequalities previously introduced to rewrite the jumps for the two components of the solid displacement:

$$|u_z^s(0) - u_z^s(d)| \leqslant k_s d\left(u_z^s(d) + 2\frac{\hat{A}}{\hat{P}}u_x^s(d)\right), \qquad |u_x^s(0) - u_x^s(d)| \leqslant k_s d\Big(2u_z^s(d) + u_x^s(d)\Big) \tag{9}$$

Provided that the frequency or the thickness are sufficiently small such that $k_s d \ll 1$, it is reasonable to assume that , and thus to neglect all terms on lines 2 and 6 in (6) except the unit diagonal.

Moreover, it is proposed to neglect two other effects:

— the influence of the saturating fluid on the evolution of *in vacuo* shear solid stresses $\hat{\sigma}_{xz}$;

— the coupling of the tangential solid and normal total displacement.

These assumptions respectively cancel $\boldsymbol{T}_{14}$ and $\boldsymbol{T}_{41}$, $\boldsymbol{T}_{15}$ and $\boldsymbol{T}_{36}$.

The transfer matrix may then be rewritten as:

$$\boldsymbol{T}(d) \approx \mathbf{I} - d\begin{bmatrix} 0 & 0 & 0 & 0 & 0 & -\frac{\hat{A}^2-\hat{P}^2}{\hat{P}}k_x^2 - \tilde{\rho}\omega^2 \\ 0 & 0 & 0 & 0 & 0 & 0 \\ 0 & 0 & 0 & 0 & -\frac{1}{\tilde{K}_{eq}} + \frac{k_x^2}{\tilde{\rho}_{eq}\omega^2} & 0 \\ 0 & -\tilde{\rho}_s\omega^2 & -\tilde{\rho}_{eq}\tilde{\gamma}\omega^2 & 0 & 0 & 0 \\ 0 & \tilde{\rho}_{eq}\tilde{\gamma}\omega^2 & \tilde{\rho}_{eq}\omega^2 & 0 & 0 & 0 \\ 0 & 0 & 0 & 0 & 0 & 0 \end{bmatrix}. \tag{10}$$

So far, the proposed modifications mostly impact the structure of the transfer matrix without significantly reducing the number of physical parameters required to describe the system behaviour. Considering the small thickness of the coatings, it is proposed to neglect the effects of tortuosity and set $\tilde{\alpha}_\infty \approx 1$ and . This last assumption leads to simplified forms for the equivalent fluid quantities $\tilde{K}_{eq}$ and $\tilde{\rho}_{eq}$:

$$\tilde{K}_{eq} \approx \frac{P_0}{\phi}, \quad \tilde{\rho}_{eq} \approx \frac{\rho_0}{\phi} + \frac{\sigma}{\mathrm{j}\omega} \tag{11}$$

The first of these relations suggests that the compression is isothermal. The imaginary part of the simplified equivalent density represents a phase shift of the fluid-borne wave often referred to as a pressure jump or pressure drop[8]. The real part of the simplified expression of $\tilde{\rho}_{eq}$ is actually a second order term (whereas

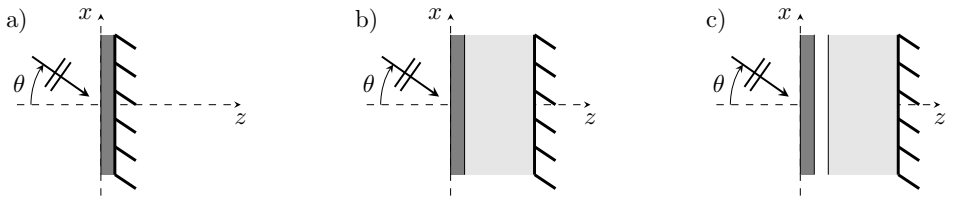

Figure 1 – Configurations used during the development of the method and used in the tests.

the imaginary part is of the first order) that corrects the loss of accuracy at high frequencies due to the simplifications.

This last set of simplifications brings down the number of parameters in the model to six : three mechanical parameters ($\hat{A}$, N and the structural loss parameters η), the flow resistivity σ, the porosity ϕ and the bulk density ρ_1. Investigations involving neglected frame mechanical parameters were performed, however the resulting levels of error were higher than the target. Hence, it was decided to keep the elastic contributions in the proposed model.

3 Validating the simplified model

In this section, the simplified model is tested for different configurations against a reference solution corresponding to a full Biot-JCA Transfer Matrix model. In order to validate the proposed approach, attention must be paid to special cases such as the change of backing condition, grazing incidence and different materials. A large range of configurations have then been tested in order to assess the robustness of the proposed model. The three configurations shown on Figure 1 were used in the development process. They present three different types of boundary conditions backing the simplified layer and helps understanding how the errors build up. It has been observed during the refinement of the proposed method, that the backing condition featuring an air-gap (1.c) leads to results very similar to those obtained with a PoroElastic Material (PEM) backing (1.b) whereas the rigidly backed configuration (1.a) behaves differently. Consequently, only the configurations of Figure 1.a and 1.b are used in the results shown hereafter.

The numerical values for the parameters used to model the films are taken from a work discussing the characterization procedure for films[19]. These values are gathered in Table 1 along with the parameters of the backing foam. In the simulations, the thicknesses of the films and foam are respectively 0.5mm and 50mm and the following properties are used for air $\rho_0 = 1.213\ \mathrm{kg \cdot m^{-3}}$, $\mathrm{Pr} = 0.71$, $\eta_0 = 1.839 \cdot 10^{-5}\ \mathrm{Pa \cdot s}$, $P_0 = 1.01325 \cdot 10^5\ \mathrm{Pa}$, $\gamma_0 = 1.4$. Note that in this table and for the reference solution, the values for for films but they are set to unity for the simulations when evaluating the simplified model.

Table 1 – Physical parameters of the foam and films (woven and non-woven) used in the validation cases of section 3.

Parameters (unit)	Foam	Woven	Non-woven
ϕ	0.994	0.72	0.04
σ (N·s·m^{-4})	9045	$87{\cdot}10^3$	$775{\cdot}10^3$
$\tilde{\alpha}_\infty$	1.02	1.02	1.15
Λ' (μm)	197	480	230
Λ (μm)	103	480	230
ρ_1 (kg·m^{-3})	8.43	171	809
ν	0.42	0	0.3
E (Pa)	$194.9{\cdot}10^3$	$50{\cdot}10^3$	$260{\cdot}10^6$
η	0.05	0.5	0.5

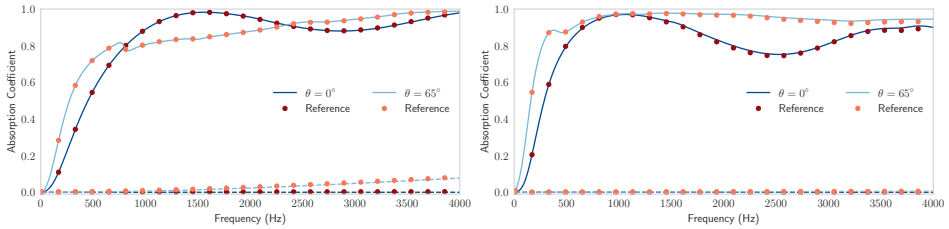

Figure 2 – Absorption coefficient for two different materials (one per sub-figure), two angles of incidence (different colours) and two configurations (different line styles). Left: Non-woven film. Right: Wowen film. The graphs showing low absorption (dashed lines) are computed for the configuration of Figure 1.a with the film directly laid on the backing, the others correspond to configuration 1.b with an inserted PEM layer. The reference results are shown using marker symbols. (Color online)

As seen from Figure 2, the agreement between the proposed simplified model and a complete Biot-JCA model for the film is tested for two materials, two angles (0° and 65°) and two boundary conditions (rigid backing and PEM backing). Clearly, the results obtained by the proposed method stay close to the reference. The agreement is even perfect at low frequencies and some very small discrepancies discussed below are observed at higher frequencies.

In order to systematize the analysis, the evolution of the absolute error

$$\epsilon = |\alpha_{\text{biot}} - \alpha_{\text{screen}}| \tag{12}$$

is computed over the (f, θ) plane with α_{biot} and α_{screen} being respectively the absorption coefficients calculated using the complete Biot-JCA model for the film and the simplified model. The results are shown on Figure 3 for different films and backing conditions.

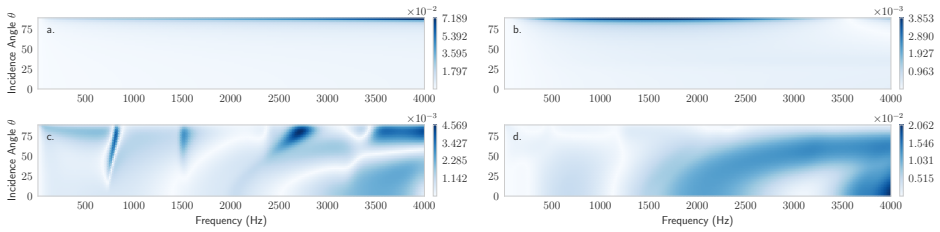

Figure 3 – Evolution of the relative error in the (f, θ) plane. Left: (a. and c.) non-woven film; Right (b. and d.): woven film. Top: (a. and b.) configuration as in Figure 1.a; Bottom: (c. and d.) configuration as in Figure 1.b. (Color online)

Near grazing incidence, an expected drop of precision is observed, particularly when the film is directly laid on a rigid backing. This difference between the two setups suggests that a compensatory effect is introduced when the backing is a PEM. Indeed, whereas the absorption occurs only in the film when directly laid on a rigid surface, it occurs mainly in the PEM in the other case, smoothing the effect of the film. At grazing incidence, the proposed model (where most of the shear effects have been neglected) obviously breaks down. The path travelled by the waves in the film is also much longer, invalidating the hypothesis of a thin film and leading to excessive absorption. Despite these points, the corresponding relative error is lower than 3% in the observed cases.

4 Conclusion

In the present work, a simplified model for the transfer matrix of acoustic films is proposed. Approximations based on physical reasoning lead to both a simpler propagation model (with expanded matrix exponential) and a reduction of the number of parameters. It is demonstrated that these simplifications hold for thin poroelastic layers and that the resulting model behaves best when used in a transfer matrix model on top of another PEM or air layer. For rigid backing conditions, some discrepancies may be observed, mainly due to some of the parameters being neglected. Despite these aspects, the model still exhibits a reasonable accuracy.

References

[1] C. Lagarrigue et al. Absorption of sound by porous layers with embedded periodic arrays of resonant inclusions. *The Journal of the Acoustical Society of America*, 134 (**6**), 2013, pp. 4670–4680.

[2] N. Jiménez et al. Quasiperfect absorption by subwavelength acoustic panels in transmission using accumulation of resonances due to slow sound. en. *Physical Review B*, 95 (**1**), 2017. DOI: 10.1103/PhysRevB.95.014205.

[3] J. Yang, J. S. Lee, and Y. Y. Kim. Metaporous layer to overcome the thickness constraint for broadband sound absorption. *Journal of Applied Physics*, 117 (**17**), 2015, p. 174903.

[4] J. P. Parra Martinez et al. Acoustic analysis of anisotropic poroelastic multilayered systems. en. *Journal of Applied Physics*, 119 (**8**), 2016, p. 084907. DOI: 10.1063/1.4942443.

[5] N. Atalla and F. Sgard. Modeling of Perforated Plates and Screens Using Rigid Frame Porous Models. *Journal of Sound and Vibration*, 303 (**1-2**), 2007, pp. 195–208. DOI: 10.1016/j.jsv.2007.01.012.

[6] S. Sugie, J. Yoshimura, and H. Ogawa. Absorption characteristics of fibrous material covered with perforated facing and film. *Acoustical science and technology*, 27 (**2**), 2006, pp. 87–96.

[7] J.-F. Allard and N. Atalla. Propagation of sound in porous media: modelling sound absorbing materials. 2nd. Hoboken, N.J: Wiley, 2009.

[8] A. D. Pierce. Acoustics: an introduction to its physical principles and applications. 1989th ed. Woodbury, N.Y: Acoustical Society of America, 1989.

[9] M. A. Biot. Theory of Propagation of Elastic Waves in a Fluid-Saturated Porous Solid. en. *The Journal of the Acoustical Society of America*, 28 (**2**), 1956, p. 168. DOI: 10.1121/1.1908239.

[10] D. L. Johnson, J. Koplik, and R. Dashen. Theory of Dynamic Permeability and Tortuosity in Fluid-Saturated Porous Media. *Journal of fluid mechanics*, 176 (**1**), 1987, pp. 379–402.

[11] Y. Champoux and J.-F. Allard. Dynamic Tortuosity and Bulk Modulus in Air-Saturated Porous Media. *Journal of Applied Physics*, 70 (**4**), 1991, p. 1975. DOI: 10.1063/1.349482.

[12] O. Dazel et al. An alternative Biot's displacement formulation for porous materials. en. *The Journal of the Acoustical Society of America*, 121 (**6**), 2007, p. 3509. DOI: 10.1121/1.2734482.

[13] F.-X. Bécot and L. Jaouen. An Alternative Biot's Formulation for Dissipative Porous Media with Skeleton Deformation. *The Journal of the Acoustical Society of America*, 134 (**6**), 2013, pp. 4801–4807. DOI: 10.1121/1.4826175.

[14] J. Kanfoud et al. Development of an Analytical Solution of Modified Biot's Equations for the Optimization of Lightweight Acoustic Protection. *The Journal of the Acoustical Society of America*, 125 (**2**), 2009, pp. 863–872. DOI: 10.1121/1.2973197.

[15] M. A. Biot and D. Willis. The Elastic Coefficients of the Theory of Consolidation. *Journal of Applied Mechanics*, 1957.

[16] O. Dazel et al. A stable method to model the acoustic response of multilayered structures. en. *Journal of Applied Physics*, 113 (**8**), 2013, p. 083506. DOI: 10.1063/1.4790629.

[17] Q. Serra, M. N. Ichchou, and J.-F. Deü. On the Use of Transfer Approaches to Predict the Vibroacoustic Response of Poroelastic Media. *Journal of Computational Acoustics*, 24 (**02**), 2016. DOI: 10.1142/S0218396X15500204.

[18] J. P. Parra Martinez et al. Derivation of the state matrix for dynamic analysis of linear homogeneous media. en. *The Journal of the Acoustical Society of America*, 140 (**2**), 2016, EL218–EL220. DOI: 10.1121/1.4960624.

[19] L. Jaouen and F.-X. Bécot. Acoustical characterization of perforated facings. *The Journal of the Acoustical Society of America*, 129 (**3**), 2011, pp. 1400–1406.

Paper B

Response envelope generation for thin acoustic screens with uncertain parameters

M. Gaborit[1,2,@], O. Dazel[1], P. Göransson[2] L. Jaouen[3],

Submitted to the Journal of the Acoustical Society of America on September 23rd

1. LAUM, UMR CNRS 6613, Université du Maine, Le Mans, France
2. MWL, KTH Royal Institute of Technology, Stockholm, Sweden
3. Matelys Research Lab, Vaulx-en-Velin, France

@ Corresponding author

Abstract

The properties of the materials used for building sound proofing systems are known to exhibit large variations. These may lead to significant differences in the acoustic responses within a given material batch, particularly when resistive screens are used as a surface component for a multi-layered absorbing panel. In such thin films, it is mostly the thickness and the flow resistivity, but in some cases also the porosity, that are difficult to control in the production process. All these potential variations influence the acoustic response of the complete panel. In the present contribution, a method to isolate and evaluate the effect of uncertainties in a film is proposed. Using a transmission line approach, it is shown to be possible to predict the modification of the response induced by the uncertainties. The proposed technique is then adapted to determine envelopes, for experimentally acquired responses, that are closer to measured envelopes as compared to those generated using Monte Carlo simulations or naive approaches. The method is tested both on numerical and experimental cases and shows, in both cases, a very good agreement with the reference solutions. Unlike Monte Carlo approaches, the proposed method does not require a massive computational effort which makes it suitable for real life applications.

1 Introduction

Reducing noise through dedicated acoustic treatments is essential in modern society to counteract the negative impact on health that is linked to exposure. Many approaches have been proposed over the years, either with a broadband noise reduction objective[1] or targeting a given frequency band[2–4]. Recent reports and directives[5–7] set evermore ambitious targets in term of noise mitigation for the future. This overall endeavour to reduce noise and its impact requires the development of efficient, versatile strategies to be combined with punctual, more specific solutions to mitigate particular features of the noise content (emerging tones for instance).

A widely used and rather inexpensive approach to noise reduction over a fairly large frequency band uses poro-elastic materials (foam, fibre panels, etc.) arranged as a multi-layered laminate. These composite structures usually involve a small number of foam/fibrous layers with carefully chosen properties and thicknesses in order to meet specific absorption objectives[1]. To protect the panel and sometimes fine tune its properties, thin films can be added on the free surface[8,9]. Often highly resistive, such films are known to play a prominent role in the behaviour of the overall systems[10–12]. As their precise characterisation might be challenging[13], it is of primary importance to understand how the uncertainties on the film parameters induce variations of the overall system response. Apart from this objective, another goal of the study is to propose an efficient method to compute the associated response envelope curves both on simulated response and on experimental results. It is shown that the proposed approach allows to merge statistical data from the char-

acterisation of the screen with a single measurement of the overall system response. The resulting envelopes are shown to convey the same statistical information as Monte Carlo results obtained by measuring a large number of samples.

The paper is organised as follows. In the first section a study model is introduced and used to derive the influence of the film and its the uncertain parameters on the response. A technique for combining an existing deterministic response of a panel and statistical information on the film to infer the associated envelope is discussed. In a second section, the proposed developments are tested against Monte Carlo simulations and validated. A third section presents an experimental set-up to measure the absorption coefficient of different laminates. Using a large number of samples from two different films, a statistical characterisation is performed following a procedure described in the literature[13], Using the same rig, different systems composed of an absorbing backing lined by of of these films are measured for an important number of film samples in order to obtain experimental envelopes. The experimental results are compared to those given by the proposed envelope annotation technique. A final section discusses the results.

2 Theoretical background

2.1 Position of the problem

The key idea of this section is to write the system response such that it is possible to isolate the contribution of uncertain film parameters. The chosen configuration is presented in Figure 1 and involves a backing represented by its surface impedance Z_B, a resistive but permeable layer (film, screen, etc.) of thickness d and the so-called incident medium in which the excitation propagates.

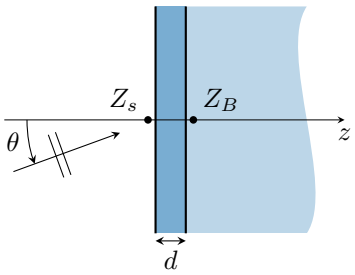

Figure 1 – Configuration under study. The backing is known through its surface impedance Z_B, the system is impinged by a plane wave propagating at an angle θ from the normal to the surface.

In the following, a positive time convention $e^{\mathrm{j}\omega t}$ is assumed where ω is the pulsation, t the time variable and $\mathrm{j}^2 = -1$.

2.2 Transmission through the film

Throughout this work, the film layer is assumed to be thin, of the order of half a millimetre. It is furthermore assumed that the elastic deformation of the film may be neglected. This allows for a class of simplified models where the film may be regarded as an equivalent fluid[1,14].

Based on the above assumptions, the thin film layer is modelled through an equivalent characteristic impedance:

$$Z_f = \sqrt{\rho_f K_f}, \tag{1}$$

where ρ_f and K_f are respectively the equivalent density and dynamic bulk modulus. Different expressions of these quantities exist in the literature[1,15,16] but are out of the scope of this paper and will not be discussed in the present contribution.

2.2.1 Evaluating the surface impedance

In order to determine the response of the multi-layered system to a plane wave excitation, one needs its surface impedance Z_s. Using an equivalent fluid model for the film, this quantity can be deduced from the backing surface impedance Z_B and the film properties using the impedance translation formula[1]:

$$Z_s = Z_f \frac{Z_B + \mathrm{j} Z_f \tan(k_f d)}{Z_f + \mathrm{j} Z_B \tan(k_f d)}, \tag{2}$$

where

$$k_f = \omega \cos\theta \sqrt{\rho_f / K_f} \tag{3}$$

is the wavenumber in the film.

As the thickness of the film is small compared to the wavelength ($\varepsilon = k_f d \ll 1$), a first order Taylor expansion of the tangent gives $\tan(k_f d) = k_f d + \mathcal{O}(k_f d)$. After substitution in (2) and simplification, this may be rewritten as

$$Z_s \approx \frac{Z_B + \mathrm{j} Z_f k_f d}{1 + \mathrm{j} Z_B Z_f^{-1} k_f d}, \tag{4}$$

which may be simplified further, through a Taylor expansion of the denominator:

$$Z_s = Z_B - \mathrm{j} Z_B^2 Z_f^{-1} k_f d + \mathrm{j} Z_f k_f d + \mathcal{O}\Big((k_f d)^2\Big). \tag{5}$$

Finally, substituting Eqs. (3) and (1), and neglecting the $(k_f d)^2$ term gives

$$Z_s = Z_B + \underbrace{\mathrm{j}\omega d \cos\theta \left(\rho_f - Z_B^2 K_f^{-1}\right)}_{Z_F}. \tag{6}$$

The influence of the film is then entirely captured in Z_F which, apart from the angle of incidence and the thickness of the screen, shows a dependency on the backing impedance Z_B.

2.2.2 Introducing uncertainties

As indicated in the introduction, the parameters of acoustic screens are seldom known with perfect accuracy. The sources of uncertainty can be either linked to sample-wise variations or to the characterisation itself. These films, woven or non-woven, are rather delicate and it is difficult to ensure that cutting and manipulating the samples does not alter their properties. Thus, different factors tend to render these media challenging to characterise even though standardised procedures are available[13,17]. Their influence on the acoustic performance is mainly controlled by two properties, the airflow resistivity σ and the thickness d[1,12]. In this section, the corresponding uncertainties induced on the model parameters of the medium are considered in terms of the higher level descriptors: ρ_f and K_f. Through these two descriptors, and the thickness d, the resulting deviation may be directly introduced into (6). It should be noted that the hypotheses leading to (6) henceforth are assumed to apply.

Each quantity ξ that is considered uncertain, is written as the sum of a nominal part $\bar{\xi}$ and a deviation $\Delta\xi$. Through this the overall deviation of the surface impedance Z_F in (1), i.e. ΔZ_F, may be evaluated as discussed in the following.

Equivalent density ρ_f Considering a deviation of the equivalent density $\rho_f = \bar{\rho}_f + \Delta\rho_f$ only, Z_F it is possible to write,

$$Z_F = \mathrm{j}\omega d\cos\theta\left(\bar{\rho}_f - Z_B^2 K_f^{-1}\right) + \underbrace{\mathrm{j}\omega d\cos\theta\Delta\rho_f}_{\Delta Z_F}. \tag{7}$$

Equivalent compressibility K_f A deviation of the equivalent compressibility alone can be treated in a similar fashion assuming that it is small compared to the nominal value (i.e. $\Delta K_f \bar{K}_f^{-1} \ll 1$). Substituting $\bar{K}_f + \Delta K_f$ into (6) and simplifying yields

$$Z_F = \mathrm{j}\omega d\cos\theta\left(\rho_f - Z_B^2 \bar{K}_f^{-1}\right) + \underbrace{\mathrm{j}\omega d\cos\theta Z_B^2 \frac{\Delta K_f}{\bar{K}_f^2}}_{\Delta Z_F}. \tag{8}$$

Equivalent density and compressibility In specific cases, such as for an uncertainty on the porosity ϕ in the JCA model, both K_f and ρ_f are modified. In this situation, both are replaced as before which allows to easily separate the terms and identify ΔZ_s, in terms of ΔK_f and $\Delta \rho_f$, as:

$$\begin{aligned} Z_s = {} & \mathrm{j}\omega d \cos\theta \left(\bar{\rho}_f - Z_B^2 \bar{K}_f^{-1} \right) \\ & + \underbrace{\mathrm{j}\omega d \cos\theta \left(\Delta\rho_f - Z_B^2 \frac{\Delta K_f}{\bar{K}_f^2} \right)}_{\Delta Z_F} . \end{aligned} \tag{9}$$

Thickness d Finally, the effect of a deviation of the thickness d leads to

$$\begin{aligned} Z_F = {} & \mathrm{j}\omega \cos\theta \left(\rho_f - Z_B^2 K_f^{-1} \right) \bar{d} \\ & + \underbrace{\mathrm{j}\omega \cos\theta \left(\rho_f - Z_B^2 K_f^{-1} \right) \Delta d}_{\Delta Z_F} . \end{aligned} \tag{10}$$

Note that in the above cases, there is no need for any but the films parameters (or even just the deviations of the descriptors themselves) and sometimes the surface impedance of the backing system at the frequency of interest. The cases for which this last quantities is not readily available are discussed in section 2.3.

2.2.3 Deriving reflection and absorption coefficients

Considering the deviation of the surface impedance $Z_s = \bar{Z}_s + \Delta Z_s$, it is straightforward to compute the reflection coefficient:

$$R = \frac{\bar{Z}_s + \Delta Z_s - Z_0}{\bar{Z}_s + \Delta Z_s + Z_0} . \tag{11}$$

and factorising $\bar{Z}_s + Z_0$, the denominator contains a small parameter $\Delta Z_s (\bar{Z}_s + Z_0)^{-1}$ and thus may be expanded in a Taylor series, which allows to separate the nominal and deviated part of R as,

$$R = \underbrace{\frac{\bar{Z}_s - Z_0}{\bar{Z}_s + Z_0}}_{\bar{R}} \left(1 + \underbrace{\frac{2 Z_0 \Delta Z_s}{\bar{Z}_s^2 - Z_0^2}}_{\eta} \right) + \mathcal{O}\left(\frac{\Delta Z_s^2}{\bar{Z}_s^2 - Z_0^2} \right) . \tag{12}$$

From (12), one can derive the absorption coefficient as (with $\mathcal{R}(\eta)$ denoting the real part of η)

$$\begin{aligned}\alpha &= 1 - |\bar{R}|^2|1+\eta|^2 \\ &= \underbrace{1-|R|^2}_{\bar{\alpha}} \underbrace{-|R|^2\left(2\mathcal{R}(\eta)+|\eta|^2\right)}_{\Delta\alpha}\end{aligned} \tag{13}$$

2.3 Envelope determination

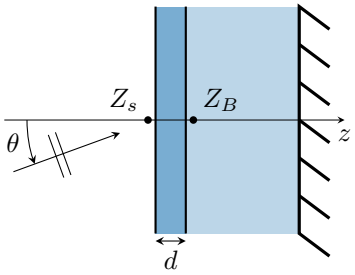

Figure 2 – System considered for the addition of the envelopes on a precomputed response.

Having established equations (7) - (10), it is now possible to generate an envelope curve using as input a single response of the overall system and information on the uncertainties in the film. This process will be outlined in the following, based on the notation introduced in Figure 2. Here two possibly independent sets of measurements are used. On one hand, a characterisation of the film is required including a rather accurate estimation of how properties are statistically distributed, for which different techniques exist, either based on quasi-static or dynamic measurements[13,17]. On the other hand, a deterministic response of the overall system is needed which may be readily measured using e.g. standard impedance tube techniques[18].

Depending on which of the JCA parameters that are affected, and thus on the type of uncertainty considered, the envelope generation process follows slightly different routes, essentially following Section 2.2.2. In cases when the uncertainty in ρ_f is evaluated, the overall surface impedance and its computed deviation are independent. On the other hand, if either d or K_f are afflicted by uncertainties, generating the envelope requires the computation of Z_B and thus the overall surface impedance Z_s needs to be known. To obtain Z_B, the impedance translation theorem is used anew, and the value of the overall surface impedance Z_S has to be obtained implying a translation through the film thus its parameters has to be known. These may be obtained by averaging the corresponding experimentally characterised values, in order to obtain the average value of the impedance $\bar{Z}_B$. Once $\bar{Z}_B$ is entirely deter-

mined, there only remains the computation of the deviation to the mean response from the equations (7) to (10).

3 Numerical validation

As a validation of the proposed approach, numerical simulations are employed. In the current work, envelopes generated using the previously presented steps are compared to results obtained from a Monte Carlo based analysis.

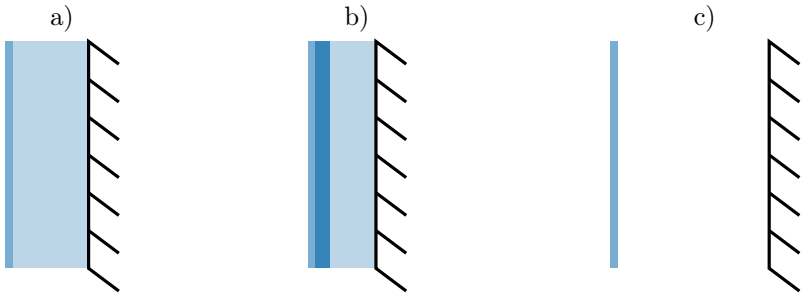

Figure 3 – Test systems considered. a) the film is placed on a single layer backing. Two configurations are tested: foam backing ($L = 50$ mm). b) the film is set on a two-layers backing (thickness of the backing layers is respectively 10 mm and 30 mm). c) an air plenum ($L = 200$ mm) if formed behind the film. The properties of the media used for these tests are reported in Table 1.

For the numerical validation, three different configurations are used, see Figure 3. In order to assess the limitations of the proposed method in relation to thin films of different design and manufacturing processes, a woven and a non-woven film are investigated. The physical parameters of the media are taken from the literature[1,11,13] and gathered in Table 1 for reference. The following properties are used for air: $\rho_0 = 1.213$ kg $\cdot$ m^{-3}, Pr $= 0.71$, $\eta_0 = 1.839 \cdot 10^{-5}$ Pa $\cdot$ s, $P_0 = 1.01325 \cdot 10^5$ Pa and $\gamma_0 = 1.4$.

The two different films attached to a slab of foam and impinged by a plane wave at an angle $\theta = 0$ deg or $\theta = 60$ deg, give the results shown in Figure 4. In this figure, the results from the proposed approach are compared with the Monte Carlo (MC) generated reference solutions. The MC references are statistical indicators (standard deviation and extrema) generated from a population of responses corresponding to 300 samples of the varying parameter ξ drawn from a normal distribution $\mathcal{N}\left(\bar{\xi}, \Delta\xi\right)$ with $\Delta\xi = 0.1\bar{\xi}$. The solutions from the proposed approach are generated for different deviations $n\Delta\xi$ with $n = 1, 2, 3$ in order to reach different confidence levels.

Two different representations are proposed: the response envelope, plotted as a regular absorption coefficient and the centred envelope where the mean curve is

Table 1 – Properties of media used in simulated tests, taken from the literature and especially[1,11,13]. CL stands for characteristic length.

Property [unit]	Foam 1	Foam 2	Non-woven Film	Woven film
Open-Porosity ϕ	0.994	0.99	0.72	0.04
Airflow resistivity σ [N $\cdot$ s $\cdot$ m^{-4}]	9045	65000	$87{\cdot}10^3$	$775{\cdot}10^3$
Tortuosity α_∞	1.02	1.98	1.02	1.15
Thermal CL Λ' [μm]	197	120	480	230
Viscous CL Λ [μm]	103	37	480	230
Density ρ_1 [kg $\cdot$ m^{-3}]	8.43	16	171	809
Poisson ratio ν	0.42	0.3	0	0.3
Young's modulus E [Pa]	$194.9{\cdot}10^3$	$46.8{\cdot}10^6$	$50{\cdot}10^3$	$260{\cdot}10^6$
Loss factor η	0.05	0.1	0.5	0.5

subtracted from the envelope curves. This second representation (shown on the four bottom plots of Figure 4) is especially useful when the comparison involves the generated envelope amplitudes over the entire frequency range under consideration.

Several points are worth noting about the results presented in Figure 4. The good agreement between the $n = 1$ envelopes predicted by the proposed approach and the MC standard deviation envelopes could perhaps have been anticipated given that this envelope correspond to a 68% confidence interval. Similarly, almost all the realisations are inside the $n = 2$ envelope (corresponding to a 95% confidence level). Over the considered frequency range, no realisation is completely outside the predicted envelopes) but some are partially outside of the envelope corresponding to a 99.7% confidence level ($n = 3$).

One must keep in mind that the differences between the predicted and empirical envelopes are of very low amplitudes and that a slight change in the model could cause such effects. It is also important to remember that the proposed approach is based on several approximations supported by the fact that the film is thin which might impair the overall accuracy. Furthermore, it is important to note that no major difference in accuracy is observed when increasing the angle of incidence θ.

In order to demonstrate that the proposed approach works for different backings, two more cases are studied. Figure 5 shows the results obtained for a facing placed upstream a 200 mm air plenum which correspond to configuration in Figure 3.c) . This case triggers a large number of resonances but the predicted envelopes are very similar to the empirical ones. It is interesting to note, from a modelling point of view, that the envelopes constrict near resonances and expand in a very repeatable pattern. This feature was also visible in Figure 4 to a certain extent even though the resonances are not as sharp. An interesting phenomenon is observed on the

$\theta = 0\,\text{deg}$ responses of Figure 4: constrictions of the envelope occur even though no resonance is visible for the absorption coefficient.

As a last validation test, Figure 6 shows the response and envelopes when the film facings are placed onto two layers of PEM. This configuration is expected to be more damped meaning that the envelopes should be smoother. This effect is indeed observed and the standard deviation envelope of the experimental results is rather smooth and very well captured by the proposed method for $n = 1$. Note that the empirical envelopes might be asymmetrical (for $\theta = 60\,\text{deg}$ for instance) and that this effect is not quite captured by the proposed approach. Nevertheless, the above results support the validity of the proposed approach.

4 Experimental validation

Besides the numerical validation of the approach presented in Section 3, a number of experiments presented in the present section allow to assess the capabilities of the proposed method. These experiments use once again two different kinds of facing, one woven and the other non-woven mimicking their numerical counterpart presented previously, and two different backing media. When needed for the proposed method, the properties of air were chosen the same as in Section 3. Photographs of samples used in the experiments are available in Figure 7

As a first part of the experimental investigation, the screens and the different backing materials were characterised. The result of this first part is presented in Table 2 in terms of mean value over the measured samples. Note that only the parameters of the JCA model are used in the following. The characterisation procedure is based on three samples of melamine foam, two samples of glass wool and forty samples of each of the facings. The large number of samples in the last case was chosen in order to have statistically significant data.

A second part of the experiments consists in using an impedance tube to measure the response of twenty samples of each film set on one of the samples of melamine and one of the samples of glass wool. This process once again allows to obtain meaningful statistical indicators regarding the response of each system.

The remainder of this section comprises a note on the measurement rig and the post-processing followed by a section of results where the proposed approached is leveraged to predict envelope curves.

The measurements used in the present paper are released online and free to download for further examination or use[19].

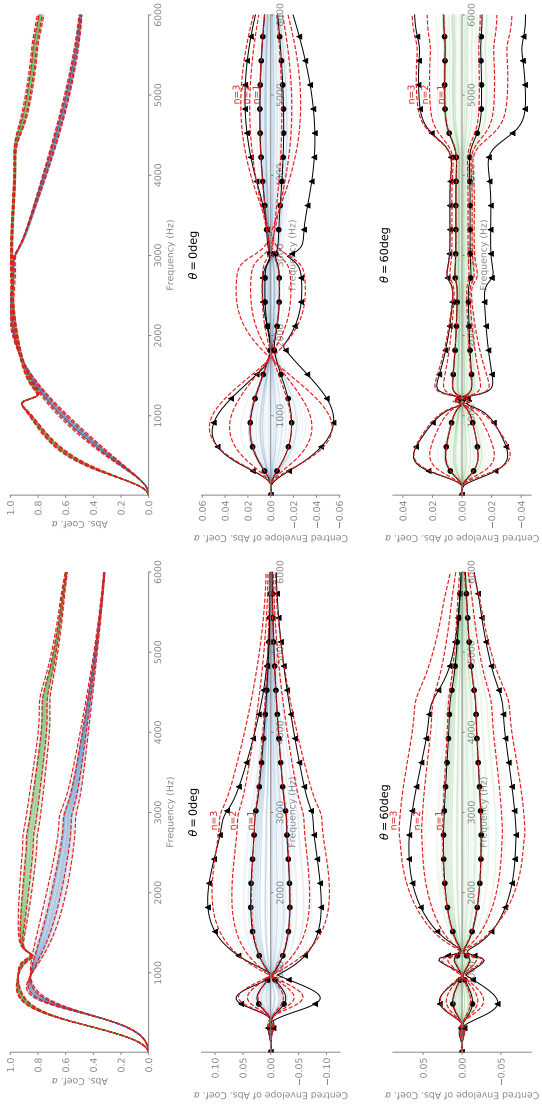

Figure 4 – Case of a varying thin film placed over a poro-elastic slab with a rigid backing. Comparison between Monte Carlo envelopes (realisations in blue/green, realisation-wise standard deviation envelope with bullets • and extremal envelopes with triangles ▲) and envelope from the proposed method (dashed red, n being the multiplier to the standard deviation of the varying parameter). Absorption coefficient (two top most axes) and centred envelopes (four lower axes) for two films (non-woven on the left, woven on the right) and two angles of incidence (0 in blue and 60 deg in green). (Color Online)

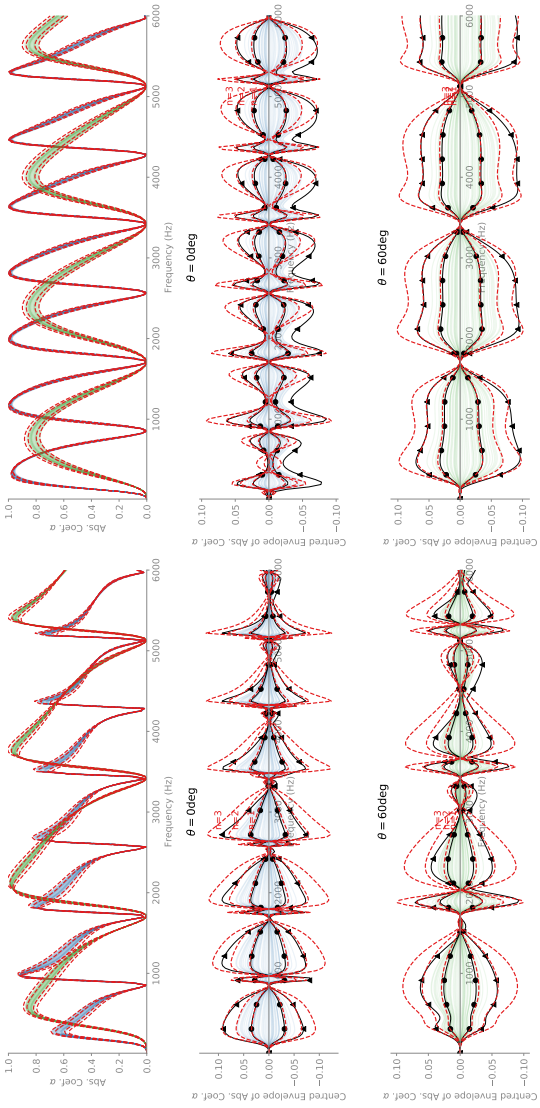

Figure 5 – Case of a varying thin film upstream a 200 mm air plenum. Quantities and line styles identical to Figure 4. (Color online)

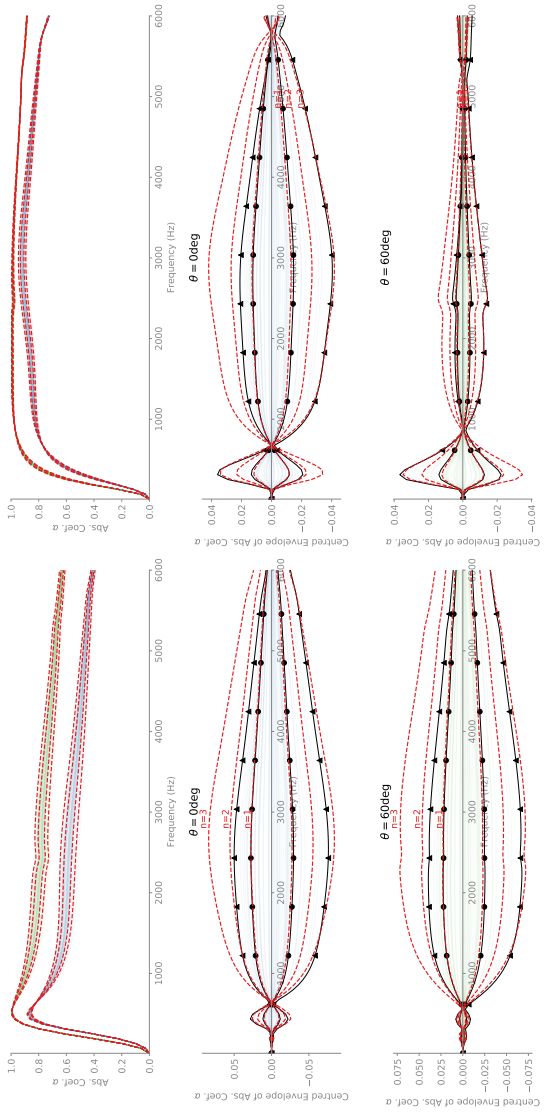

Figure 6 – Case of a varying thin film placed over two layers of poro-elastic media of thickness 10 mm and 30 mm. Quantities and line styles identical to Figure 4. (Color online)

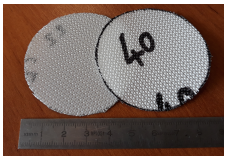

(a) Woven facing

(b) Non-woven facing

(c) Glass wool backing

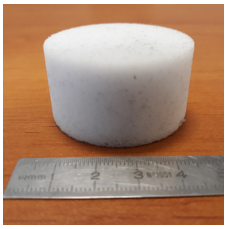

(d) Melamine backing

Figure 7 – Photographs of samples of backing and facing media under study.

Table 2 – Material properties from the characterisation process as a first step to the experimental validation (see Section 4). CL stands for characteristic length.

Property [unit]	Melamine	Glass wool	Non-woven Film	Woven film
Open-Porosity ϕ	0.99	0.97	0.096 ± 0.01	0.022 ± 0.003
Airflow resistivity σ [$\mathrm{N \cdot s \cdot m^{-4}}$]	11400 ±300	76100 ± 4400	$(7189 \pm 1043) \cdot 10^2$	$(55799 \pm 8305) \cdot 10^2$
Tortuosity α_∞	1.03 ±0.02	1.5 ± 0.55	1.07 ± 0.01	1.13 ± 0.01
Thermal CL Λ' [μm]	155 ±66	64 ± 30	46 ± 3	35 ± 3
Viscous CL Λ [μm]	91 ±18	30 ± 17	46 ± 3	35 ± 3
Density ρ_1 [$\mathrm{kg \cdot m^{-3}}$]	9.2 ±0.4	94.1 ± 2.7	427 ± 14	1243.5 ± 27.3
Thickness d (mm)	24.2±0.3	48.9±0.1	0.59±0.01	0.369

4.1 Measurement rig & post-processing

Both for the characterisation of all samples and for the actual measurement of the response of the studied film-backing configurations, an impedance tube of diameter 44.44 mm was used together with a dedicated commercial software[20]. All measurements use a three-microphones procedure[21,22] and span over the frequency band 10-4250 Hz. A schematic of the measurement rig is presented on Figure 8. The tube is split in two parts to allow for sample insertion and when needed, the film samples are clamped in the seam. Note that these are thin enough not to create leakage.

Note that the tube is split in two parts which overlap when assembled. If the tube's inner diameter is not impacted by this design, it provides a slight seam located at the beginning of the sample section which can be used for clamping the film samples.

Characterising the samples is entirely based on impedance tube measurements,

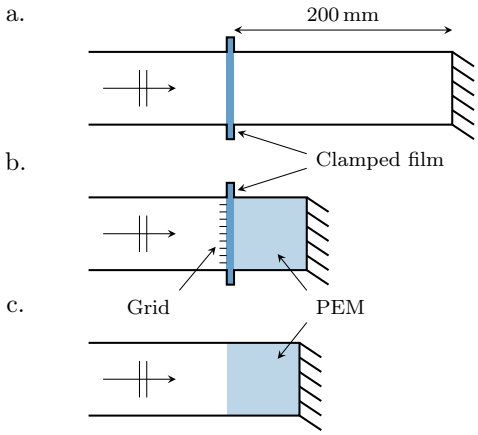

Figure 8 – Schematics of the different measurement set-ups. The incident wave is a plane wave, travelling normal to the sample's surface. A three-microphones method is used, one being mounted through the rigid backing, the two others on the side wall between the source and the sample.

Figure 9 – Plastic grid positioned inside the tube to prevent the facings from bending. It adds a 0.89 mm shift due to its shoulder.

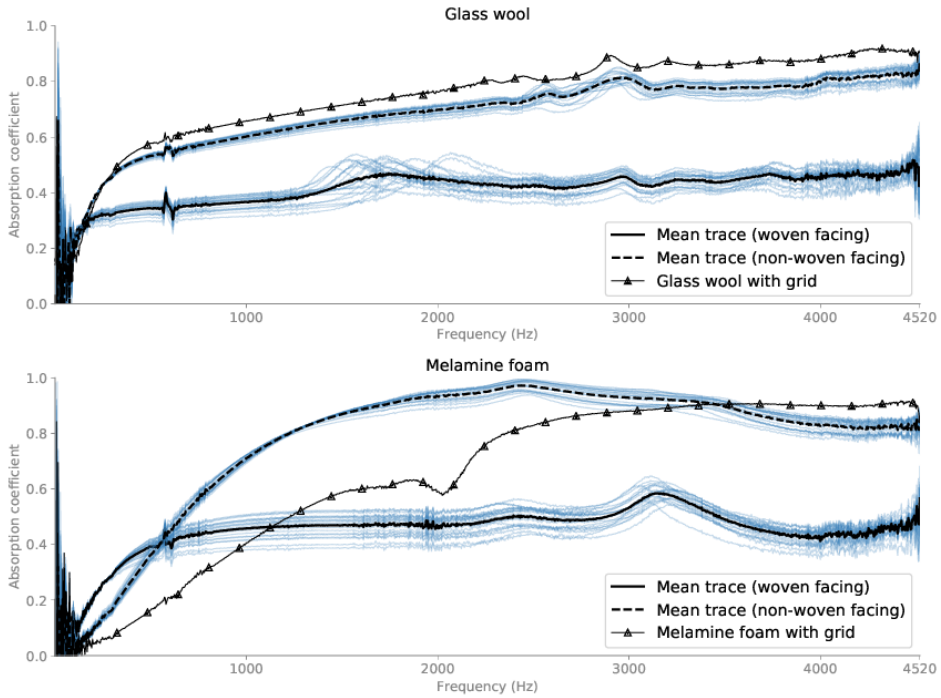

Figure 10 – Measured absorption coefficients for the glass wool (top) and melamine (bottom) stacked with each facing (average with woven in solid black line and with the non-woven one in dashed lines) and with only the grid (triangle ▲ markers). Thin blue lines are the traces associated to the different film samples. (Color online)

following procedures described in the literature for facings[13] and backings[23,24]. In the first case, a 200mm plenum is formed behind the screen sample by moving a piston located at the end of the tube. For characterising the backing samples, the piston is adjusted to their length such that the surface of each sample sits flush with the tube split line (i.e. exactly at the position of the seam).

When measuring the response of the multi-layered systems, in the second part of the experiments, a plastic grid shown in Figure 9 was inserted inside the tube to prevent the facing from bending. This grid has a known thickness of 0.89mm which could be compensated for to achieve better accuracy although this was not considered to be necessary here. In an attempt to reduce most of the sources of variation except for these linked to the tested films, the same sample of backing material is used to measure the response with the twenty samples of film. To make this possible, the tested facings are not glued to the backings but simply clamped and mounted tight between the grid and the backing sample. This technique gives

satisfying results while being very flexible.

Figure 10 show the absorption coefficient for the two considered backing (melamine foam and glass wool) with the upstream grid as well as the absorption coefficients for each of the twenty samples of film and each backing. On this figure, the influence of the film is clearly visible. Analysing these results, it appears that the variability of the parameters of the film leads to a slight spreading of the responses with occasional features distributed over the spectrum. A glitch is seen around 600Hz and is present on all measurements, it is linked to the measurement rig and will not be discussed any further.

To better understand the origin of the observed variations, Figure 11 show the range of variation of the physical parameters for both films in terms of percentage of deviation with respect to the average value. In this figure, it is seen that σ is the most varying parameter for both screens, closely followed by the porosity ϕ and the two characteristic lengths Λ and Λ'. It is known that the airflow resistivity, together with the thickness d, is of prime importance as it plays a prominent role in the airflow resistance. Even though the thickness does not vary much amongst the samples considered here, it has been observed to have high deviations for other facings and might sometimes have an important impact.

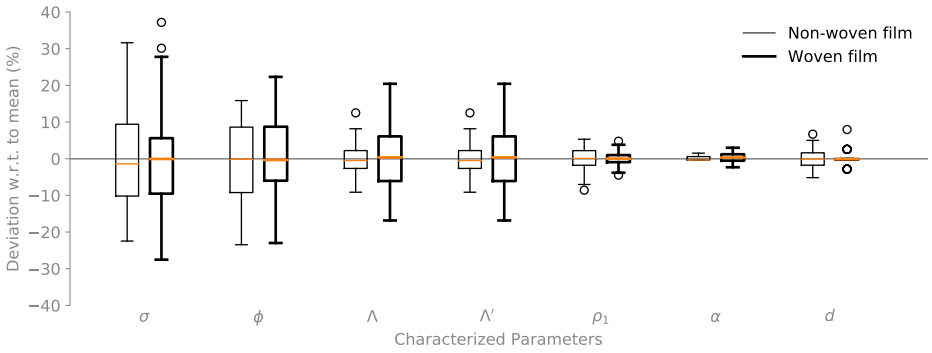

Figure 11 – Spread of the JCA parameters and thickness for both facings. The orange line marks the median, outliers are represented with circles and the box spans between the first and third quartiles. Thin lines correspond to the non-woven facing, thick ones to the woven film. (Color online)

4.2 Generating envelopes for experimental data

In this subsection the envelope response is observed and two techniques to reconstruct these are compared. First a naive approach, consisting in reusing the mean values and standard deviations of the parameters of the thin facings as well as the backing parameters to compute a upper- and lower bound response. These responses are computed by using the average value of all parameters except the supposedly varying one (for instance σ) for which n times the standard deviation is added/subtracted to mean value.

The other approach is the one described in Section 2 where statistical information on the facing parameter is embedded in an annotated envelope. When needed, the backing impedance Z_B is computed using the average value of the parameters. All envelopes in this section are computed with the proposed method for $n = 1$ or $n = 2$. On Figure 12, the cases with a melamine backing is presented, on Figure 13 the one with a glass wool backing is shown. Note that in these figures, both films are considered for both approaches.

From these figures, it is clear that the naive approach is rarely a good approximation of the actual envelope, particularly at low frequencies. On the top rows of both Figure 12 and 13, one easily notices the discrepancies introduced by considering a JCA model both for the backing and for the film. Indeed, even though this hypothesis is reasonable for the film thanks to its very specific effect and thinness, it is a strong approximation for the poro-elastic backing in which solid-borne waves also propagate.

On the other hand the proposed approach closely follows the empirical envelope particularly the predicted envelope for $n = 1$ which almost exactly follows the standard deviation envelope. Some discrepancies are observed around 1750 Hz on Figure 13 with a woven fabric, which might be linked to the fact that the surface of the glasswool sample is not perfectly flat and that the woven film is rather soft. Around this frequency, the proposed approach traces a plausible envelope but does not account for the existing resonance.

5 Conclusion

In the present contribution, a method to generate envelopes responses for multilayered systems including a film with uncertain parameters is introduced. The proposed method uses a set of Taylor expansions to introduce a way to separate the contributions of uncertainties from the average trend. The said method is both suitable for standalone computations of envelope responses or as a tool to compute envelopes from a single response from the system and the parameters of the facing.

The method is tested both on simulated cases with materials and configurations sourced from the literature and on actual experiments. In both cases, the method is shown to give good results with predicted envelopes having similar trends and amplitudes as the ones based on measurements. The proposed solution is fitting the

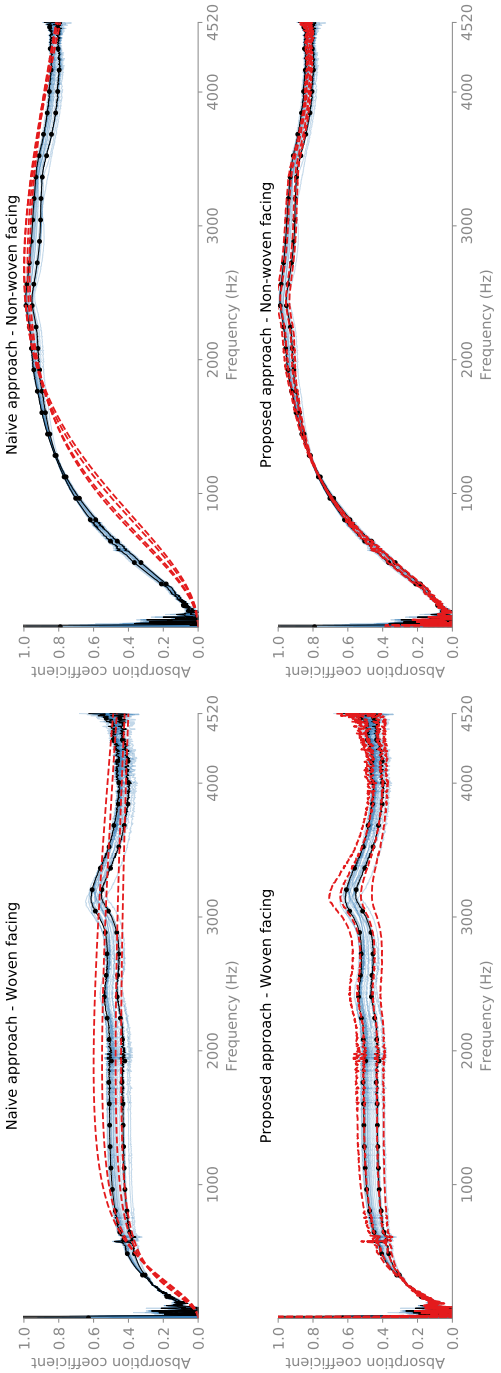

Figure 12 – Case of a melamine backing. Comparison of envelopes (in red) annotated on the mean response as proposed in section 2.3 (bottom) and envelopes generated using the JCA characterisation of the backing and the film (top). For a woven film (left) and a non-woven (right). The blue light traces are sample responses and the black curve with bullets • is the standard deviation envelope. (Color online)

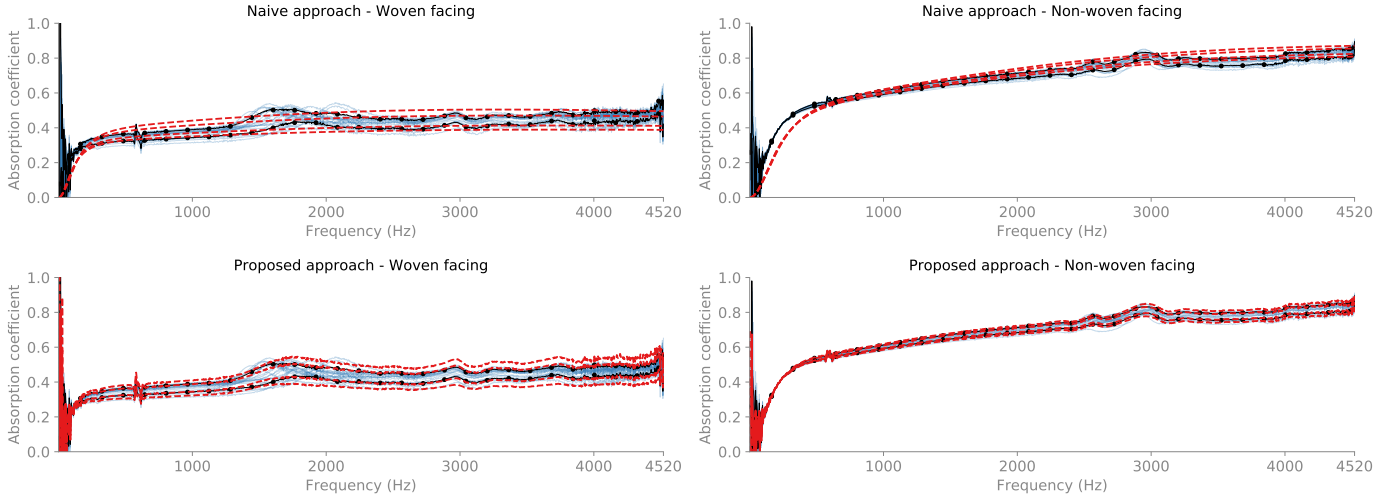

Figure 13 – Case of a glass wool backing. Comparison of envelopes (in red) annotated on the mean response as proposed in section 2.3 (bottom) and envelopes generated using the JCA characterisation of the backing and the film (top). For a woven film (left) and a non-woven (right). The blue light traces are sample responses and the black curve with bullets • is the standard deviation envelope. (Color online)

measured reference better than a naive approach based on the bounds of a given variation interval of the parameters.

References

[1] J.-F. Allard and N. Atalla. Propagation of Sound in Porous Media: Modelling Sound Absorbing Materials. 2nd. Hoboken, N.J: Wiley, 2009.

[2] T. Weisser et al. Acoustic Behavior of a Rigidly Backed Poroelastic Layer with Periodic Resonant Inclusions by a Multiple Scattering Approach. *The Journal of the Acoustical Society of America*, 139 (**2**), 2016, pp. 617–629. DOI: 10.1121/1.4940669.

[3] N. Jiménez et al. Rainbow-Trapping Absorbers: Broadband, Perfect and Asymmetric Sound Absorption by Subwavelength Panels for Transmission Problems. en. *Scientific Reports*, 7 (**1**), 2017. DOI: 10.1038/s41598-017-13706-4.

[4] C. Boutin. Acoustics of Porous Media with Inner Resonators. en. *The Journal of the Acoustical Society of America*, 134 (**6**), 2013, pp. 4717–4729. DOI: 10.1121/1.4824965.

[5] M. E. Beutel et al. Noise Annoyance Is Associated with Depression and Anxiety in the General Population- The Contribution of Aircraft Noise. en. *PLOS ONE*, 11 (**5**), 2016. Ed. by M. A. Andrade-Navarro, e0155357. DOI: 10.1371/journal.pone.0155357.

[6] The European Parliament. Regulation (EU) No 540/2014 of the European Parliament and of the Council of 16 April 2014 on the Sound Level of Motor Vehicles and of Replacement Silencing Systems, and Amending Directive 2007/46/EC and Repealing Directive 70/157/EEC. *Official Journal of the European Communities*, L158, 2014, pp. 131–195.

[7] W. Babisch. The Noise/Stress Concept, Risk Assessment and Research Needs. eng. *Noise & Health*, 4 (**16**), 2002, pp. 1–11.

[8] F. Chevillotte. Controlling Sound Absorption by an Upstream Resistive Layer. en. *Applied Acoustics*, 73 (**1**), 2012, pp. 56–60. DOI: 10.1016/j.apacoust.2011.07.005.

[9] S. Sugie, J. Yoshimura, and H. Ogawa. Absorption Characteristics of Fibrous Material Covered with Perforated Facing and Film. *Acoustical science and technology*, 27 (**2**), 2006, pp. 87–96.

[10] N. Atalla and F. Sgard. Modeling of Perforated Plates and Screens Using Rigid Frame Porous Models. en. *Journal of Sound and Vibration*, 303 (**1-2**), 2007, pp. 195–208. DOI: 10.1016/j.jsv.2007.01.012.

[11] M. Gaborit, O. Dazel, and P. Göransson. A Simplified Model for Thin Acoustic Screens. en. *The Journal of the Acoustical Society of America*, 144 (**1**), 2018, EL76–EL81. DOI: 10.1121/1.5047929.

[12] A. D. Pierce. Acoustics: An Introduction to Its Physical Principles and Applications. 1989th ed. Woodbury, N.Y: Acoustical Society of America, 1989.

[13] L. Jaouen and F.-X. Bécot. Acoustical Characterization of Perforated Facings. *The Journal of the Acoustical Society of America*, 129 (**3**), 2011, pp. 1400–1406. DOI: 10.1121/1.3552887.

[14] O. Dazel et al. An Alternative Biot's Displacement Formulation for Porous Materials. en. *The Journal of the Acoustical Society of America*, 121 (**6**), 2007, p. 3509. DOI: 10.1121/1.2734482.

[15] Y. Champoux and J.-F. Allard. Dynamic Tortuosity and Bulk Modulus in Air-Saturated Porous Media. en. *Journal of Applied Physics*, 70 (**4**), 1991, p. 1975. DOI: 10.1063/1.349482.

[16] D. L. Johnson, J. Koplik, and R. Dashen. Theory of Dynamic Permeability and Tortuosity in Fluid-Saturated Porous Media. *Journal of fluid mechanics*, 176 (**1**), 1987, pp. 379–402.

[17] ISO. ISO 9053-1 - Acoustics - Determination of Airflow Resistance - Static Airflow Method. 2018.

[18] ISO. ISO 10534-2 Acoustics - Determination of Sound Absorption Coefficient and Impedance in Impedance Tubes - Part 2 : Transfer-Function Method. 1998.

[19] M. Gaborit et al. Statistical Characterisation and Responses of Acoustics Screens and Two-Layers Systems. en. 2019. DOI: 10.5281/zenodo.3358921.

[20] Matelys. TubeCell. Vaulx-en-Velin, France, 2019.

[21] T. Iwase and Y. Izumi. A new sound tube measuring method for propagation constant in porous material–Method without any air space at the back of test material. jp. *Journal of the Acoustical Society of Japan*, 52 (**6**), 1996.

[22] T. Iwase, Y. Izumi, and R. Kawabata. A New Measuring Method for Sound Propagation Constant by Using Sound Tube without Any Air Spaces Back of a Test Material. *INTER-NOISE and NOISE-CON Congress and Conference Proceedings*. Vol. 1998. 1998, pp. 1265–1268.

[23] R. Panneton and X. Olny. Acoustical Determination of the Parameters Governing Viscous Dissipation in Porous Media. en. *The Journal of the Acoustical Society of America*, 119 (**4**), 2006, p. 2027. DOI: 10.1121/1.2169923.

[24] X. Olny and R. Panneton. Acoustical Determination of the Parameters Governing Thermal Dissipation in Porous Media. en. *The Journal of the Acoustical Society of America*, 123 (**2**), 2008, pp. 814–824. DOI: 10.1121/1.2828066.

Paper C

Coupling FEM, Bloch Waves and TMM in Meta Poroelastic Laminates

M. Gaborit[1,3,@], L. Schwan[1], O. Dazel[1], J-P. Groby[1], T. Weisser[2], P. Göransson[3]

Published in Acta Acustica United with Acustica
Vol. 104 (2018), pp. 220-227, DOI: 10.3813/AAA.919163

1. LAUM, UMR CNRS 6613, Université du Maine, Le Mans, France
2. MIPS Laboratory, Université de Haute Alsace, Mulhouse, France
3. MWL, KTH Royal Institute of Technology, Stockholm, Sweden
@ Corresponding author

Abstract

The propagation of airborne plane waves in the presence of a meta poroelastic laminate, that is a poroelastic matrix coated with thin elastic layers at its facings and periodically-embedded with inclusions, is studied. Using the Finite Element Method (FEM) only would result in a drastic increase of the degrees of freedom due to the fine mesh required to account for the very thin coatings. Here, the approach relies on: the Bloch wave expansion of the fields in air; the modal Transfer Matrix Method to account for the coatings; and the coupling with the FEM model of the poroelastic matrix and the resonant inclusions. The model is developed for reflection and transmission problems and it can account for coatings with multiple layers. The procedure induces the addition of the Bloch coefficients in the FEM's linear system at a negligible additional computational cost. It is applied to the meta poroelastic laminates with poroelastic inclusions and rubber shell inclusions. The results are compared with those from the Multiple Scattering Theory and an excellent agreement between the methods is found. The approach offers a numerically-efficient way to account for coatings applied to meta poroelastic layers, and finds applications in industrial prototypes where coatings are widely used.

1 Introduction

Sound insulation is a prominent research topic in acoustics and the development of tailored absorbers using structured media has gained even more interest with the emergence of the so-called metamaterials[1–5]. Recently, the use of meta-poroelastic media, consisting of micro-structures periodically embedded in a poroelastic matrix, has been put forward[4,6,7]. Such materials rely on the acoustic/elastodynamic energy reduction, while energy dissipation is achieved through visco-thermal phenomena in the matrix pores.

Besides, audacious designs are becoming more and more accessible, and new manufacturing solutions such as 3-D printing[8–10] now allow materializing algorithmically generated structures with a high fidelity. In particular, manufacturing numerous quasi-identical unit cells is made possible and allows for full scale measurements. Such prototyping techniques motivate the use of advanced optimization techniques such as genetic algorithms or nonlinear programming to simulate systems under realistic conditions.[11,12]

To this end, efficient and accurate numerical models of systems are required and several options have been considered. On one hand, semi-analytical approaches such as Multiple Scattering Theory[13], allow for very fast evaluation of system responses at the cost of an initial analytical resolution. Nevertheless, Multiple Scattering Theory (MST) is limited to simple inclusion geometries. On the other hand, more versatile purely numerical techniques may be used to model one elementary cell with periodicity conditions but tend to exhibit a much higher computational cost at each evaluation. The Finite-Element Method (FEM) is part of this second group and the cost of evaluation is directly linked to the mesh refinement which, in turn,

is related to both the frequency of interest and the size of the smallest geometrical features. The latter is of particular interest in the scope of meta-poroelastic systems for which the free surface may be protected by thin layers (e.g. films or fabric) that have an impact on the acoustic response and tend to drive the mesh refinement, increasing considerably the computational cost. Considering these points, it proves interesting to develop a method combining the versatility and ease of modelling associated to the FEM while alleviating the cost of added layers by accounting for them separately.

The present work is concerned with the plane wave reflection/ transmission of airborne sound from a laminate panel made of a metaporoelastic layer sandwiched between very thin elastic coatings. A method is presented which couples the FE model of a meta-poroelastic layer and the Bloch expansions of the fields in the surrounding media. The proposed approach efficiently accounts for elastic coatings that may be added to the poroelastic matrix and modelled with only a few additional degrees of freedom. The model can give access to the reflection and transmission coefficients not only for the specular modes but also for the Bloch modes of higher order. The problem is tackled in 2-D and no particular assumption is made about the inner design of the metaporoelastic layer. The method is presented in Section 2, and the results are compared with those from the Multiple Scattering Theory (MST) for poroelastic media[6] in Section 3.

2 Numerical model

2.1 Statement of the problem

The meta-poroelastic laminate consists of the infinite D-periodic arrangement along the x axis of the elementary cell made of (1) a poroelastic matrix; (2) one or several periodically embedded inclusions of arbitrary shape in the poroelastic matrix; and (3) a thin elastic coating at the plane boundary Γ_- of the poroelastic matrix, see figure 1. The coating is supposed to be made of homogeneous elastic material. Furthermore, the exact nature of the inclusions is not specified at this stage, but they are supposed to be sufficiently long to tackle the problem in the 2-D cross section (x, z). In this Cartesian coordinate system, the interface Γ_+ is given by $z = z_+$ while the coating boundary Γ_- on the other side is given by $z = z_-$. For simplicity in the derivation, the meta-poroelastic laminate is arranged against a rigid backing at the boundary Γ_b and a single-layer coating is considered. The model will be extended to transmission problems and multi-coating configurations in Section 2.4.

The meta-poroelastic laminate is supposed to be in contact with air at the boundary Γ_-, see sigure 1. The reflection of an airborne unitary plane wave from the meta-poroelastic laminate is studied in the linear harmonic regime at the circular frequency ω (using $e^{j\omega t}$ time convention). Taking advantage of the adaptivity of the FEM and its ability to model various types of inclusions, the meta-poroelastic layer comprising the poroelastic matrix with the inclusion will be modelled using

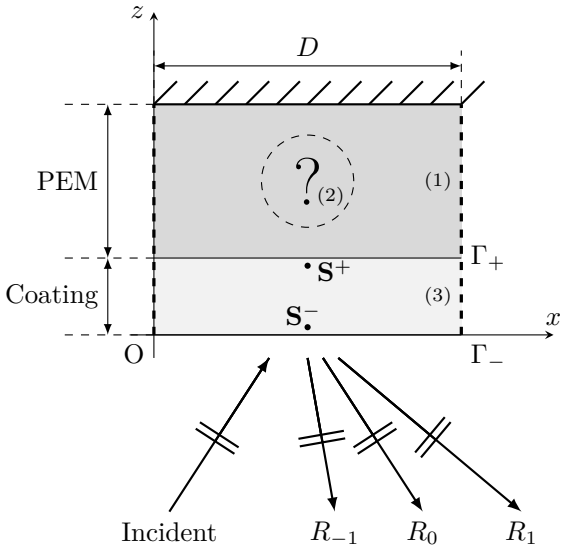

Figure 1 – A generic elementary cell of an infinitely periodic system. The dotted lines on each side denotes periodicity conditions (applied in the FE scheme). A detailed description of the cell is given in section 2. The inclusion is not detailed and is of very little importance: only counts the homogeneity of the interface Γ_+.

the FEM. As a first step to the Finite Element Method[14], the equations governing the equilibrium in the poroelastic matrix and the inclusions are formulated in their weak form. The two classical approaches to model poroelastic with the FEM use the solid displacement $\mathbf{u}^s$ and interstitial pressure p as main variables. They differ in their way of accounting for boundaries: Ref. [15] proposes a boundary operator coupling naturally with fluid media, whereas the formulation in Ref. [16] couples best with elastic and poroelastic media. This last formulation uses the total stress tensor $\underline{\underline{\sigma}}^t$ and relative displacement $\boldsymbol{w}$ between solid and fluid phase as secondary variables used in the boundary operators. While the full weak form associated to the FEM domain is beyond the scope of the present work, the expression of the boundary operator along Γ_+, here expressed with the normal $\mathbf{n}$ pointing outwards the FE domain, is given by:

$$\mathcal{I} = \int_{\Gamma_+} \delta\mathbf{u}^s \cdot [\underline{\underline{\sigma}}^t \cdot \mathbf{n}] \, \mathrm{d}\Gamma + \int_{\Gamma_+} \delta p \, [\mathbf{w} \cdot \mathbf{n}] \, \mathrm{d}\Gamma. \tag{1}$$

A crucial point is that all the other boundaries of the FE domain are treated classically by the FEM. They will not be discussed in the present paper.

Evaluating this integral is hence one key of the FEM model. To avoid modeling the coating with the FEM (which would inevitably lead to a drastic increase in

the number of degrees of freedom due to the very fine mesh required by very small thickness), an alternative procedure is presented here, that takes advantage of the quasi-periodicity in the system. The present approach relies on the transfer of the unknown Bloch coefficients from the fluid medium to the poroelastic matrix. A technique similar to the transfer matrix method is used for transferring the Bloch expansions and allows to account for the coating by rewriting the FEM boundary operator $\mathcal{I}$ and the associated set of continuity conditions.

2.2 Bloch wave expansions and modal Transfer Matrix Method

Due to the D-periodicity of the meta-poroelastic laminate, the pressure field p^a in air can be expanded as follows in terms of Bloch waves:

$$p^a(\mathbf{r}) = \sum_{l\in\mathbb{Z}} \left[\delta_{0l} e^{-\mathrm{j}k_z^l z} + R_l e^{+\mathrm{j}k_z^l z}\right] e^{-\mathrm{j}k_x^l x}, \tag{2}$$

where δ_{0l} is the Kronecker symbol and represents the amplitude of the incident wave, R_l are complex reflection coefficients and k_x^l and k_z^l are the Bloch wavenumbers defined as:

$$k_x^l = k_x^i + \frac{2\pi l}{D} \;;\quad k_z^l = \sqrt{\left(\frac{\omega}{c}\right)^2 - (k_x^l)^2}, \tag{3}$$

where k_x^i is the wavenumber of the incident field in the direction x, c is the sound speed in the fluid medium of density ρ. Besides, the particle displacement $\mathbf{u}^a = \left\{u_x^a,\ u_z^a\right\}^T$ in air is given by the momentum conservation $\rho\omega^2\mathbf{u}^a = \mathbf{grad}(p^a)$ and, using equation (2), its component along z reads:

$$u_z^a = \sum_{l\in\mathbb{Z}} \left[u_z^{a,i}\delta_{0l} e^{-\mathrm{j}k_z^l z} + u_z^{a,l} R_l e^{+\mathrm{j}k_z^l z}\right] e^{-\mathrm{j}k_x^l x}, \tag{4}$$

where the harmonic displacement coefficients $u_z^{a,i}$ for the incident field and $u_z^{a,l}$ for the Bloch reflections read:

$$u_z^{a,i} = \frac{-\mathrm{j}k_z^i}{\rho\omega^2} \;;\quad u_z^{a,l} = \frac{\mathrm{j}k_z^l}{\rho\omega^2}. \tag{5}$$

Similarly, the solid particle displacement $\mathbf{u}^e(x, z_\pm)$ at the boundary $\Gamma_\pm$ of the elastic coating (fixed value of $z = z_\pm$) can be expanded as:

$$\mathbf{u}^e(x, z_\pm) = \sum_{l\in\mathbb{Z}} \left[\mathbf{u}^{e,l}(z_\pm)\right] e^{-\mathrm{j}k_x^l x}, \tag{6}$$

where the vectors $\mathbf{u}^{e,l}(z_\pm) = \left\{u_x^{e,l}(z_\pm),\ u_z^{e,l}(z_\pm)\right\}^T$ are the complex amplitudes of the displacement $\mathbf{u}^e(x, z_\pm)$ in its Spatial Fourier Transform along x, that is its projection on Bloch waves. Likewise, the surface stress vector $\boldsymbol{\sigma}^e = \left\{\sigma_{zx}^e,\ \sigma_{zz}^e\right\}^T$ at the boundary $\Gamma_\pm$ is expanded as:

$$\boldsymbol{\sigma}^e(x, z_\pm) = \sum_{l\in\mathbb{Z}} \left[\boldsymbol{\sigma}^{e,l}(z_\pm)\right] e^{-\mathrm{j}k_x^l x}. \tag{7}$$

At the interface Γ_- between the fluid medium and the coating, that is at $z = z_-$, the following boundary conditions hold, stating the continuity of the normal flux and of the surface stress vector:

$$u_z^e = u_z^a \ ; \quad \sigma_{zx}^e = 0 \ ; \quad \sigma_{zz}^e = -p^a \qquad \text{at } \Gamma_-. \tag{8}$$

Note that the x-component of the displacement $\mathbf{u}^e$ does not appear in those conditions, and its modal components $u_x^{e,i}(z_-)$ and $u_x^{e,l}(z_-)$ are hence unknowns of the problem. Using equations (2), (4), (6), (7) and the orthogonality of the Bloch waves, the interface conditions (8) leads to the following relations, where the Bloch modes are decoupled from one another:

$$\begin{cases} u_x^{e,l}(z_-) = \text{unknown}, \\ u_z^{e,l}(z_-) = u_z^{a,i}\delta_{0l} + u_z^{a,l} R_l, \\ \sigma_{zx}^{e,l}(z_-) = 0, \\ \sigma_{zz}^{e,l}(z_-) = -\delta_{0l} - R_l. \end{cases} \tag{9}$$

The components on the left-hand side of equations (9) can be advantageously arranged in the state vector $\mathbf{S}_l^-$ for Bloch mode l at the boundary $\Gamma_-(z = z_-)$ as follows:

$$\mathbf{S}_l^- = \left\{ u_x^{e,l}(z_-),\ u_z^{e,l}(z_-),\ \sigma_{zx}^{e,l}(z_-),\ \sigma_{zz}^{e,l}(z_-) \right\}^T. \tag{10}$$

Then, using expression (5) for the displacements $u_z^{a,i}$ and $u_z^{a,l}$, equation (9) can be written in the following matrix formulation:

$$\mathbf{S}_l^- = \mathbf{E}^- \delta_{0l} + [\mathbf{I}_l^-]\mathbf{Q}_l, \tag{11}$$

with the vector $\mathbf{E}^-$ being related to the incident field, $\mathbf{Q}_l = \left\{ u_x^{e,l}(z_-),\ R_l \right\}^T$ being the vector of unknowns and $[\mathbf{I}_l^-]$ a matrix implementing the continuity conditions for the reflections. These quantities are defined by:

$$\mathbf{E}^- = \begin{Bmatrix} 0 \\ \frac{-\mathrm{j}k_z^i}{\rho\omega^2} \\ 0 \\ -1 \end{Bmatrix} \ ; \quad [\mathbf{I}_l^-] = \begin{bmatrix} 1 & 0 \\ 0 & \frac{\mathrm{j}k_z^l}{\rho\omega^2} \\ 0 & 0 \\ 0 & -1 \end{bmatrix}. \tag{12}$$

Likewise, the state vector $\mathbf{S}_l^+$ for the Bloch mode l at the boundary $\Gamma_+(z = z_+)$ reads:

$$\mathbf{S}_l^+ = \left\{ u_x^{e,l}(z_+),\ u_z^{e,l}(z_+),\ \sigma_{zx}^{e,l}(z_+),\ \sigma_{zz}^{e,l}(z_+) \right\}^T. \tag{13}$$

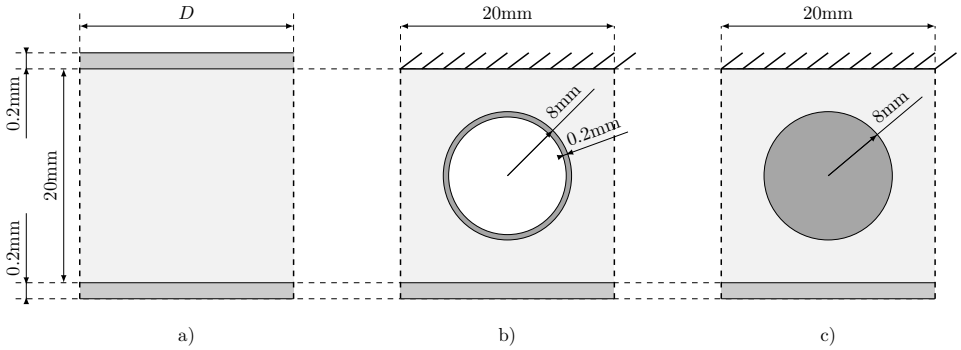

Figure 2 – The three elementary cells used in the examples, **a)** rubber-poroelastic-rubber sandwich panel with no inclusion, **b)** rubber coated poroelastic slab with an air-filled rubber shell inclusion, **c)** rubber coated poroelastic slab with a poroelastic inclusion.

Considering the orthogonality of the Bloch waves (exponential functions), each Bloch mode l at the boundary Γ_+ depends linearly on the Bloch mode of the same order l at the boundary Γ_-. Introducing a modal transfer matrix $[\mathbf{T}_l]$ for each Bloch mode l, this linear relation is given by the relation:

$$\mathbf{S}_l^+ = [\mathbf{T}_l]\mathbf{S}_l^-. \tag{14}$$

The expression for the modal transfer matrices $[\mathbf{T}_l]$ related to the elastic coating can be found in Ref. [17].
Now, substituting (11) into (14), the state vector $\mathbf{S}_l^+$ is found to take the form:

$$\mathbf{S}_l^+ = \mathbf{E}^+\delta_{0l} + [\mathbf{I}_l^+]\mathbf{Q}_l, \tag{15}$$

where the vector $\mathbf{E}^+$ and the matrix $[\mathbf{I}_l^+]$ are given by:

$$\mathbf{E}^+ = [\mathbf{T}_0]\mathbf{E}^-; \quad [\mathbf{I}_l^+] = [\mathbf{T}_l][\mathbf{I}_l^-]. \tag{16}$$

Note in equation (15) that the state vector $\mathbf{S}_l^+$ for the Bloch mode l at the boundary Γ_+ actually depends on the vector $\mathbf{Q}_l$ of unknowns, that are the modal displacement $u_x^{e,l}(z_-)$ in the x-direction at the boundary Γ_-, and the reflection coefficients R_l in air. In other words, these unknowns have been transferred to the interface Γ_+ between the coating and the meta-poroelastic layer. In the next section, the method to incorporate these unknowns into the FEM model of the meta-poroelastic layer is presented.

2.3 FEM implementation

At the interface Γ_+ between the elastic coating and the poroelastic matrix, the following conditions hold, which state the imperviousness of the coating, and the continuity of the normal surface stress and solid displacements:

$$\mathbf{w}\cdot\mathbf{n}=0\ ;\quad \underline{\underline{\sigma}}^t.\mathbf{n}=-\boldsymbol{\sigma}^e\ ;\quad \mathbf{u}^s=\mathbf{u}^e\qquad \text{at } \Gamma_+. \tag{17}$$

The minus sign in the balance of surface stresses has been introduced to comply with the orientation of the normal vector at Γ_+. Using equations (7) and (13), the surface stress $\underline{\underline{\sigma}}^t.\mathbf{n}=-\boldsymbol{\sigma}^e(z_+)$ at Γ_+ reads:

$$\underline{\underline{\sigma}}^t.\mathbf{n}(x,z_+)=-\sum_{l\in\mathbb{Z}}\mathbf{S}_l^+\Big|_{3,4}e^{-\mathrm{j}k_x^l x}, \tag{18}$$

where the subscripts $3,4$ denote the extraction of the 3rd and 4th row of the tensor. Combining equation (18) with (15) results in:

$$\underline{\underline{\sigma}}^t.\mathbf{n}(x,z_+)=-\sum_{l\in\mathbb{Z}}\left(\mathbf{E}^+\Big|_{3,4}\delta_{0l}+[\mathbf{I}_l^+]\Big|_{3,4}\mathbf{Q}_l\right)e^{-\mathrm{j}k_x^l x}. \tag{19}$$

Substituting this expression back into the expression of $\mathcal{I}$ in equation (1) and using the impervious surface condition $\mathbf{w}\cdot\mathbf{n}=0$ at Γ_+ from equation (18), the boundary operator reads:

$$\begin{aligned}\mathcal{I}=\ & -\int_{\Gamma_+}\left(\mathbf{E}^+\Big|_{3,4}e^{-\mathrm{j}k_x^l x}\right)\cdot\delta\mathbf{u}^s\ \mathrm{d}\Gamma\\ & -\sum_{l\in\mathbb{Z}}\int_{\Gamma_+}\left([\mathbf{I}_l^+]\Big|_{3,4}\mathbf{Q}_l e^{-\mathrm{j}k_x^l x}\right)\cdot\delta\mathbf{u}^s\ \mathrm{d}\Gamma.\end{aligned} \tag{20}$$

Similarly, using the last condition of (17) as well as equations (13) and (6), the displacement at the surface of the poroelastic matrix is retrieved. Directly substituting $\mathbf{S}_l^+$ from (15), $\mathbf{u}^s$ reads:

$$\mathbf{u}^s=-\sum_{l\in\mathbb{Z}}\left(\mathbf{E}^+\Big|_{1,2}\delta_{0l}+[\mathbf{I}_l^+]\Big|_{1,2}\mathbf{Q}_l\right)e^{-\mathrm{j}k_x^l x}, \tag{21}$$

where the subscripts 1,2 denote the extraction of the first and second rows of the vector or matrix.

Projecting the continuity of the solid displacement in equation (21) on each Bloch mode along Γ_+ and using the orthogonality of the Bloch series' components yields a set of continuity conditions depending on the unknown coefficients and the fields from the FEM:

$$\int_0^D\mathbf{u}^s(x,z_+)e^{\mathrm{j}k_x^l x}\ \mathrm{d}x=D\mathbf{E}^+\Big|_{1,2}\delta_{0l}+D[\mathbf{I}_l^+]\Big|_{1,2}\mathbf{Q}_l. \tag{22}$$

Both equations (20) and (22) can now be implemented in the FEM model of the poroelastic matrix with the inclusion. After the spacial discretization and the Galerkin expansion over a set of shape functions, the FEM process results in a linear system:

$$[\boldsymbol{A}]\boldsymbol{X} = \boldsymbol{B}, \tag{23}$$

where the matrix $[\boldsymbol{A}]$ describes the propagation in the volume; the vector $\boldsymbol{B}$ comes from the discretization of the boundary operator; and the vector $\boldsymbol{X}$ contains the N_{FE} nodal values for the fields[14].

To perfectly represent the reflected field, the Bloch wave expansion involves infinite sums on $\mathbb{Z}$, but for practical reasons, only a truncation to $2N+1$ terms ranging from $-N$ to N is considered. The integer N is chosen according to an empirical rule based on previous numerical experiments[6,18,19] and is large enough for the Bloch waves' series to represent the fields' complexity:

$$N = \left\lfloor \frac{D}{2\pi} \left(3\mathrm{Re}\left(\frac{\omega}{c}\right) - k_x^0 \right) \right\rfloor + 5, \tag{24}$$

where $\mathrm{Re}(x)$ represents the real part of x and 5 is chosen as a security term.

The vectors $\mathbf{Q}_l$ of unknowns are gathered in the overall vector $\mathbf{Q}$:

$$\mathbf{Q} = \left\{ \mathbf{Q}_{-N} \ \ldots \ \mathbf{Q}_{-1}, \ \mathbf{Q}_0, \ \mathbf{Q}_1 \ \ldots \ \mathbf{Q}_N \right\}^T.$$

The discretization of the boundary operator $\mathcal{I}$ as expressed in (20) is included in the right-hand side term $\boldsymbol{B}$ along with the terms from the other boundaries (gathered in $\boldsymbol{F_0}$ but not detailed in this work):

$$\boldsymbol{B} = \boldsymbol{F_0} + \boldsymbol{F}_{\mathcal{I}} = \boldsymbol{F_0} + \boldsymbol{F} - [\boldsymbol{C}]\mathbf{Q}, \tag{25}$$

where the N_{FE} vector $\boldsymbol{F}$ and $N_{FE} \times 2(2N+1)$ coupling matrix $[\boldsymbol{C}]$ come from the discretization of the first and second terms in (20), respectively. The evaluation of these terms must be handled with care since they might require integration of exponential-polynomial products.

Likewise, the discretization of (22) yields the following relation:

$$[\boldsymbol{C'}]\boldsymbol{X} = \boldsymbol{F'} - [\boldsymbol{A'}]\mathbf{Q}, \tag{26}$$

where the $2(2N+1) \times N_{FE}$ matrix $[\boldsymbol{C'}]$, comes from the discretization of the left-hand-side term of (22) while the $2(2N+1)$ vector $\boldsymbol{F'}$ and the $2(2N+1)$ diagonal matrix $[\boldsymbol{A'}]$ come from the discretization of the first and second terms in the right-hand-side of (22). Note that $\boldsymbol{F'}$ is zero for all l except for $l=0$ where it takes the value D. Finally, combining equations (23) to (26), the following overall FEM/Bloch coupled-system is formed:

$$\begin{bmatrix} [\boldsymbol{A}] & [\boldsymbol{C}] \\ [\boldsymbol{C'}] & [\boldsymbol{A'}] \end{bmatrix} \begin{Bmatrix} \boldsymbol{X} \\ \mathbf{Q} \end{Bmatrix} = \begin{Bmatrix} \boldsymbol{F} \\ \boldsymbol{F'} \end{Bmatrix} + \begin{Bmatrix} \boldsymbol{F_0} \\ \mathbf{0} \end{Bmatrix}. \tag{27}$$

Hence, the vector of the FEM unknowns $\boldsymbol{X}$ is extended by the $2(2N+1)$ vector of unknowns $\mathbf{Q}$ from the Bloch expansions.

2.4 Extension to transmission problems and multi-coating configurations

The method has been presented for the reflection problem on a meta-poroelastic laminate with a rigid backing and a single coating above the meta-poroelastic layer. It is now extended to the transmission problem and multi-layer coating configurations.

Extension to transmission problems The fields transmitted through the system are accounted for in a manner similar to the reflected ones. Based on Bloch wave expansion, expressions similar to (2) can be written for the transmitted fields. This implies introducing a new set of unknown coefficients $\mathbf{Q}_{\mathbf{T}l}$ to be added to the linear system. The continuity relations between the FE domain and the coatings are rewritten in terms similar to (17). This procedure leads to a new extension of the linear system for the transmission case:

$$\begin{bmatrix} [\boldsymbol{A}] & [\boldsymbol{C}] & [\boldsymbol{C}_{\mathbf{T}}] \\ [\boldsymbol{C}'] & [\boldsymbol{A}'] & [\mathbf{0}] \\ [\boldsymbol{C}'_{\mathbf{T}}] & [\mathbf{0}] & [\boldsymbol{A}'_{\mathbf{T}}] \end{bmatrix} \begin{Bmatrix} \boldsymbol{X} \\ \mathbf{Q} \\ \mathbf{Q}_{\mathbf{T}} \end{Bmatrix} = \begin{Bmatrix} \boldsymbol{F} \\ \boldsymbol{F}' \\ \mathbf{0} \end{Bmatrix}, \tag{28}$$

with $[\boldsymbol{A}']$, $[\boldsymbol{C}']$, $[\boldsymbol{C}]$, $\boldsymbol{Q}$, $\boldsymbol{F}'$ being related to the reflection side and their counterparts subscripted with $\mathbf{T}$ to the transmission one. Note that the second forcing vector is null since no excitation is considered on the transmission side.

Extension to multi-coating configurations For multi-coating configurations, the approach relies on the modal Transfer Matrix Method (TMM) to transfer the fields through the different coating layers. A generalised transfer matrix for the whole multilayer can be deduced by multiplying the transfer matrices $[\mathbf{T}(n)]$ related to each of the N_L layers in the system[20]. This leads to a new set of $[\mathbf{T}_l]$ matrices that can be substituted into (14) to account for a multilayer coating.

3 Applications

Three different cases are presented in this section, one is a transmission case without inclusion and the two others are reflection cases with periodic embeddings. The reference for the transmission case is computed using the TMM. On the other hand, the reflection cases reference solutions are computed using a semi-analytical Multiple Scattering[21] approach. Schematics of the test cases can be found in figure 2 and physical properties of the materials in table 1.

Table 1 – Physical parameters used in the test suite, taken from Ref. [21] or manufacturer data (inclusion's poroelastic material is based on a sample from Eurocell). V/T.c.l: Viscous/Thermal characteristic length.

Air properties

Parameter	Symbol	Value	Unit
Density	ρ	1.213	$\mathrm{kg{\cdot}m^{-3}}$
Prandlt number	Pr	0.71	—
Viscosity	η	$1.839 \cdot 10^{-5}$	Pa·s
Atmospheric pressure	P_0	$1.01325 \cdot 10^5$	Pa
Polytropic index	γ	1.4	—
Sound speed	c	$\sqrt{\gamma \mathrm{P}_0/\rho}$	$\mathrm{m{\cdot}s^{-1}}$

Rubber properties

Parameter	Symbol	Value	Unit
Density	ρ	1800	$\mathrm{kg{\cdot}m^{-3}}$
Young's modulus	E	$1.9 \cdot 10^6 - 796\mathrm{j}\omega$	Pa
Poisson ratio	ν	0.48	—

Poroelastic media properties

Parameter	Symbol	Slab	Inclusion	Unit
Porosity	ϕ	0.989	0.95	—
Resistivity	σ	8060	$42 \cdot 10^3$	$\mathrm{N{\cdot}s{\cdot}m^{-4}}$
Tortuosity	α_∞	1	1.1	—
V.c.l.	Λ	214	15	μm
T.c.l.	Λ'	214	45	μm
Density	ρ	6.1	126	$\mathrm{kg{\cdot}m^{-3}}$
Shear modulus	N	$2.28 \cdot 10^4$	$2.8 \cdot 10^5$	Pa
Poisson ratio	ν	0.24	0.24	—
Structural damping	η_s	0.02	0.05	—

3.1 Transmission Case

This first test computes the absorption coefficient and transmission loss of a rubber-poroelastic-rubber sandwich panel. The problem is of infinite extent along the x direction, which is enforced using periodicity conditions on both sides of an elementary cell depicted in figure 2(a). Two tests are conducted: one with a period $D = 20$ mm and another with $D = 150$ mm and both use 10 elements per period. The goal of the second case is to demonstrate that the proposed approach allows reducing the number of elements while controlling the loss of accuracy. A plane wave impinges the surface of the multilayer at an angle θ with respect to the normal to the surface and, given the problem geometry, only specular reflection and transmission might exist. In order to test the proposed method, the solution is computed considering 11 Bloch waves both in transmission and reflection and as

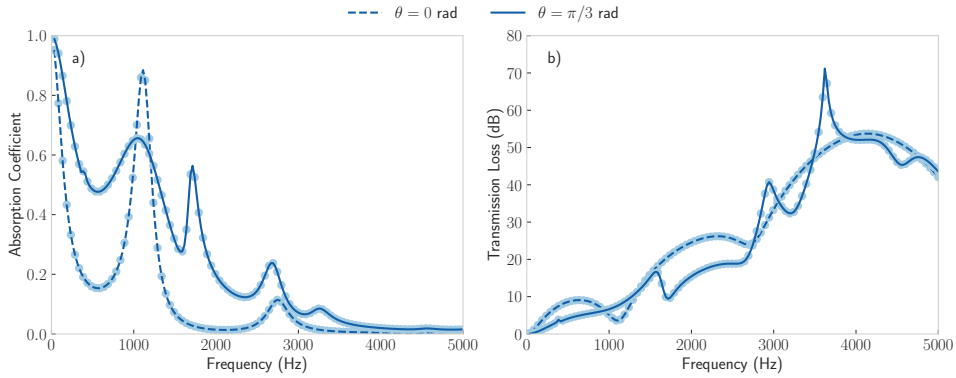

Figure 3 – a) Absorption coefficient & b) Transmission loss for a rubber-poroelastic-rubber panel at two two angles of incidence $\theta = 0\,\text{rad}$ (dashed) and $\theta = \pi/3\,\text{rad}$ (solid). The circle markers correspond to the TMM reference solution.

many terms in each of the two expansions for u_x. The higher-order reflection and transmission coefficients are all expected to be null.

Using the TMM solution as a reference, one can validate the proposed approach by computing the evolution of the absorption coefficient and transmission loss with regard to the frequency. The results for this test are presented in figure 3 where solid lines correspond to the proposed method and the markers to the TMM reference. This figure shows a perfect agreement between both methods over the whole frequency range and particularly around the peaks of large absorption and transmission. The FE mesh is sufficiently refined and this first result suggests that the proposed method does not induce any loss of precision.

In order to check that the solution vector is consistent with the expectations, one may plot the evolution of the coefficients from the Bloch series with respect to the frequency, as proposed in figure 4. The null-order coefficients (specular) are plotted in figure 4(a) and the higher-order ones in 4(b). One clearly sees that, except for the coefficients R_0 and T_0, all values are down to the order of 10^{-7}. This validates that the method gives consistent results and does not generate artifacts.

In order to highlight another ability of the method, the period is increased ($D = 150$ mm) while keeping the same number of elements. The comparison is made between the TMM reference (same as above), a solution using the proposed approach and a pure FEM solution modeling both the core and the coating using the FEM. Because of the period increase, the elements are slightly larger than in the previous case and the agreement with the reference solution is expected to be worse.

The results are shown in figure 5 with the TMM reference in black dots, the proposed method in light solid line and the FEM in dark solid line. One sees that at low frequency, all approaches produce similar results. As the frequency increases,

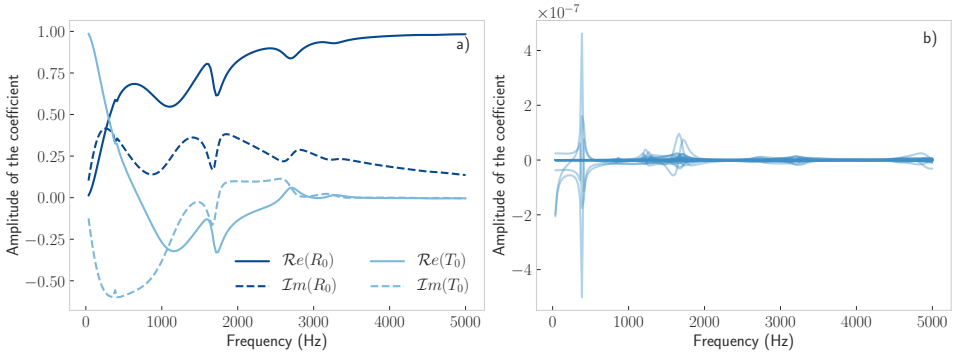

Figure 4 – Bloch series coefficients for a rubber-poroelastic-rubber panel with the incidence angle $\theta = \pi/3$ rad. a) Real (solid line) and imaginary (dashed line) parts of the null-order coefficients for transmission (light) and reflection (dark). b) Higher order coefficients with real and imaginary part superimposed (note the 10^{-7} scale factor).

the under-refined mesh leads to discrepancies in the pure FEM, the method being unable to represent the phenomena above 1 kHz. This is a side effect of distortion induced by an insufficiently refined mesh. The proposed approach does not experience the same issue: the coarse mesh tends to produce a slight shift of the peak towards low frequencies compared to TMM but the agreement is still good even without adding elements. Up to 5 kHz, no major disagreement between the TMM reference and the proposed approach can be noted, neither in amplitude nor peaks positions.

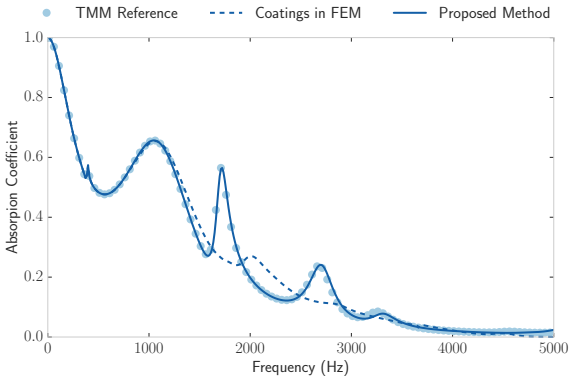

Figure 5 – Comparison of the absorption coefficient computed using TMM (circle markers), the proposed method (solid line) or including the coatings in a Finite Element model (dashed line). The number of elements in the core is the same for the two last methods, chosen such as one of them cat least complies with the reference.

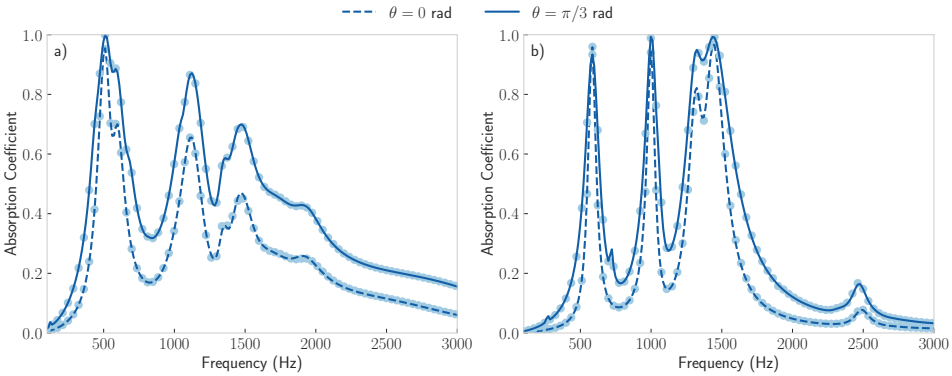

Figure 6 – Absorption coefficient for two meta porous panels bonded on a rigid backing with a) an air-filled rubber shell or b) a poroelastic circular inclusion. The panels are coated with rubber and excited by a plane wave for two different incidence angles $\theta = 0\,\text{rad}$ (dashed) and $\theta = \pi/3\,\text{rad}$ (solid). Results from the Multiple Scattering Theory are used as reference and shown with circle markers.

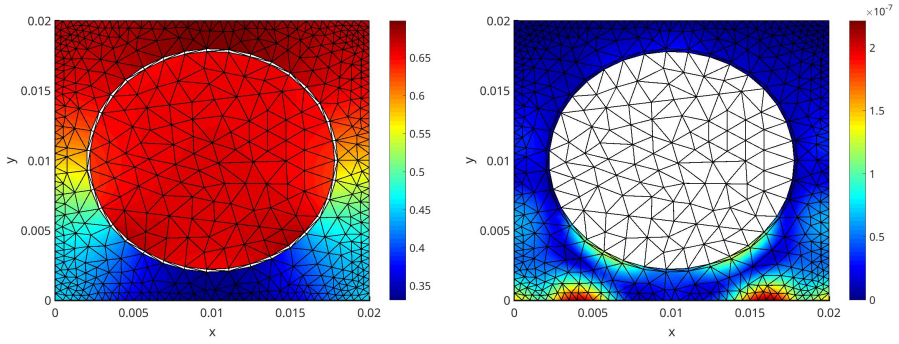

(a) Fluid pressure

(b) Norm of the solid displacement vector $\|\boldsymbol{u}\|$

Figure 7 – Fields' maps for the rubber shell case at $f = 1945\,\text{Hz}$ and $\theta = \pi/6$.

3.2 Reflection cases with inclusions

To illustrate the effects of the meta-poroelastic laminates on wave reflection, two configurations are studied. In the first case, the inclusion is made of poroelastic material, while in the second case the inclusion consists of a rubber shell with a 0.2 mm thickness filled with air, see figures 2(b) and 2(c). In both configurations, circular inclusions have an external radius of 8 mm, the period is $D = 20$ mm, the poroelastic matrix is 20 mm thick and is placed on a rigid backing while its free surface is coated with a 0.2 mm rubber layer. Results are presented in figure 6, and are compared with those obtained by the Multiple Scattering Theory for poroelastic media[21]. Two angles of incidence are considered: normal incidence ($\theta = 0$) and oblique incidence with $\theta = \pi/3$. The overall agreement between both methods is excellent and both the amplitude and the position of maxima match well.

4 Conclusion

In the present work, a method to account for thin plane structures at the boundary of a Finite-Element model is proposed. This method does not require to mesh the considered coating, limiting both the increase in complexity of the model and the potential distortion effects. The method is based on a transfer matrix approach and allows accounting for single- and multilayer coatings for a negligible increase of the model's size, while keeping the versatility of the FEM. The proposed approach was compared to the semi-analytical Multiple Scattering Technique to assess its accuracy. Results were in excellent agreement and the method is thus deemed reliable for the considered cases. Although the theoretical discussion was focused on a single layer elastic coating placed on a meta poroelastic layer, the approach could be extended to other types of media (anisotropic, for instance).

The whole development has been thought for meta materials design. Actually, the technique presented in this work has the potential to facilitate design of new meta absorbers. It alleviates the cost of meshing the coatings and allows to resolve separately all Bloch coefficients while still taking advantage of the FEM's versatility. Based on the FEM, the method allows to visually explore the on-going phenomena by generating maps as could be done with pure FEM typically implemented in commercial software. Examples of such maps for the system presented in figure 2(b) are depicted in figure 7. These field representations allow to finely investigate localization and radiation properties of such systems and can eventually serve as a guide towards new designs.

Applications of this work may concern a numerical approach to the design of meta materials and meta poroelastic laminates, especially in industrial applications where multilayer coatings are heavily used for protection, aesthetics, etc. and where the efficient simulation of their effect is crucial to the design process.

Acknowledgements

O. D., L. S., and J.-P. G. are grateful to the French ANR project Metaudible (ANR-13-BS09-0003). This article is based upon work from COST Action DENORMS CA15125, supported by COST (European Cooperation in Science and Technology).

References

[1] L. Schwan, O. Umnova, and C. Boutin. Sound absorption and reflection from a resonant metasurface: Homogenisation model with experimental validation. en. *Wave Motion*, 72, 2017, pp. 154–172. DOI: 10.1016/j.wavemoti.2017.02.004.

[2] M. D. Guild et al. Acoustic metamaterial absorbers based on multilayered sonic crystals. en. *Journal of Applied Physics*, 117 (**11**), 2015, p. 114902. DOI: 10.1063/1.4915346.

[3] J.-P. Groby et al. Enhancing the absorption properties of acoustic porous plates by periodically embedding Helmholtz resonators. *The Journal of the Acoustical Society of America*, 137 (**1**), 2015, pp. 273–280.

[4] C. Lagarrigue et al. Absorption of sound by porous layers with embedded periodic arrays of resonant inclusions. *The Journal of the Acoustical Society of America*, 134 (**6**), 2013, pp. 4670–4680.

[5] J. V. Sánchez-Pérez et al. Sound attenuation by a two-dimensional array of rigid cylinders. *Physical Review Letters*, 80 (**24**), 1998, p. 5325.

[6] T. Weisser et al. High broadband absorption of acoustic waves by elastic-framed metaporous layer. *Advanced Electromagnetic Materials in Microwaves and Optics (METAMATERIALS), 2016 10th International Congress on*. IEEE, 2016, pp. 322–324.

[7] C. Boutin and P. Royer. On models of double porosity poroelastic media. en. *Geophysical Journal International*, 203 (**3**), 2015, pp. 1694–1725. DOI: 10.1093/gji/ggv378.

[8] C. R. Garcia et al. 3D printing of anisotropic metamaterials. *Progress In Electromagnetics Research Letters*, 34, 2012, pp. 75–82.

[9] N. Jiménez et al. Quasiperfect absorption by subwavelength acoustic panels in transmission using accumulation of resonances due to slow sound. en. *Physical Review B*, 95 (**1**), 2017. DOI: 10.1103/PhysRevB.95.014205.

[10] M. Kadic et al. On the practicability of pentamode mechanical metamaterials. *Applied Physics Letters*, 100 (**19**), 2012, p. 191901.

[11] C. Lagarrigue et al. Design of metaporous supercells by genetic algorithm for absorption optimization on a wide frequency band. en. *Applied Acoustics*, 102, 2016, pp. 49–54. DOI: 10.1016/j.apacoust.2015.09.011.

[12] P. M. Pardalos et al., eds. Machine Learning, Optimization, and Big Data. Vol. 10122. Lecture Notes in Computer Science. Cham: Springer International Publishing, 2016.

[13] L. C. Botten et al. Rayleigh multipole methods for photonic crystal calculations. *Progress In Electromagnetics Research*, 41, 2003, pp. 21–60.

[14] O. C. Zienkiewicz and R. L. Taylor. The finite element method: the basis. 5th ed. Oxford ; Boston: Butterworth-Heinemann, 2000.

[15] N. Atalla, R. Panneton, and P. Debergue. A mixed displacement-pressure formulation for poroelastic materials. en. *The Journal of the Acoustical Society of America*, 104 (**3**), 1998, p. 1444. DOI: 10.1121/1.424355.

[16] N. Atalla, M. A. Hamdi, and R. Panneton. Enhanced weak integral formulation for the mixed (u,p) poroelastic equations. en. *The Journal of the Acoustical Society of America*, 109 (**6**), 2001, p. 3065. DOI: 10.1121/1.1365423.

[17] H. Bufler. Theory of elasticity of a multilayered medium. *Journal of Elasticity*, 1 (**2**), 1971, pp. 125–143.

[18] J.-P. Groby, A. Wirgin, and E. Ogam. Acoustic response of a periodic distribution of macroscopic inclusions within a rigid frame porous plate. *Waves in Random and Complex Media*, 18 (**3**), 2008, pp. 409–433.

[19] J.-P. Groby, W. Lauriks, and T. E. Vigran. Total absorption peak by use of a rigid frame porous layer backed by a rigid multi-irregularities grating. en. *The Journal of the Acoustical Society of America*, 127 (**5**), 2010, pp. 2865–2874. DOI: 10.1121/1.3337235.

[20] J.-F. Allard and N. Atalla. Propagation of sound in porous media: modelling sound absorbing materials. 2nd ed. Hoboken, N.J: Wiley, 2009.

[21] T. Weisser et al. Acoustic behavior of a rigidly backed poroelastic layer with periodic resonant inclusions by a multiple scattering approach. *The Journal of the Acoustical Society of America*, 139 (**2**), 2016, pp. 617–629.

Erratum
A simplified model for thin acoustic screens [J. Acoust. Soc. Am. 144 (1), EL76-EL81 (2018)]

M. Gaborit[1,2,@], O. Dazel[1], P. Göransson[2]
Published in the Journal of the Acoustical Society of America
Vol. 146 **(2)** (2019), pp. 1382-1383, DOI: 10.1121/1.5121612

1. LAUM, UMR CNRS 6613, Université du Maine, Le Mans, France
2. MWL, KTH Royal Institute of Technology, Stockholm, Sweden
@ Corresponding author

Abstract

The present erratum reports an error impacting the figures of a contribution published in 2018 about a simplified model for thin acoustic screens in a transfer matrix context (doi: 10.1121/1.5047929). A mistake in the implementation of the rigid termination condition for the systems under study is identified and a rectified version is proposed along with the corrected figures. It is shown that this error did not impact the conclusions of the original contribution and that the model proposed therein keeps its advantages as the approximation error remains very similar to the previously reported values.

1 Introduction

In 2018, the authors published the letter "A simplified model for thin acoustic screens" in the present Journal[1] which describes a strategy towards a model for very thin poroelastic layers based on transfer matrices. The original contribution uses a Taylor expansion justified by the film thinness to linearise the transfer matrix. Once this first step is completed, an analysis of the coupling between the different fields inside the film allows to reduce the number of non-zero elements in the transfer matrix. Finally, the proposed approach is tested on different cases and is shown to only induce a small error that is explained in the text.

It should be stressed that the following discussion does neither alter the relevance of the original contribution nor the correctness of its conclusions. Indeed, the published work is focused on modelling the effect of a porous film, whereas the implementation error only affects the backing conditions, which *per se* has no influence on the effectiveness of the proposed approach.

2 Termination conditions

In the original contribution, all the results shown are absorption coefficients of multi-layered systems set on a rigid backing. The film with the simplifications is always the first layer to be impinged by the incident wave. The mistake in the implementation causes the conditions on the fields at the termination to differ from the usual rigid backing conditions for a poroelastic medium.

In the case of the poroelastic model used in the contribution[1,2] a rigid backing is modelled by setting all displacements to zero and by considering the *in vacuo* stresses and the interstitial pressure unknown. In the implementation of the backing condition used to generate the results shown in the original figures, the conditions differed: the *in-vacuo* stresses were set to zero and the solid displacements considered unknown. This mistake led to much stiffer and less resonant test systems which implies that the correct implementation is a more challenging task for the proposed model than the erroneous one.

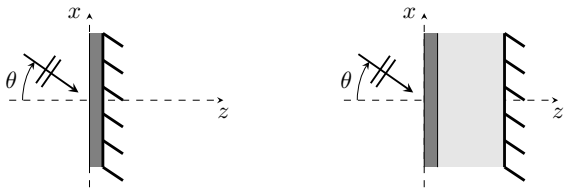

Figure 8 – Configurations used for the results presented in the original contribution. The darkest layer is a resistive screen, the light one a slab of poroelastic medium.

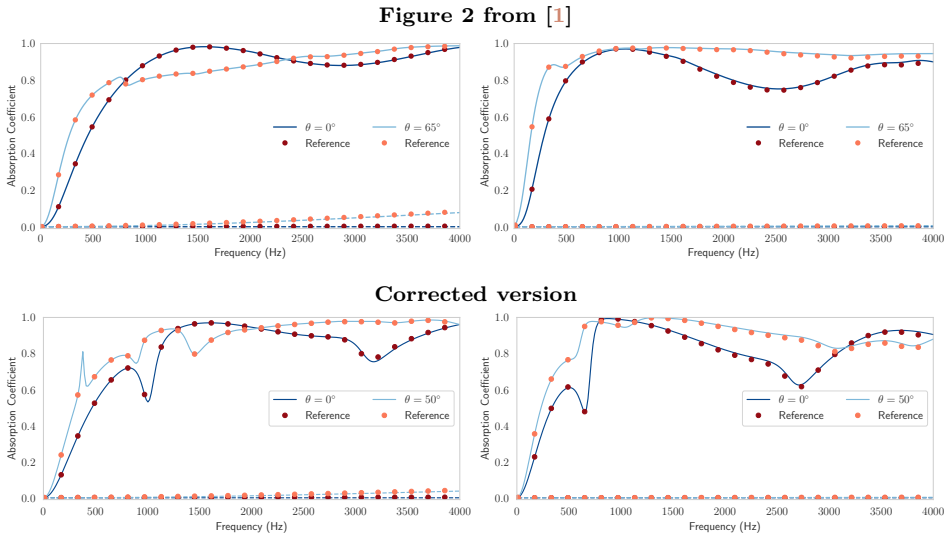

Figure 9 – Absorption coefficient for two materials, two angles and configurations presented on Figures 8.a (dashed lines) and 8.b (solid lines). For each result the lines correspond to the proposed approach and markers to the reference method. (Color online)

3 Impact on the results from the original contribution

In the original contribution,[1] the two configurations presented in Figure 8 are considered and tested for two different films. The remainder of the present contribution presents two versions of each figure: one before correcting the error (identical to these of the original contribution) and one after applying the correction.

Comparing the two versions of each figure, it is clear that the resonances and global trends are modified by the correction. Nevertheless, it is important to keep in mind that the original contribution does not discuss the system's absorbing properties but only the agreement between the reference solution and the proposed model's result. In Figure 9, it is clear that even though the trend is modified, the

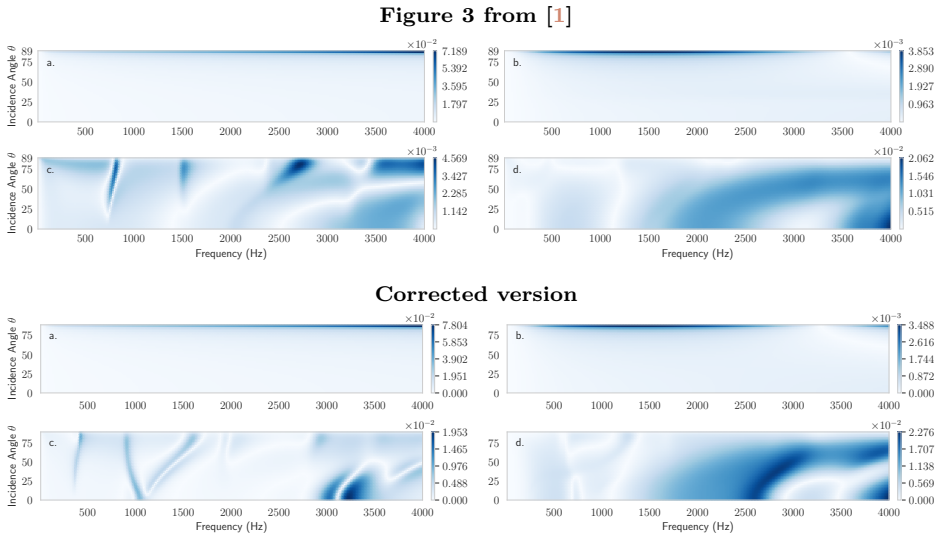

Figure 10 – Evolution of the absolute error $|\alpha_{biot} - \alpha_{screen}|$ in the (f, θ) plane. Two films are used, the first column (a. & c.) uses a non woven film, the second (b. & d.) a woven one. Similarly two backing conditions are tested, the one of Figure 8.a for the first line(a. & b.) and of Figure 8.b for the second (c. & d.).

proposed model's solution (solid lines) closely follows the reference (dots) as it did for the previous version. The same is observed on Figure 10 where the order of magnitude of the absolute difference between the two solutions is very similar to the one before the mistake was corrected. These observations, associated with other test results generated to assess the effectiveness of the correction and omitted here, support the claim that the mistake did not induce erroneous conclusions.

As succinctly presented in the introduction, this situation is easily explained by the fact that the original contribution focuses on the representation of the screens and is completely independent from the backing system. A modification of how the termination is modelled does indeed change the resonances and the overall response but as the proposed model for the screen remains unchanged, so does the associated approximation error.

4 Conclusion

In the present note, an issue with the figures from[1] is presented and addressed. It is shown that the mistake comes from the representation of the rigid backing in the implementation of the simulation method. This error modifies the response of the observed systems but does not impact the accuracy of the proposed screen model as observed when comparing the figures before and after correction.

References

[1] M. Gaborit, O. Dazel, and P. Göransson. A Simplified Model for Thin Acoustic Screens. *The Journal of the Acoustical Society of America*, 144 (**1**), 2018, EL76–EL81. DOI: 10.1121/1.5047929.

[2] O. Dazel et al. An Alternative Biot's Displacement Formulation for Porous Materials. *The Journal of the Acoustical Society of America*, 121 (**6**), 2007, p. 3509. DOI: 10.1121/1.2734482.

Part III

Published versions of the appended papers